

PREDICTING THE DEVELOPMENT OF CRESCENTIC BED PATTERNS

A comparison of linear stability model results with field observations

Meinard C.H. Tiessen, M.Sc.

Thesis submitted to the University of Nottingham
for the degree of Doctor of Philosophy

Nottingham, September 2009

Abstract

Large scale patterns in the seabed often occur in the nearshore zone of sandy beaches. A widely occurring bed pattern is the crescentic bar. These bed patterns develop under moderate wave conditions, and form a lunate shaped alongshore pattern in front of a coast. Over recent years, knowledge concerning the development, occurrence, and characteristics of these bed patterns has been significantly expanded through field studies and modelling attempts. An example of such a model is the linear stability analysis, which describes the initial development of crescentic bed patterns along an undisturbed beach.

To date, comparisons between field measurements and modelling results have been general in nature. The purpose of this research is to investigate whether a linear stability analysis, which is useful for understanding the physics of emerging bed-forms, can be used to make quantitative predictions in the field. To this end a morphodynamical linear stability model (Morfo60, [Calvete et al., 2005]) is used to describe the development of crescentic bed patterns at the coast at the USACE Field Research Facility in Duck, North Carolina, USA. Wave, tide and bathymetry data recorded at Duck over a two month period in 1998 are used to model the development of these morphodynamical patterns. The model predictions are compared with field observations made at Duck, over the same two month period, reported by van Enckevort et al. [2004].

A direct comparison shows that predicted length scales of crescentic bed patterns are similar to those observed. However, the model predictions show more

fluctuations than are observed in the field. This is because the model describes the development of crescentic bed patterns starting from an alongshore constant bed, whereas in reality bed patterns already exist in most situations.

An algorithm is developed to overcome these fluctuations and identifies the more physically significant model predictions based on large growth rates and consistency in length scales. The moments at which physically significant model predictions occur correspond better with field observations than the original model predictions.

The effects of pre-existing bed-forms on the development of crescentic bed patterns are investigated using a non-linear model (Morfo55, [Garnier, 2006]). Results show that pre-existing bed patterns can have significant effects, however, the finally dominant length scale, the linear growth and decay rates, and the migration rate can be accurately described by a linear stability model. Pre-existing length scales that exhibit significant linear growth will remain and undergo further development, whereas length scales that are outside the linear growth rate curve decay and give rise to a bed pattern with a bigger linear growth rate.

The conclusions drawn from the research concerning pre-existing bed patterns are applied to improve predictions linear stability model. This results in considerable improvements in the comparison of model predictions with field observations, for certain periods of time.

Acknowledgements

A PhD research project is a big undertaking, and although my name is the only one on the front of this thesis, there are many more people involved this project, who I would like to thank.

First of all I would like to thank Nick for, first of all offering me this opportunity, but mainly for his help and support. When I would come into his office, and in my enthusiasm forget to tell three quarters of my idea, he was patient and would ask again and again until the idea was clearly defined, not only for him, but also for me. I would also like to thank Daniel for his help. He was, as remote semi-supervisor, very good at explaining Morfo60 to me and my trip to Barcelona was a great experience, thanks to his hospitality.

Secondly, I would like to thank the Engineering and Physical Sciences Research Council (EPSRC) for generously funding my Ph.D. research project along with the University of Nottingham.

I would like to thank Hans, Trineke and Ansje for my home in the Netherlands. Their support and many visits made that the UK remained a bit of a holiday destination for me too!

I would also like to thank all my housemates here. But in particular Costas, Iorgos, Eleni, Cesar, Torsten and Tim: thank you for being fantastic housemates in the different places that I have called (and still call) my home here.

The usefulness of coffee-breaks and pub-visits cannot be overstated, and my office-mates are to thank for that: Thank you Karwan, Julia, Diego, Sebastian, Omar, Bruce, Dave², Jeff, Roland, Riccardo, Tom, Fangfang, Athena, Haider and Anurak. Finally, Rachel thank you so much for being such a fabulous lady!

Meinard Tiessen

Nottingham, September 24th, 2009

Contents

Abstract	ii
Acknowledgements	iv
List of Figures	x
List of Tables	xvi
1 Introduction	1
1.1 Coastal management	2
1.2 Natural beaches	4
1.3 Crescentic bed patterns	5
1.4 Understanding natural beaches	6
1.5 Linear stability analysis	7
1.6 Research goal and questions	8
1.7 Thesis outline	10
2 Morphodynamics in the nearshore zone: Background	12
2.1 Literature	12
2.1.1 The nearshore zone	12
2.1.2 Field measurements	17

2.1.3	Modelling of the nearshore zone morphology	21
2.1.4	Characteristics of crescentic bars and rip channels	24
2.1.5	In summary	30
2.2	Theoretical background	33
2.2.1	Short waves	33
2.2.2	Governing equations	36
2.2.3	Parametrisation	39
2.2.4	Dynamic unknowns	45
2.3	Stability analysis	46
2.3.1	Linear stability analysis	46
2.3.2	Non-linear stability analysis	48
2.4	Morfo60	50
2.4.1	Basic state	51
2.4.2	Perturbations	52
2.5	Morfo55	60
3	A field test of a linear stability model for crescentic bars	70
3.1	The Duck research facility	70
3.2	Field data	72
3.2.1	Wave conditions	72
3.2.2	Bathymetry	75
3.2.3	Tide	76
3.2.4	Argus images	77
3.3	Development over time	79
3.4	Relationships between input and output parameters	83

3.4.1	Wave conditions	83
3.4.2	Bed profile	86
3.4.3	Tidal variation	89
3.5	Physically significant developments algorithm	97
3.5.1	Introduction	97
3.5.2	Testing different algorithms	99
3.5.3	Comparison with field observations	109
3.6	Discussion	113
3.7	Conclusions	117
4	Non-linear analysis of pre-existing crescentic bed patterns	120
4.1	Linear compared to non-linear results	123
4.1.1	Basic state	127
4.1.2	Perturbations	128
4.2	Undisturbed evolution	135
4.3	Evolution of pre-existing bed patterns	140
4.4	Output analysis of pre-existing bed-forms	151
4.4.1	Length scale	151
4.4.2	Amplitude	153
4.4.3	Growth rate	164
4.4.4	Migration rate	173
4.5	Discussion	180
4.6	Conclusions	184
5	Pre-existing bed patterns in a linear stability model	186

5.1	Assumptions of the pre-existing algorithm	186
5.2	Comparison with field observations	192
5.3	Discussion	200
5.4	Conclusions	204
6	Conclusions and recommendations	206
6.1	Answers to research questions	206
6.2	Conclusion	210
6.3	Recommendations for further research	211
6.3.1	Comparison of linear model predictions with reality	211
6.3.2	Comparison of a time-domain model with reality	214
6.3.3	Shoreface nourishments	214
	Bibliography	216

List of Figures

1.1	(a) Warning for the dangers of rip currents. (b) Coastal erosion at Happisburgh, UK.	2
1.2	The dissipative and reflective beach state.	4
1.3	The crescentic bed pattern.	5
2.1	The formation of rip currents under (a) normal, and (b) oblique wave incidence [The Open University, 1989].	15
2.2	Crescentic and transverse bed patterns at Duck, North Carolina, USA.	16
2.3	The coordinate system for (a) normal, and (b) oblique wave incidence, applied to describe the nearshore dynamics [originally from Garnier, 2006].	35
2.4	An example of the linear and Feddersen et al. [2000] friction distribution.	41
2.5	An example of the Thornton and Guza [1983] and Church and Thornton [1993] dissipation rate distribution.	43
2.6	The Morfo60 distribution of different basic state variables.	50
2.7	The growth rate and migration rate curve according to Morfo60.	53

2.8	The effect of the inclusion of perturbed effects of refraction over the current and the depth perturbation terms on the growth rate curve.	55
2.9	The Morfo60 distribution of different perturbation variables.	56
2.10	Alongshore and cross shore distribution of the Morfo60 output.	57
2.11	A numerical analogue of a Dirac-delta function with an amplitude of 3 cm, applied to excite all frequencies to the same extent.	62
2.12	Analysis of the bed evolution according to Morfo55.	65
2.13	Fourier analysis of the bed evolution according to Morfo55.	67
3.1	The Duck research facility.	71
3.2	The wave conditions recorded during the two month observation period.	72
3.3	The nearshore bathymetry at Duck at August 12 th 1998.	74
3.4	The evolution of the bathymetry over 1998.	74
3.5	The tidal variation at Duck during the observation period.	76
3.6	Argus imaging at Duck.	77
3.7	Input and output of the various runs of Morfo60 describing the two month observation period at Duck.	80
3.8	The accumulated growth ($\sum \omega_r \Delta t$) for each wave number ($k_{FGM} = \frac{2\pi}{\lambda_{FGM}}$) for all model predictions during the observation period.	82
3.9	The distribution of the recorded wave conditions and model predictions.	84
3.10	The different wave energy distributions for different bed profiles.	87
3.11	The growth rate (ω_r [1/d]) as a function of the wave number (k [rad/m]) for different bed profiles.	87

3.12	The wave energy distribution for different tidal levels.	90
3.13	The growth rate as a function of the wave number for different tidal levels.	91
3.14	The effects of different tidal levels on the <i>FGM</i> for different wave conditions.	93
3.15	Output analysis of the Morfo60 results of Duck as a result of tidal variation.	95
3.16	The <i>PSD</i> algorithm results in time for case 1.	102
3.17	The accumulated growth captured by the <i>PSD</i> algorithm for case 1.	103
3.18	The <i>PSD</i> algorithm results in time for case 2.	105
3.19	The accumulated growth captured by the <i>PSD</i> algorithm for case 2.	105
3.20	The <i>PSD</i> algorithm results in time for case 3.	107
3.21	The accumulated growth captured by the <i>PSD</i> algorithm for case 3.	108
3.22	Comparison between the original and <i>PSD</i> length scale predictions, and what is observed in the field.	109
3.23	The post-storm evolution of the crescentic bed pattern length according to the <i>PSD</i> algorithm.	110
4.1	A crescentic bed pattern breaks up.	120
4.2	A comparison between the basic state profiles of Morfo55 and Morfo60.	126
4.3	A comparison between the growth rate curves of Morfo55 and Morfo60.	128
4.4	A comparison between the migration rate curves of Morfo55 and Morfo60.	131
4.5	A comparison between the perturbation profiles of Morfo55 and Morfo60.	132

4.6	The evolution of the bed under normal wave incidence.	136
4.7	The evolution of the bed under oblique wave incidence.	137
4.8	The growth rate curves for both normal and oblique wave incidence.	139
4.9	The migration rate curve for oblique wave incidence.	139
4.10	The evolution of the bed under normal wave incidence when long pre-existing bed patterns are implemented.	140
4.11	The evolution under normal wave incidence of the bed when short pre-existing bed patterns are implemented.	143
4.12	The evolution under normal wave incidence of the nearshore seabed when the pre-existing bed patterns have a length scale that is close to the optimum length scale in the undisturbed development.	144
4.13	Examples of the evolution of the nearshore seabed when pre-existing bed patterns are implemented, under oblique wave incidence.	145
4.14	The evolution of the nearshore bed under various pre-existing bed pattern length scales and amplitudes, for normal wave incidence.	146
4.15	The evolution of the nearshore bed under various pre-existing bed pattern length scales and amplitudes, for oblique wave incidence.	149
4.16	An example of the development of the amplitude of crescentic bed patterns, when bed patterns pre-exist.	153
4.17	Amplitude characteristics of the bed pattern evolution for different pre-existing amplitudes.	156
4.18	Characteristic moment during the bed pattern evolution for differ- ent pre-existing conditions.	158
4.19	The minimum amplitudes for different pre-existing conditions.	161

4.20	The final amplitude for different pre-existing conditions.	163
4.21	An example of the development of the linear growth rate of crescentic bed patterns, when bed patterns pre-exist.	165
4.22	Growth rate characteristics of the bed pattern evolution for different pre-existing amplitudes.	167
4.23	The linear growth and decay rate of the initially dominant mode, for different pre-existing conditions.	168
4.24	The linear growth rate of the finally dominant mode, for different pre-existing conditions.	172
4.25	An example of the migration rate of crescentic bed patterns, when bed patterns pre-exist.	174
4.26	The migration rate of the pre-existing and the finally dominant bed-forms for various initial amplitudes.	175
4.27	The migration rate of the initially dominant mode, for different pre-existing conditions.	176
4.28	The migration rate of the finally dominant mode, for different pre-existing conditions.	178
5.1	Extrapolation of the growth rate curve.	188
5.2	The amplitude development in time according to consecutive growth rate curve predictions.	190
5.3	Comparison of the <i>PEB</i> algorithm output with field observations.	193
5.4	Implementation of pre-existing bedforms in the <i>PEB</i> algorithm, after the second storm at Duck.	194

5.5	The dominant bed pattern characteristics in time, according to the <i>PEB</i> algorithm.	195
5.6	The development in time of the original, <i>PSD</i> and <i>PEB</i> length scale predictions, and what is being observed in the field.	196
5.7	Comparison between the original, <i>PSD</i> and <i>PEB</i> length scale predictions, and what is being observed in the field.	197

List of Tables

2.1	Model set-up for a linear and a non-linear stability analysis.	49
2.2	Settings used in the linear stability analysis Morfo60.	59
2.3	Settings used in the non-linear model Morfo55.	64
3.1	The characteristics of the <i>PSD</i> algorithm for the three different cases.	100
4.1	The initial and finally dominant length scales for normal and oblique wave incidence, as well as the factor by which the number of bed- forms along a certain beach width increases.	152

Chapter 1

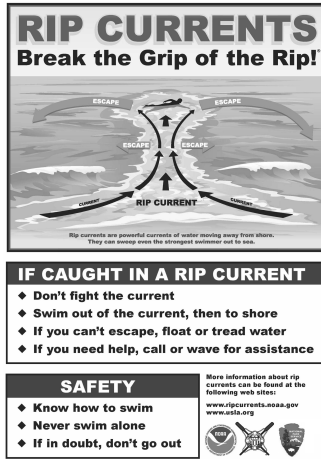
Introduction

Norfolk village being swallowed by the sea, The Independent, 2008
'Happisburgh's sea defences built in 1959 have crumbled away'

Erosion threat to protect sites, The Times, 2006
'Britain is going to have to learn to let go of certain places due to climate change'

Stark warning on Britain's shrinking coast, The Independent, 2008
'Stretches of Britain's coastline are doomed due to the rising sea and plans will soon have to be drawn up to evacuate people from the most threatened areas'

Living on the edge, The Guardian, 2006
'About 1,062,000 flats and houses, 82,000 businesses, 2.5 million people and 2 million acres of agricultural land, worth about £120 billion in all, are at risk from flooding and erosion brought on by global sea level rise'



(a)



(b)

Figure 1.1: (a) Warning for the dangers of rip currents. (b) Coastal erosion at Happisburgh, UK.

1.1 Coastal management

Sea level rise combined with the increasing severity of storms make research concerning the evolution of beaches and the nearshore region of great importance, not only to coastal engineers but also to the millions of people living, working and holidaying in coastal areas (see Fig. 1.1(a), [<http://ripcurrents.noaa.gov>]).

Coastal defences form the defence against storms, flooding and coastal erosion. However, current coastal defences in the UK were designed with 'yesterdays' storms and sea levels in mind. Ever increasing impacts of human presence in coastal areas (see Fig. 1.1(b), [<http://www.happisburgh.co.uk>]), crumbling defences and expected increase in severity of storms, combined with sea level rise due to global warming, will cause more and more challenges in coastal management [Dodson, 2009].

The management of the coastal zone is aimed at avoiding flooding and erosion and, where appropriate, creating pleasurable and safe environments for recreation.

Along with the seabed, beaches and coastal defence structures, waves, tides and currents form an interactive system that changes on wide-ranging spatial and temporal scales.

Hard defences such as sea walls and groins can form a final line of defence against floodings as well as reducing beach erosion. However, hard defences not only reduce possibilities for recreation, they can also cause negative effects down the coast and locally, by impairing the natural beach evolution. For example, groins block alongshore currents, trapping sediment at the location of the groins, but causing increased erosion downstream of the groined beach. Sea walls form a hard structure blocking storm waves from eating away dunes. However, because the sediment exchange between the beach and dune systems is disrupted, sea walls can actually cause beach erosion, as happened at the stretch of beach between Winterton and Happisburgh [Environment Agency, 2008].

Consequently, recent developments in coastal management are more orientated towards maintaining the natural beach evolution. Soft defences, such as beach nourishments, are a common practice in many countries [Hamm et al., 2002; Hanson et al., 2002], whilst shoreface nourishments form a new cheaper solution to mitigate beach erosion [Grunnet and Ruessink, 2005; Klein, 2006]. Both soft coastal management solutions involve the deposition of sand to compensate for coastal erosion and improve the protection of the coastline against the impact of storms. Where hard defences attempt to reduce natural beach evolution, soft defences only attempt to mitigate its impact with respect to coastal defence and

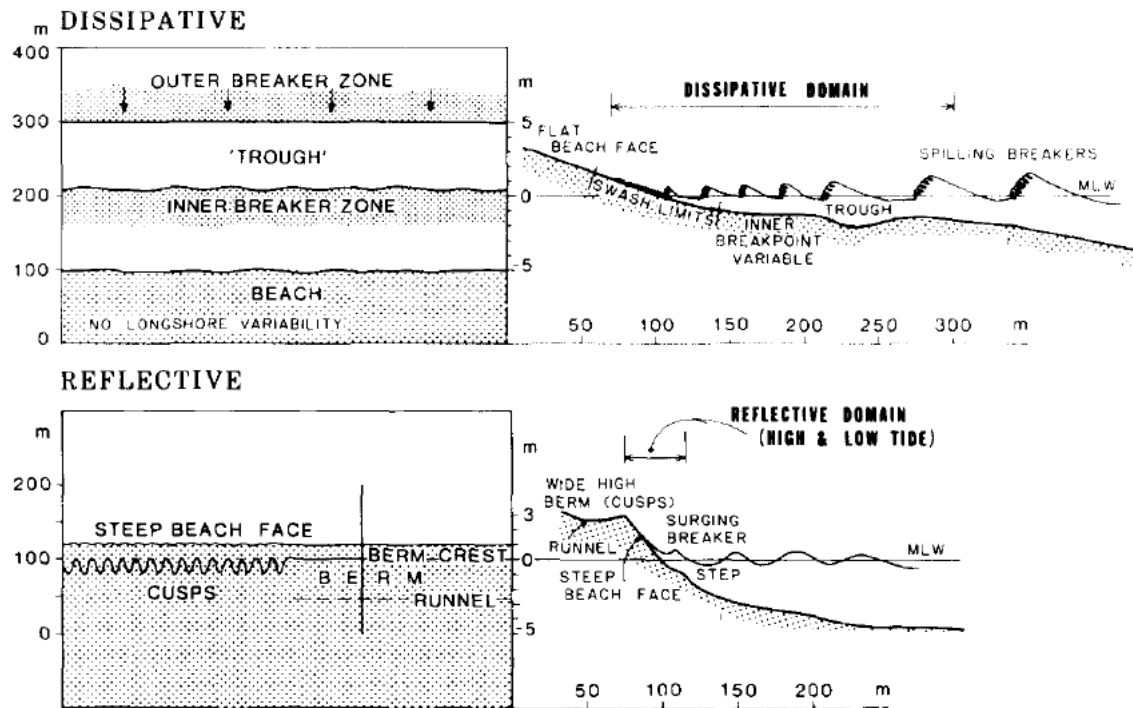


Figure 1.2: A schematic description of the dissipative and reflective beach state [adopted from Wright and Short, 1984].

recreational purposes.

1.2 Natural beaches

Natural undisturbed sandy beaches generally show non-uniform cross shore beach profiles. A natural beach can be divided into different beach states as a result of different forcing conditions: From a shallow highly dissipative beach, occurring generally during winter storms to a steep, fully reflective beach generally composed of coarse material. In between both extreme beach states, a wide range of different beach states is observed: Moderately dissipative beaches will develop an offshore bar that shows rhythmic bed patterns, such as transverse or crescentic bars, al-

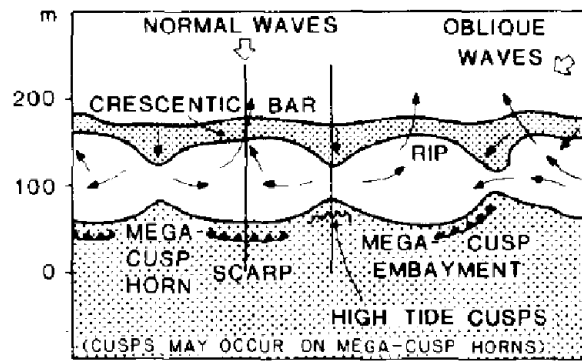


Figure 1.3: A schematic description of the crescentic bed pattern and the corresponding water circulation [adopted from Wright and Short, 1984].

though transverse bars are more commonly observed closer to the shoreline. More reflective beaches generally develop a (tidal) terrace closer to the shore, along with ridge and runnel circulation patterns and beach cusps [Wright and Short, 1984]. Natural beaches form an interactive and dynamic system with tides, currents, and waves [Wright et al., 1986]. Different bed patterns, such as beach cusps and crescentic bed patterns develop under different forcing conditions [Blondeaux, 2001]. Changing wave and tidal circumstances therefore result in changing beach states and bed patterns [van Enckevort et al., 2004].

1.3 Crescentic bed patterns

A widely occurring bed pattern in front of sandy beaches is the crescentic bar [van Enckevort et al., 2004] (see Fig. 1.3). Many beaches around the world display alongshore bars at a certain distance from the beach [van Enckevort and Ruessink, 2003b]. Under certain conditions, these bars will deform into lunate shaped bed-forms along a beach, called crescentic bars, with length scales varying

from 30 to 3000 m [Blondeaux, 2001]. The existence of crescentic bed patterns has been shown to correspond with water circulation cells [Fredsoe and Deigaard, 1992]. Water moves onshore on the crest of the crescentic bed patterns, and offshore in the shoals. The offshore water motion, called rip currents, represents a danger for bathers (see Fig. 1.1(a)). Both rip currents and crescentic bed patterns interact with nourishments, and for the successful application of nourishments, the ability to make predictions of the development of crescentic bed-forms and rip currents, with a reasonable degree of accuracy and within limited periods of time is therefore of significant importance.

1.4 Understanding natural beaches

For the successful application of coastal defences, understanding of the natural behaviour of beaches is necessary [Ojeda et al., 2008]. The processes behind the behaviour of natural beaches have been investigated over the last decades. Field measurement techniques, such as Argus imaging [Lippmann and Holman, 1989], have greatly expanded the knowledge concerning the occurrence of bed patterns. Further, a wide range of modelling techniques have been applied to the study of natural beach behaviour: From empirical formulations to describe specific processes [eg. Plant et al., 2006]; the description of the development of bed patterns due to forcing templates [eg. Bowen and Inman, 1971] or free instabilities [eg. Falqués et al., 2000]; to full time-domain models describing actual beach locations with a high degree of accuracy [eg. Klein and Schuttelaars, 2006]. Each type of model furthers the understanding of the dynamics of the nearshore bed evolution

with regards to hydrodynamic conditions. Empirical models tend to focus on relating different measured quantities with each other, while models based on the Newtonian equations attempt to describe the evolution of the seabed as a result of physical relationships.

1.5 Linear stability analysis

An example of a model based on physical relationships is the linear stability analysis, which investigates whether, for example, an alongshore uniform shoreline is stable, or whether crescentic bed patterns would develop under certain forcing conditions. This type of model needs less calculation time and input data to produce a prediction for the development of the nearshore seabed than traditional time-domain models. However, such a model assumes alongshore constant conditions and can only describe the initial development of bed patterns. Until now, both limitations have restricted the use of this type of model mainly to the investigation of the effects of different physical processes and model settings on the development of crescentic bed patterns. Despite these limitations, comparisons of linear stability analysis results with field data have shown similar crescentic bed pattern characteristics [Deigaard et al., 1999; Falqués et al., 2000; Calvete et al., 2005; van Leeuwen et al., 2006].

Linear stability models have the potential for providing useful information to engineers. They not only provide information concerning the likelihood of developing bed patterns (and accompanied rip channels), but can also give insight into

the length scale of emerging bed-forms and the time over which they are likely to develop. Additionally, they can provide information concerning the migration rates of bed-forms. In a quasi-alongshore uniform coast this information informs the engineer of how likely crescentic bed patterns and rip currents are to form, and their approximate alongshore spacing - information which is very useful for assessing bather safety and beach erosion. Both of these aspects also impact on shoreface nourishment projects, in that shoreface nourishments have the potential to develop into, or trigger rip current systems. This information can, moreover, be provided in very small computational times and with limited data input, compared to traditional time-domain models.

To date, a comprehensive comparison of this type of model prediction with a large number of field observations has not been carried out, but could show the extent to which a linear stability analysis can accurately describe the development of crescentic bed patterns and rip spacings. Such a study is carried out in the research presented in this thesis. In order to do so, actual field data from a specific site is compared with linear stability model predictions of the development of crescentic bed patterns under the same wave, tidal and topographical circumstances.

1.6 Research goal and questions

This research presents a study of the capabilities of a linear stability model in predicting crescentic bed pattern developments through direct comparison with field observations. The objective is to examine whether a linear stability analysis can

generate similar bed pattern predictions as are observed in reality, under the same circumstances. The model used is Morfo60 [Calvete et al., 2005] and the observed data are from the USACE Field Research Facility in Duck, North Carolina, USA, during a two month period in 1998, this data has previously been analysed by van Enckevort et al. [2004].

The main research questions are formulated as follows:

- **How capable is a linear stability analysis in describing the observed development of crescentic bed patterns under variable wave forcing?**

A direct comparison of Argus field observations of the development of crescentic bed patterns, with model predictions made by the linear stability model Morfo60, using wave, tidal and bathymetric conditions as they were measured during the observation period.

- **Can current understanding of the development of crescentic bars be applied to improve the implementation of linear stability analysis predictions?**

Development of an algorithm to overcome limitations inherent to linear stability models. This algorithm is tested for the Duck site comparison to examine the extent to which it can improve the predictive skills of linear stability analysis in describing the actual development of crescentic bed patterns.

- **How do pre-existing crescentic bed patterns interfere with the development of crescentic bed patterns?**

A non-linear stability model is used to investigate the implications of assuming an alongshore constant beach profile in the linear stability model.

- **To what extent can a linear stability analysis be of use in describing the development of crescentic bed patterns, when crescentic bed-forms already exist?**

Conclusions drawn from the previous research question are applied on the Duck site comparison of linear stability analysis results with field observations.

1.7 Thesis outline

Chapter 2: *Morphodynamics in the nearshore zone: Background*

An overview of current and past research in the field of modelling and observing nearshore morphodynamics. Secondly, a description of the physics involved in nearshore coastal dynamics. Finally, a description of the modelling techniques used in this research is presented.

Chapter 3: *A field test of a linear stability model for crescentic bars*

A comparison between the linear stability model results created using the wide variety of input data from Duck and field observations is presented. An analysis of the effects of input parameters on the model predictions, including a more thorough sensitivity analysis of the effects of beach evolution and tidal variation on the crescentic bed pattern characteristics is given. The development of an algorithm to emphasise the more physically significant model predictions is described and a

direct comparison of field observations with the model predictions and physically significant developments is presented.

Chapter 4: *Non-linear analysis of pre-existing crescentic bed patterns*

A brief comparison of the linear and non-linear stability model results is presented. The effects of pre-existing bed patterns on the development of crescentic bed patterns is examined using a non-linear stability model.

Chapter 5: *Pre-existing bed patterns in a linear stability model*

Knowledge obtained from the research concerning pre-existing crescentic bed patterns is applied to the interpretation of the linear results for the Duck site in order to establish to what extent this can improve the comparison with field observations.

Chapter 6: *Conclusions and recommendations*

Presentation of the answers to research questions posed. Finally, an overview of possible research topics that lead from this PhD research is given.

Chapter 2

Morphodynamics in the nearshore zone: Background

2.1 Literature

In this section an overview of the more recent publications concerning the development of crescentic bed patterns will be presented. The section is divided into four parts; firstly an introduction of the nearshore zone is given, presenting a description of various terms. Secondly a brief look at field observations and measurements of processes and bed-forms is presented. Then a description of the mathematical models used to describe these processes is given. Finally, characteristics of crescentic bed patterns are discussed.

2.1.1 The nearshore zone

As water depth decreases, waves propagating towards a shore start to sense the bed and the orbital particle motion underneath a wave becomes increasingly hori-

zontal [Svendsen, 2006]. When the wave height and the water depth are of similar order, wave breaking can occur [Mei, 1989]. The location where waves first start to break is called the **breaker line**, dividing the **shoaling zone** (offshore of the breaker line) from the surf zone [Mei, 1989]. The **surf zone** can be defined in general terms, as the region where waves are breaking and extends from the dry beach to the seaward limit of breaking, or the breaking line [Dean and Dalrymple, 1984]. However, variable wave conditions mean that wave breaking on real beaches is not constantly occurring at the same location. Furthermore, tidal variation and wave run-up create an area at the beach that is only submerged for certain periods of time. It is, therefore, more realistic to define the surf zone as the area of the beach that is always submerged, with the offshore boundary at the alongshore bar crest (where wave breaking generally occurs during most wave conditions).

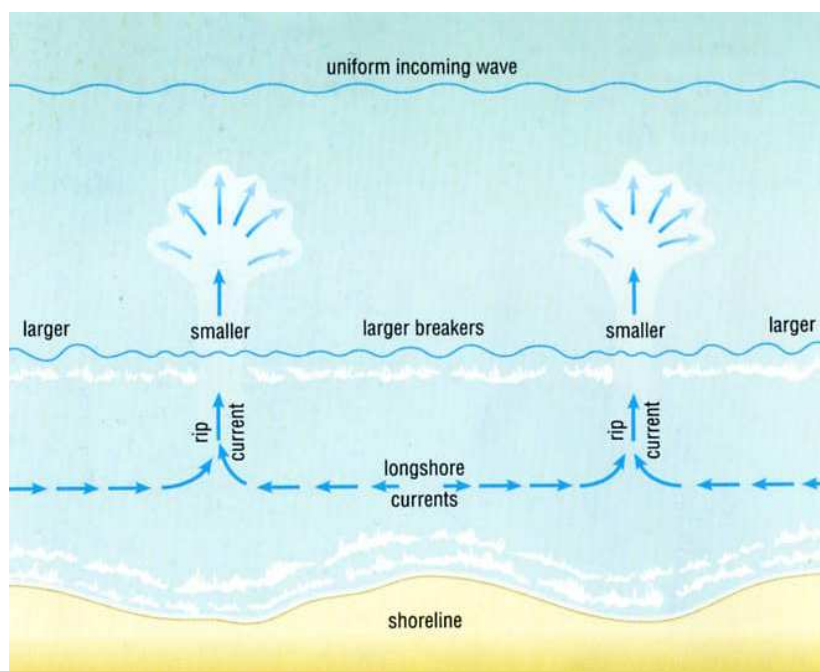
The surf zone is the area where wave energy is converted to turbulence and heat [Fredsoe and Deigaard, 1992]. Wave energy dissipation gives rise to the formation of currents, due to **radiation stresses**. Longuet-Higgins and Stewart [1964] describe radiation stresses as 'the excess flow of momentum due to the presence of waves'. In front of many beaches, the water motion shows horizontal **circulation patterns** in and out of the surf zone. Waves approaching the shore at an oblique angle can result in dominant water motion along the beach, the **alongshore current**. Both circulation patterns and the alongshore current are well documented in front of many beaches [Fredsoe and Deigaard, 1992; Bowen and Inman, 1969].

Beaches generally do not have a constant beach slope, since the wave climate of-

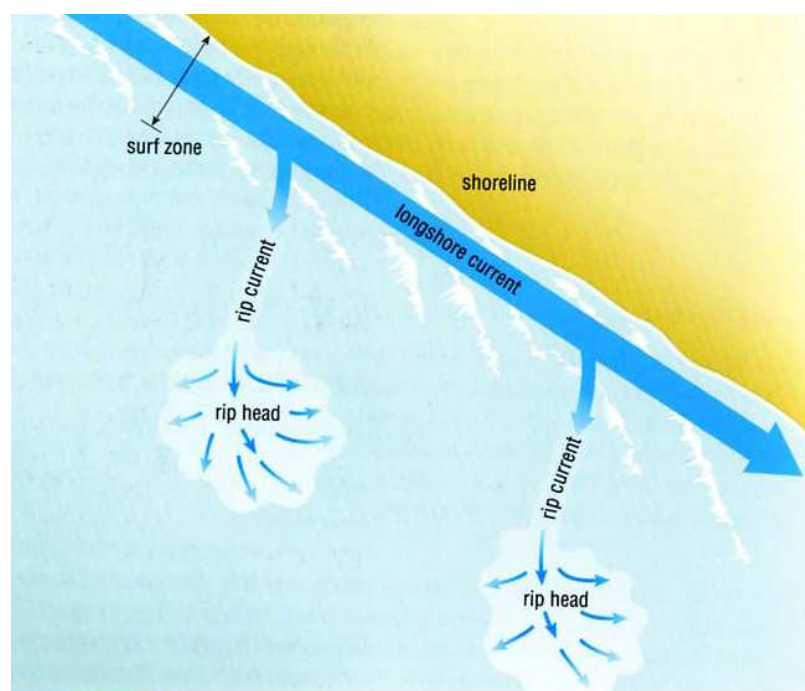
ten results in **alongshore bars** and terraces being formed [Fredsoe and Deigaard, 1992]. A range of different factors give rise to various beach states. The two extreme beach states are the dissipative and reflective beach [Wright and Short, 1984]. **Dissipative beaches** are very mild sloping beaches with several along-shore bars at different distances from the shore, which are generally associated with spilling breakers. This form of wave breaking results in a continual decrease in wave height, while the wave propagates forward [Sorensen, 1993]. Highly **reflective beaches** show, on the other hand, very steep beach faces, with a constant beach slope. The type of wave breaking, in this case, is more likely to be surging, which is progressing towards a standing or reflecting wave [Sorensen, 1993].

In between both extremes, a range of different beach states and breaker types are observed. Where the two extreme beach states are generally uniform along the shore in the surf zone, the intermediate beach states show a wide range of three dimensional bed-forms [Wright and Short, 1984]. These bed-forms generally occur in combination with flow patterns and interact with both waves and currents. The flow patterns can give rise to **rip currents** (see Fig. 2.1), which are strong offshore-directed currents that form inside the surf zone, and flow through a trough between surf zone bed-forms out of the surf and into the shoaling zone. [Wright and Short, 1984]

A moderately dissipative beach will show one or more alongshore bars that can deform into crescentic bed-forms under the right forcing conditions [Wright and Short, 1984]. A **crescentic bar** (see Fig. 2.2(a)) is a rhythmic lunate shaped



(a)



(b)

Figure 2.1: The formation of rip currents under (a) normal, and (b) oblique wave incidence [The Open University, 1989].



(a)



(b)

Figure 2.2: (a) Crescentic bed patterns at Duck, North Carolina, USA. The bar pattern shows up as a white band in the Argus image. [Dodd et al., 2003].
(b) Transverse bed patterns at Duck. [Konicki and Holman, 2000].

bed-form that forms out of an alongshore constant bar, during moderate wave conditions [Blondeaux, 2001]. A less dissipative beach will generally give rise to the development of **transverse bars** (see Fig. 2.2(b)). These bed-forms run perpendicularly or obliquely from a bar or beach into the sea [Konicki and Holman, 2000] and are separated by rip currents [MacMahan et al., 2005]. The **ridge and runnel system** combines a dissipative tidal berm in combination with a reflective beach. **Beach cusps** can be found at reflective beaches and develop due to the run up and backwash of waves [Inman and Guza, 1982]. However, many intermediate beach states also locally display a reflective beach profile at the swash zone, giving rise to beach cusps. **Mega cusps** result from the water motion circulation pattern originating from surf zone bed-forms, such as crescentic bars. These bed-forms generally mirror offshore bed-forms in length [Wright and Short, 1984].

2.1.2 Field measurements

Many techniques exist to monitor the nearshore zone and surf zone processes, from probing techniques to determine the bed level, and pressure gauges to determine wave characteristics, to remote imaging techniques determining the location of offshore bed-forms. In the past, elaborate techniques were employed to obtain quantitative information of nearshore processes. The seabed level was measured using echo sounding and physical probing techniques [Wright and Short, 1984], while waves and currents were monitored using visual observations and drifters [MacMahan et al., 2007]. Pressure gauges could give information about the wave field [van Enckevort et al., 2004], and velocity sensors were used to measure the

surf zone water circulation patterns [Wright et al., 1979]. Additionally, physical reproductions of the surf zone in laboratories provided a means of studying specific processes and investigating the development of certain bed-forms under idealised circumstances [Bowen and Inman, 1969]. However, scaling problems and a difference in the representation of processes in a 2D and 3D laboratory environment complicate the application of this knowledge to real scenarios [Kamphuis, 1995].

The current state of field data collection incorporates these techniques but also enables researchers to analyse surf zone dynamics remotely from the shore. Lidar, Radar and improved photographic image processing techniques reveal nearshore processes, the development of bed-forms, and erosion and accretion patterns at the beach [van Enckevort et al., 2004; Holman and Stanley, 2007; Thornton et al., 2007]. In particular, the introduction of the Argus imaging technique by Lippmann and Holman [1989] greatly expanded the quantitative and qualitative database available to coastal researchers. Prior to this, bathymetric measurements were cumbersome and labour intensive to obtain. The Argus imaging technique [Lippmann and Holman, 1989] (discussed in section 3.2.4) can provide highly detailed and very frequent information about the changing bathymetry and is applied extensively [Holman and Stanley, 2007]. Initially, Argus was mainly used to reveal the bar crest position along a stretch of beach [van Enckevort et al., 2004]. Recently, however, this technique has also been applied to the study of other processes. For example, the swash beach morphology can be examined due to images of the variable shoreline positions under different tidal levels, while wave conditions can be observed by sampling intensity variations over a number of wave periods

[Holman and Stanley, 2007]. Alongshore current velocities can also be observed in Argus images, by measuring the drift of foam inside the surf zone [Chickadel et al., 2003].

The numerous techniques used in the monitoring of the nearshore zone and bed-forms have resulted in a range of processes and bathymetries being documented. Different beach states were described by Wright and Short [1984] and also observed on the Australian Gold Coast [Wright et al., 1986]. Field observations as well as reproduction of rip currents and circulation patterns under laboratory circumstances were presented by Bowen [1969]. An extensive description of field observations prior to the Argus imaging technique is presented by Komar and Holman [1986], where both beach cusps and crescentic bars are reported in combination with rip currents and beach erosion. Recently, remote data collection expanded the data available to researchers enormously. Wide ranging beach states were observed, as well as transitions between the different beach states due to seasonal changes in the wave climate [Lafon et al., 2005; Castelle et al., 2007]. Rip currents and circulation patterns spanning the different beach states, resulting in the development of different bed-forms, have been widely reported [van Enckevort and Ruessink, 2003a; van Enckevort et al., 2004; Castelle et al., 2007].

The relationship between field observations and wave conditions has shown that during storms, most three dimensional bed-forms, such as transverse and crescentic bars, are removed, and only alongshore constant bars persist [van Enckevort et al., 2004; Lafon et al., 2005; Ribas and Kroon, 2007]. However, the alongshore bar itself

can also migrate as a result of various wave conditions. Offshore bar migration has been observed extensively during high wave conditions, while shoreward migration generally corresponds to mild wave conditions [Wright et al., 1986; Plant et al., 1999; Pope et al., 2007]. Different bed patterns evolve under different forcing circumstances. Crescentic bed-forms develop during moderate wave conditions [van Enckevort et al., 2004], while transverse bars generally develop under milder wave conditions [Ribas and Kroon, 2007]. The angle at which waves approach the shore is of importance for the formation of either bed-form. Crescentic bed-forms generally develop at normal and near normal wave angles, with increased bed pattern lengths for oblique wave angles. Transverse bars evolve only when waves approach the shore at an oblique angle, and disappear when the waves approach the shore perpendicular to the coast [Ribas and Kroon, 2007].

It is common that beaches show a combination of bed-forms, either in sequence or simultaneously. Over time, variable forcing conditions can cause different bed-forms to develop. However, several bed-forms can also occur at the same time and location. Beaches can show both a transverse bar profile at the beach or nearshore bar, and crescentic bed-forms at the offshore bar, [for instance: Castelle et al., 2007]. Double-barred systems can even show two systems of crescentic bed-forms that can show coupled or non-coupled behaviour, depending on the significance of the bed-forms, the size of the circulation patterns [Ruessink et al., 2007] and the forcing conditions [Castelle et al., 2007].

2.1.3 Modelling of the nearshore zone morphology

Observations of morphodynamics and coastal processes are not the only type of research carried out to further the understanding of coastal processes. Mathematical modelling techniques were developed in order to understand the formation of bed patterns as well as to analyse relationships between different processes. Two main types exist for the analysis of the development of morpho- and hydrodynamics in the coastal zone.

Empirical models describe a certain characteristic as a result of certain input parameters, without including the physical processes involved. This type of modelling technique consists of a function that is aimed to fit the data. An example of this is presented by Plant et al. [1999], where a relationship between wave height and bar position is investigated. This model was later extended, to include the sinuosity of the alongshore bar into the analysis [Plant et al., 2006].

A second type of model, the **process based model** uses the physical (Newtonian) equations to describe coastal processes. This model can use survey data as input to physical equations to describe wave transformation, water motion, and sediment transport in an attempt to describe the resulting physical processes as erosion and accretion. It can also be used to describe the formation of rip currents and bed-forms as well as to investigate more idealised circumstances [Fredsoe and Deigaard, 1992]. A more comprehensive description of this modelling technique will be presented in section 2.2.

In the past, it was assumed that circulation patterns and bed-forms in the nearshore zone were the result of a forcing template in the wave conditions. For example, the theory of **edge waves** describes fluctuations in the free surface elevation due to the release of long wave group energy, when short waves break as the driving force for the development of water circulation patterns and bed-forms [Fredsoe and Deigaard, 1992]. This theory has been described by many authors, and several attempts are made to relate edge waves with the formation of bed-forms and circulation processes [Bowen, 1969; Wright and Short, 1984; Wright et al., 1986]. Current understanding suggests, however, that the driving force behind the formation of bed-forms in the surf zone and the accompanying circulation patterns is due to the evolution of free instabilities in the coastal system [Hino, 1974]. **Self-organisation** of waves, currents, erosion and accretion gives rise to the development of a wide range of bed-forms, depending on the local conditions [Coco and Murray, 2007]. Initially, this modelling technique was mainly used to describe nearshore circulation patterns and shear waves [Bowen and Holman, 1989; Dodd and Thornton, 1990; Falqués and Iranzo, 1994]. Recently however, this type of model has been used extensively for research concerning the formation and evolution of surf zone bed-forms [see Blondeaux, 2001; Dodd et al., 2003; Coco and Murray, 2007; Falqués et al., 2008, for several reviews on this topic].

Within the range of process-based models, different types of modelling techniques exist. A **full time-domain model** describes the temporal evolution of the nearshore zone and can use wave, tide and bathymetric data from a specific field location to describe the temporal evolution of this beach and surf zone with a high

level of accuracy. This type of model is even able to investigate the effects of human interference, such as shoreface nourishments [Grunnet et al., 2004]. However, this modelling technique also has limitations. The predictive skills of the model are closely linked with the amount and quality of field measurements that can be implemented into the model. Secondly, the elaborate equations make model predictions time consuming and challenging to obtain [Garnier, 2006; Klein, 2006].

Alternatively, process-based models can be used to describe more idealised circumstances to investigate the occurrence of quasi-rhythmic features and other phenomena and are used to understand the physics behind these phenomena. This modelling technique is called a **stability analysis**, where the stability of the bed and water motions in the surf zone are investigated under certain forcing circumstances. If circulation patterns arise and bed patterns start to develop, the system is called unstable [Deigaard et al., 1999]. This modelling technique is a useful tool to investigate the driving forces behind the evolution of different bed-forms and has been applied in the description of crescentic bars, transverse bars, rip currents, cusped features and circulation patterns [eg. Blondeaux, 2001; Dodd et al., 2003]. This modelling technique can be split into two different analyses: the **linear stability analysis**, which only describes the initial development of instabilities, and the **non-linear stability analysis**, which describes the long term evolution of instabilities.

A linear stability analysis only uses a limited part of the modelling equations to give insight into the initial development of perturbations such as crescentic

bars. In this type of model only the linear terms concerning the perturbations are included in the equations. Such a model can, therefore, only describe the initial development of perturbations, since for very small perturbations the influence of the non-linear terms is assumed to be negligible [eg. Dodd et al., 2003].

A non-linear stability analysis can describe the evolution of bed-forms and circulation patterns as they arise from an undisturbed initial situation, using the full non-linear equations. This model can be a full time-domain model, used to analyse specific settings and conditions. For instance, Delft3D is used to describe the physical circumstances at Terschelling by Grunnet et al. [2004], but also to investigate to what extent various hydrodynamic circumstances influence the development of bed perturbations [Smit et al., 2008]. This model can give information concerning the long term development of bed-forms and flow patterns, however, it is also more time consuming and more prone to develop numerical instabilities than a linear stability analysis [Garnier, 2006].

Finally, a **weakly non-linear stability analysis** incorporates linear stability techniques, but attempts to mitigate its limitations. First a linear stability analysis is used to determine the initial growth rate, and then incorporates non-linear terms to describe the evolution of the bed using terms of the Ginzburg-Landau equation [Schielen et al., 1993].

2.1.4 Characteristics of crescentic bars and rip channels

In the last decade, work on understanding the physics of the formation of morphodynamical features such as crescentic bed patterns has yielded insights into

the growth and kinematics of these bed-forms. Stability analyses, in particular, have furthered our understanding of these bed patterns, which result from the interaction between waves, currents and beach morphology.

Stability analyses predict emerging bed patterns with similar length scales to those observed in reality. Deigaard et al. [1999], Damgaard et al. [2002], and Calvete et al. [2005] show that the alongshore wavelength of bed patterns is between 50 and 1000 m. Field observations show a similar range of observed length scales [van Enkevort et al., 2004; Blondeaux, 2001], but spacings are generally between 200 and 500 m [Komar and Holman, 1986]. Lafon et al. [2005] suggests a slight negative correlation between wave height and length scale of the bed-forms in their observations of Truc Vert beach in France. However, van Enkevort et al. [2004] observe the opposite at Duck (USA), Miyazaki (Japan) and the Gold Coast (Australia)

Under constant wave conditions, the formation time of crescentic bed patterns is about 1 to 3 days [Falqués et al., 2008], but under changing wave conditions the development of crescentic bed patterns can take up to 3 weeks [van Enkevort et al., 2004]. Tidal variation can also slow down the development of crescentic bars significantly [Castelle et al., 2007]. The growth rates of crescentic bed patterns in stability analyses vary, but growth rates that are similar to field observations are presented by Deigaard et al. [1999], Falqués et al. [2000], Calvete et al. [2005], Klein and Schuttelaars [2006], Dronen and Deigaard [2007] and Smit et al. [2008].

While the overall migration of crescentic bed patterns along the coastline is small over several days due to changing wave conditions [Lafon et al., 2005; Turner et al., 2007], observed daily migration rates can be as big as 180 m/day [van Enckevort and Ruessink, 2003b]. Generally, however, migration rates are in the order of tens of metres a day [Falqués et al., 2008] and similar migration rates are predicted by stability analyses [Deigaard et al., 1999; Dronen and Deigaard, 2007; Falqués et al., 2008].

A comparison between a linear stability analysis and a full time-domain model was presented by Damgaard et al. [2002], showing that similar length scales can be obtained. Klein and Schuttelaars [2006] showed that either model predicted the initial formation of similar crescentic bed pattern spacings, at double-barred beaches. Further, the initial growth predicted by the non-linear model corresponded with the linear growth rate.

Linear stability models have been used in previous studies to examine the physics behind the development of crescentic bed patterns. The coupling between the developing topography and the flow was first presented by Deigaard et al. [1999], while the 'bed-surf' coupling and the influence of different stirring functions was studied by Falqués et al. [2000]. This research showed that the ratio of stirring function (α) and the water depth (D) is important for the determination of which bed pattern will develop. The stirring function describes the tendency of the waves to mobilise sediment. Transverse bars develop for a stirring function which is constant over depth, in other words $\frac{\alpha}{D}$ decreases offshore. Crescentic bed

patterns would develop if the stirring function is increasing offshore in the surf zone.

Stability analyses have also been used to investigate the sensitivity of bed pattern formation to physical parameters. The effect of different wave conditions was examined using a linear stability analysis by Deigaard et al. [1999], Calvete et al. [2005] and Ribas et al. [2003]. Calvete et al. [2005] showed that length scales and growth rates increase for increasing wave heights, while increased wave angles result in increased length scales, but decreased growth rates. Deigaard et al. [1999], on the other hand, found that increased wave angles only result in decreasing growth rates for extreme wave angles and that the length scale remains similar, although, increased wave angles also resulted in decreased wave heights at the breaker line, reducing the nearshore processes. Ribas et al. [2003] showed that crescentic bed patterns are only obtained for moderate wave angles, and that for very oblique wave angles, oblique bars develop. The influence of the wave period was investigated by Calvete et al. [2005]. Here it was found that longer wave periods result in increased growth rates, and slightly increased length scales. However, the wave angle and the wave height have a stronger influence on the length scale of the crescentic bed patterns, than the wave period.

Non-linear stability analyses were also used to carry out sensitivity analyses of the evolution of crescentic bed-forms to various wave conditions [Garnier et al., 2008; Smit et al., 2008]. Results presented by Garnier et al. [2008] showed (similar to [Calvete et al., 2005]) that increased wave heights result in increased initial growth rates, and slightly bigger bed pattern lengths, while increasing wave angles

result in reduced growth rates in combination with increased length scales and migration rates. Changes in the wave period did not seem to have significant effects on either the growth rate or length scale. Variation of the wave conditions at a double-barred beach, investigated by Smit et al. [2008], suggested that increased wave heights result in increased initial growth rates and increased length scales at the outer bar, while increased wave angles reduce the growth rate and result in an increase in length scale of the inner and the outer bar bed-forms. The effects of wave groups on the formation of rip channels have been studied by Reniers et al. [2004], using a non-linear model. The results were compared with field observations, and showed a coupling between the computed edge wave motions and rip channels.

Different cross shore bed profiles have been studied by Deigaard et al. [1999], Damgaard et al. [2002], Garnier et al. [2007] and Calvete et al. [2007]. Deigaard et al. [1999] related the crescentic bed pattern characteristics to the dimensions of the trough between the bar and the shoreline. Increased trough depths result in increased growth rates and length scales, while increased trough widths result in increased length scales, but decreased growth rates. This relationship between trough width and length scale of the bed patterns was also observed by Damgaard et al. [2002], for both a linear and a non-linear stability analysis. Calvete et al. [2007] observes similar relationships, but reported that an increase in trough width does not result in a change in the growth rate. Calvete et al. [2007] showed that even slight changes in the bathymetry can cause significant differences in the characteristics of the developing bed-forms, however clear relations between

bathymetric characteristics and the developing bed-forms are difficult to observe, since the change in one bed parameter, generally affects the overall bathymetry. Garnier et al. [2007] used both a linear and a non-linear stability analysis to examine whether crescentic bed patterns would develop from a plain beach and a barred beach. Linear results suggested that only transverse bars would develop on a plain beach, while both types of bed patterns could develop on a barred beach. Non-linear results of a barred beach suggested that crescentic bars and transverse bars might coexist, with the transverse bed pattern occurring in front of the shoreline, and the crescentic bed pattern at the bar.

The interaction between the evolution of crescentic bed-forms and transverse bed-forms was examined by Caballeria et al. [2002] and Garnier et al. [2007]. Caballeria et al. [2002] showed that transverse bars and crescentic bars develop from the same instability mechanism, but that crescentic bed-forms would develop under higher wave conditions than transverse bars. For intermediate waves a combination of both bed-forms can develop, where an offshore crescentic bar coexists with nearshore transverse bars. Garnier et al. [2007] suggested that the initial stages of barred beach development give rise to transverse bars, but that crescentic bars would subsequently develop giving rise to transverse bars at the shoreline with the same length scale as the crescentic bed patterns further offshore.

Finally, the effects of different dissipation functions were examined by van Leeuwen et al. [2006]. Random waves are shown to break at a wider range of water depths, reducing the growth rate and length scale of the crescentic bed-forms

and give rise to the development of transverse bed patterns.

2.1.5 In summary

The presented literature overview shows that the knowledge concerning the development, occurrence and characteristics of nearshore zone rhythmic bed patterns has expanded significantly over the recent years. The advent of Argus imaging technique made it possible to observe the development of bed patterns over much longer periods, and under much wider circumstances than had been previously possible [Holman and Stanley, 2007]. The development in modelling techniques have created an ever-expanding base of understanding of the driving forces for the formation and characteristics of these bed-forms. However, comparisons of field measurements and observations with modelling results have to-date been general in nature. Only general similarities between length scales, growth rates and migration rates have been presented: see Deigaard et al. [1999], Falqués et al. [2000], Damgaard et al. [2002], Calvete et al. [2005] and van Leeuwen et al. [2006].

This thesis presents a direct comparison between field observations and model predictions. The temporal evolution of a barred beach with crescentic bed patterns under changing wave conditions is compared with model predictions made by a linear stability model. Field measurements of the development of crescentic bars over two months at Duck (USA), carried out by van Enkevort et al. [2004], are compared with model predictions using the bathymetric, tidal and wave data from this period at Duck. A linear stability analysis can provide information

concerning the length scale of crescentic bed patterns as well as their migration rate and the initial rate at which these bed-forms develop. The field observations reveal, in particular detail, the development in the length scale of the crescentic bed-forms and this characteristic is, therefore, the main focus of the comparison (presented in chapter 3).

This research is not only of interest from a scientific point of view, in that it investigates to what extent a linear stability analysis can actually describe real world scenarios, but these predictions can also be of use for coastal engineers. Furthermore, the likelihood of the development of rip currents can be assessed using this type of model, facilitating the assessment of bather safety. More fundamentally, rip / crescentic bar systems have an accompanying signature at the shore [Wright and Short, 1984], where mega-cusps frequently mirror the crescentic bars, so that their presence has an impact on beach erosion. Both these aspects also impact on shoreface nourishment projects, as these have the potential for developing into, or triggering rip systems [Ojeda et al., 2008]. This information can, moreover, be provided in very small computational times compared to traditional time-domain models.

A linear stability analysis assumes an alongshore uniform beach profile. This causes serious limitations in the direct applicability of knowledge obtained from a linear stability analysis in real-world scenarios. The beach at Duck generally shows rhythmic features, and only after storms can a (semi-) alongshore-uniform beach be observed [van Enckevort et al., 2004]. The effects of these pre-existing

bed patterns are investigated using a non-linear model (in chapter 4). Conclusions drawn from this additional research are applied in the subsequent comparison of the linear stability predictions with field observations of Duck (chapter 5).

2.2 Theoretical background

2.2.1 Short waves

Waves can occur in many ways and forms. In oceans and seas, the most interesting form of wave for engineering purposes is the surface gravity wave. These progressive waves occur at the interface between the atmosphere and the ocean. The restoring force of such waves lies with gravity, which will return the displaced water surface to its equilibrium position. A wide range of natural influences can force the development of such waves, ranging from wind, the effects of sun and moon (tides) to the effects of earthquakes [The Open University, 1989].

Monochromatic surface gravity waves are periodic features, whose wave length and height are defined as the horizontal distance between two crests (L [m]) and the vertical distance between the wave crest and trough (H [m]). The time it takes for a wave to pass a constant position in space is called the wave period (T [s]) and the speed at which waves propagate (c [m/s]) is given by:

$$c = \frac{L}{T}. \quad (2.1)$$

Assuming that waves are small in height with respect to their length, as well as to the water depth (D [m]), i.e.:

$$\frac{H}{L} \ll 1, \quad \frac{H}{D} \ll 1$$

they can be reasonably described by [Sorensen, 1993]:

$$\eta(x, t) = \frac{H}{2} \sin(\omega_w t - \kappa x), \quad (2.2)$$

where η [m] describes the surface displacement, κ is the wave number ($k = \frac{2\pi}{L}$), t represents time, x is the direction of wave propagation and ω_w represents the wave angular frequency ($\omega_w = \frac{2\pi}{T}$). A relation can be derived between κ and ω_w , called the dispersion relation [Dean and Dalrymple, 1984]:

$$\omega_w^2 = g\kappa \tanh(\kappa D), \quad (2.3)$$

where g stands for the gravitational acceleration ($g = 9.81$ [m/s²]). The propagation velocity of the wave can now be written as:

$$c = \sqrt{\frac{g}{\kappa} \tanh(\kappa D)} \quad (2.4)$$

The wave energy density is the energy per wave length, and comprises the kinetic energy and the potential energy. The wave energy can be written as [Komar, 1998]:

$$E = \frac{1}{8} \rho g H^2, \quad (2.5)$$

where ρ is the water density ($\rho = 1024$ [kg/m³]). Realistic waves in a sea or ocean have a random distribution of different wave heights, and periods. The random distribution of the wave height can be described by various measures; H_{rms} is used in (2.5).

The speed at which wave energy propagates is called the group velocity (c_g [m/s]) and is given by [Sorensen, 1993]:

$$c_g = \frac{c}{2} \left(1 + \frac{2\kappa D}{\sinh(2\kappa D)} \right) \quad (2.6)$$

In shallow water, the wave energy propagates at the same speed as the waves, while in deep water, the propagation speed of the wave energy is only half that of the actual waves [Dean and Dalrymple, 1984].

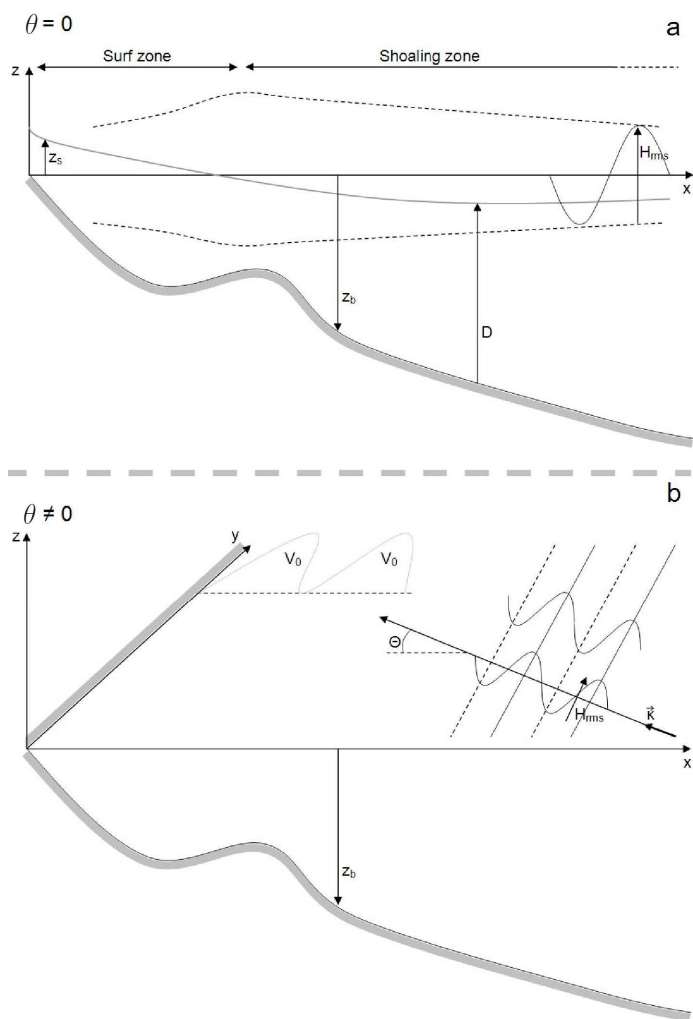


Figure 2.3: The coordinate system for (a) normal, and (b) oblique wave incidence, applied to describe the nearshore dynamics [originally from Garnier, 2006].

Waves can approach the shore at an oblique angle (θ) which creates alongshore current (V_0) in front of the beach. An overview of the coordinate system used in this thesis is shown in Fig. 2.3, which will be further explained in the following section.

2.2.2 Governing equations

The models used in this research describe the combined results of wave and water motion and the evolution of the seabed. Two models are used, a linear stability model, and a full time-domain model, which can be used to carry out a non-linear stability analysis. Each model describes the interaction between the water motions and the seabed in the nearshore region according to the same equations and same coordinate system (see Fig. 2.3). The driving forces of the system are the short gravity waves that propagate into the modelling domain from the offshore modelling boundary. In the nearshore region, wave transformation and breaking occurs. The two dimensional shallow water equations are derived from the Navier-Stokes equations, by depth averaging and averaging over the wave period [Mei, 1989; Phillips, 1966]. These 2D shallow water equations describe the conservation of mass and momentum:

Water mass conservation equation

$$\frac{\partial D}{\partial t} + \frac{\partial}{\partial x_j}(Dv_j) = 0, \quad (2.7)$$

where $j = 1, 2$; $\vec{x} = (x_1, x_2) = (x, y)$ and $\vec{v} = (v_1, v_2) = (u, v)$ and D is the total water depth. x and y are the cross- and alongshore coordinates, and u and v the cross- and alongshore depth-averaged velocities, respectively.

Momentum equations

$$\frac{\partial v_i}{\partial t} + v_j \frac{\partial v_i}{\partial x_j} = -g \frac{\partial z_s}{\partial x_i} - \frac{1}{\rho D} \frac{\partial}{\partial x_j} (S'_{ij} - S''_{ij}) - \frac{\tau_{bi}}{\rho D}, \quad (2.8)$$

where $i, j = 1, 2$, with the summation being on j . This results in two equations, one for the momentum in x -direction and in y -direction. z_s is the mean sea level over the wave period: ($z_s(x, y, t) = \frac{1}{T} \int_0^T \eta dt$); z_b is the mean bed level and D is the total mean water depth ($D = z_s - z_b$). $\vec{\tau}_b$ represents the bed shear stress ($\vec{\tau}_b = (\tau_{b1}, \tau_{b2}) = (\tau_{bx}, \tau_{by})$). S'_{ij} is the radiation stress term and S''_{ij} represents the Reynolds stresses [Calvete et al., 2005].

The left hand side of (2.8) represents the acceleration of water particles in space (x, y) and time (t) . The right hand side of the equation describes the sources of increase and decrease in momentum. The first term on the right hand side describes the pressure gradients, while the radiation stress gradients (S'_{ij}) describe how changes in wave energy result in changes in the momentum and the Reynolds' stresses describe how turbulence in the water affects the momentum. Finally, $\vec{\tau}_b$ describes the loss of momentum due to bed friction.

Wave energy equation

The wave energy density term (E) is present in the momentum conservation equation via the radiation stresses. The wave energy equation describes how energy within the waves propagates and transforms, while the waves propagate towards the shore, and its derivation can be found in Phillips [1966]; Mei [1989].

$$\frac{\partial E}{\partial t} + \frac{\partial}{\partial x_i} ((v_i + c_{gi})E) + S'_{ij} \frac{\partial v_j}{\partial x_i} = -\mathcal{D}, \quad (2.9)$$

where $i, j = 1, 2$. The wave energy conservation equation is a combination of the wave action equation [Mei, 1989] and a description of the loss of wave energy due to wave breaking and currents (\mathcal{D}). The radiation stresses (S'_{ij}) represent the transfer between wave energy and water motion.

Wave phase equation

Waves change due to the presence of currents and the changing bathymetry in the nearshore region [Svendsen, 2006]. The effects of currents on the wave phase are described by the 'conservation of waves' equation [Phillips, 1966]:

$$\frac{\partial \Phi}{\partial t} + \sigma + v_j \frac{\partial \Phi}{\partial x_j} = 0, \quad (2.10)$$

where σ is the intrinsic wave frequency, as observed when moving with the current, and Φ is the wave-averaged wave phase and can be described as:

$$\begin{aligned} \eta &= \frac{H}{2} \sin(\Phi) \\ &= \frac{H}{2} \sin\left(\int \kappa_j dx_j - \int \omega_w dt\right) \end{aligned}$$

The relation between the wave phase and the wave vector ($\vec{\kappa} = (\kappa_1, \kappa_2) = (\kappa_x, \kappa_y)$) and the wave frequency (ω_w) can be given as:

$$\frac{\partial \Phi}{\partial x_j} = \kappa_j, \quad \frac{\partial \Phi}{\partial t} = -\omega_w$$

The relation between the the intrinsic wave frequency (σ) and the absolute frequency (ω_w) can then be given by [Svendsen, 2006]:

$$\omega_w = \sigma + v_j \kappa_j$$

When no currents exist, the intrinsic frequency (σ) and the absolute frequency (ω_w) are therefore the same.

Sediment mass conservation equation

The system of equations used to describe the nearshore system is completed with the addition of an equation describing the evolution of the seabed. This equation couples the hydrodynamic variables presented above with the bottom level [Soulsby, 1997]:

$$\frac{\partial z_b}{\partial t} + \frac{1}{1-p} \frac{\partial q_i}{\partial x_i} = 0 \quad (2.11)$$

where p is the porosity of the sediment and \vec{q} represents the sediment flux ($\vec{q} = (q_1, q_2) = (q_x, q_y)$).

2.2.3 Parametrisation

The governing equations include various parameters that need defining. The following section presents the parameterisations used in this research.

Wave radiation stresses

Longuet-Higgins and Stewart [1964] describe radiation stresses as 'the excess flow of momentum due to the presence of waves'. The radiation stress tensor from linear wave theory can be written as [Mei, 1989]:

$$S'_{ij} = E \left(\frac{c_g}{c} \frac{\kappa_i \kappa_j}{\kappa^2} + \left(\frac{c_g}{c} - \frac{1}{2} \right) \delta_{ij} \right) \quad (2.12)$$

where the Kronecker delta (δ_{ij}) is defined as:

$$\delta_{ij} = \begin{cases} 1, & \text{if } i = j \\ 0, & \text{if } i \neq j \end{cases}$$

Reynolds stresses

Water motions vary in a random manner in space and time in oceans. Reynolds stresses represent dissipation through small scale turbulent processes [Phillips, 1966].

$$S''_{ij} = \rho \nu_t D \left(\frac{\partial v_i}{\partial x_j} + \frac{\partial v_j}{\partial x_i} \right), \quad (2.13)$$

where ν_t is the horizontal eddy viscosity. The Battjes [1975] model was chosen as empirical representation of the horizontal eddy viscosity (ν_t):

$$\nu_t = M \left(\frac{D}{\rho} \right)^{\frac{1}{3}} H_{rms}, \quad (2.14)$$

where M represents a dimensionless parameter that characterises the turbulence.

Bed shear stress

The friction of the bed on the water motion is extremely complex and a wide range of empirical formulations exist [Soulsby, 1997]. Both linear friction as well as friction according to Feddersen et al. [2000] are applied in this research. Linear friction describes the bed shear stress for weak currents, with respect to the wave orbital velocity, as a function of the wave orbital velocity at the edge of the modelling boundary layer (u_{rms}) and the depth-averaged water motion (v) [Mei, 1989]:

$$\vec{\tau}_b = \rho \frac{2}{\pi} c_d u_{rms} \vec{v}, \quad (2.15)$$

where c_d represents the drag coefficient, and is given by:

$$c_d = \left(\frac{0.4}{\ln(D/z_{rl}) - 1} \right)^2, \quad (2.16)$$

where z_{rl} is the roughness length due to the grain size and the occurrence of ripples on the seabed. u_{rms} in (2.15) represents the wave orbital velocity at the edge of

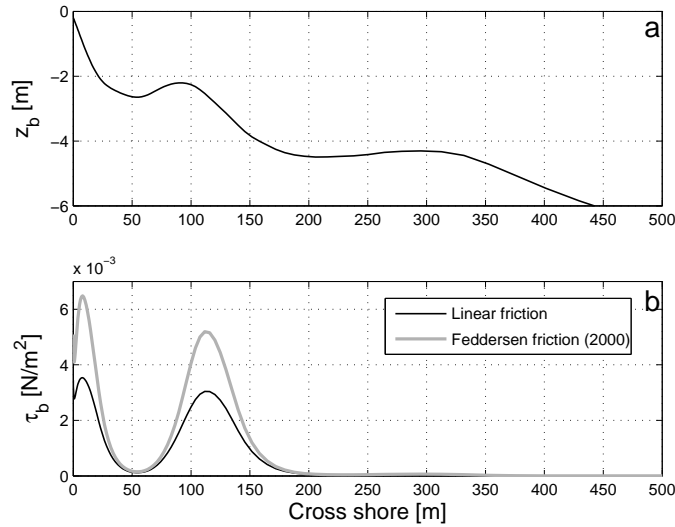


Figure 2.4: (a) The alongshore constant bed level as measured in Duck (August 1998), and (b) the linear friction (*black*) and the friction according to Feddersen et al. [2000] (2.18) (*grey*), for moderate offshore wave conditions ($H_{rms} = 1.15$ m, $T_p = 7.6$ s and $\theta = 18.7^\circ$).

the boundary layer:

$$u_{rms} = \frac{H_{rms}}{\sqrt{\pi}} \frac{|\kappa|}{\sigma} \frac{\cosh(|\kappa|z_{rl})}{\cosh(|\kappa|D)} \quad (2.17)$$

The linear equation is suitable to describe near-normal wave incidence. However, strong alongshore currents result in an underestimation of bed shear stress [Feddersen et al., 2000]. In order to describe bed friction accurately for more extreme wave angles the Feddersen friction is used, as it was applied in Morfo60 [Ribas et al., 2007].

$$\tau_{b_i} = \rho C_d \frac{u_{rms}}{\sqrt{2}} v_i \left(a_{Fed.} + 2 \frac{|\vec{v}|^2}{u_{rms}^2} \right)^{\frac{1}{2}} \quad (2.18)$$

A Feddersen friction coefficient ($a_{Fed.}$) of 1.16 gives good agreement for a random wave field at Duck [Ruessink et al., 2001].

The difference between (2.15) and (2.18) becomes apparent when waves ap-

proach the shore at an moderately oblique wave angle ($\theta = 18.7^\circ$) (see Fig. 2.4). The linear friction curves depict significantly smaller peaks than the curve according to the description of the bed shear stress from Feddersen et al. [2000].

Dissipation

Wave breaking is the process whereby wave energy is dissipated and the wave height decreases. Wave breaking can occur due to the interaction with currents, or wind, or between waves, but the main reason for waves to break close to the shoreline is the interaction of waves with the seabed. Regular waves start to break at a specific cross shore point, which is dependent on the water depth. A random wave distribution results in a wider cross shore region where waves start to dissipate energy. A formulation to describe the wave energy dissipation as a result of the interaction of the waves with the seabed for random waves is derived by Thornton and Guza [1983]:

$$\mathcal{D} = \frac{3\sqrt{\pi}}{16} B^3 f_p \rho g \frac{H_{rms}^5}{\gamma_b^2 D^3} \left(1 - \frac{1}{(1 + (H_{rms}/\gamma_b D)^2)^{5/2}} \right), \quad (2.19)$$

where B^3 is the wave dissipation coefficient, f_p represents the absolute frequency peak of the wave field ($f_p = \sigma/2\pi$) and γ_b represents the breaking index [Thornton and Guza, 1983]. However, the Thornton and Guza [1983] dissipation formulation results in significant and unrealistic dissipation far offshore, as can be seen in Fig. 2.5. A more accurate description of the dissipation is presented by Church and Thornton [1993]:

$$\mathcal{D} = \frac{3\sqrt{\pi}}{16} B^3 f_p \rho g \frac{H_{rms}^3}{D} \left(1 - \frac{1}{(1 + (H_{rms}/\gamma_b D)^2)^{5/2}} \right) \left\{ 1 + \tanh \left[8 \left(\frac{H_{rms}}{\gamma_b D} - 1 \right) \right] \right\} \quad (2.20)$$

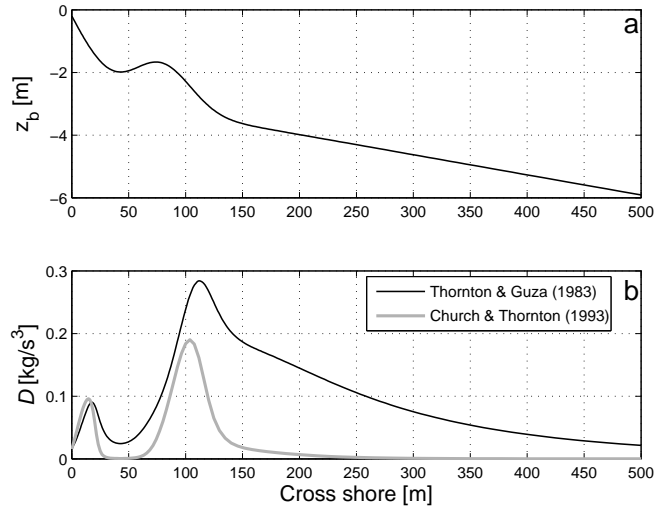


Figure 2.5: (a) The alongshore constant bed level according to Yu and Slinn [2003], and (b) the dissipation rate according to Thornton and Guza [1983] and Church and Thornton [1993], for moderate offshore wave conditions ($H_{rms} = 1.15$ m, $T_p = 7.6$ s and $\theta = 18.7^\circ$).

(2.19) and (2.20) result in a very similar dissipation profiles for mild wave conditions. For moderate and severe wave conditions, (2.20) results in dissipation closer to the shore, which corresponds to the expected location of wave breaking (see Fig. 2.5). (2.20) results in a slight reduction of the rate at which bed-forms develop. For extreme wave conditions also a slight reduction in the prevalent length scale of the developing bed patterns can be observed for the dissipation function described by Church and Thornton [1993].

Volumetric sediment flux

In order to describe the evolution of the seabed, a formulation of the total load sediment transport is used Soulsby [1997]:

$$\vec{q} = \alpha(x) \vec{v} - \gamma(x) \vec{\nabla} h, \quad (2.21)$$

where $\vec{\nabla}$ is the horizontal gradient operator: $\vec{\nabla} = (\nabla_1, \nabla_2) = (\frac{\partial}{\partial x}, \frac{\partial}{\partial y})$. α is the stirring function, γ represents the bedslope coefficient and the sediment flux (\vec{q}) is given by:

$$\vec{q}_{svr} = A_s |\vec{v}| \left[\left(|\vec{v}|^2 + \frac{0.018}{c_d} u_{rms}^2 \right)^{\frac{1}{2}} - u_{crit} \right]^{2.4} \left(\frac{\vec{v}}{|\vec{v}|} - \gamma \nabla h \right) \quad (2.22)$$

$$\vec{q} = \begin{cases} \vec{q}_{svr}, & \text{if } \left(|\vec{v}|^2 + \frac{0.018}{c_d} u_{rms}^2 \right)^{\frac{1}{2}} > u_{crit} \\ 0, & \text{otherwise} \end{cases}$$

The sediment mobility constant (A_s) depends on the sediment characteristics and the water depth, and can be split up into a part representing the suspended load (A_{ss}) and the bedload transport (A_{sb}) Soulsby [1997]:

$$A_{ss} = \frac{0.012 d_{50} D_*^{-0.6}}{[(s_{rds}-1)g d_{50}]^{1.2}}$$

$$A_{sb} = \frac{0.005 h (d_{50}/D)^{1.2}}{[(s_{rds}-1)g d_{50}]^{1.2}},$$

where d_{50} is the median grain size, s_{rds} is the relative density of sediment. D_* represents the dimensionless grain size ($D_* = \left[\frac{g(s_{rds}-1)}{\mu^2} \right]^{\frac{1}{3}} d_{50}$), where μ [m^2/s^2] is the kinematic viscosity.

The critical velocity (u_{crit}) for sediment transport is given by:

$$u_{crit} = \begin{cases} 0.19(d_{50})^{0.1} \log_{10} \frac{D}{d_{50}}, & 0.0001 \leq d_{50} \leq 0.0005 \text{ m} \\ 8.5(d_{50})^{0.6} \log_{10} \frac{D}{d_{50}}, & 0.0005 \leq d_{50} \leq 0.002 \text{ m} \end{cases}$$

2.2.4 Dynamic unknowns

The unknowns of the dynamical system of equations are [Calvete et al., 2005]:

- Depth and time averaged flow in the cross- and alongshore direction: $u(x, y, t)$
and $v(x, y, t)$
- Mean sea level: $z_s(x, y, t)$
- Wave energy density: $E(x, y, t)$
- Wave phase: $\Phi(x, y, t)$
- Mean bed level: $z_b(x, y, t)$

2.3 Stability analysis

In the past, the formation of rhythmic patterns has been attributed to hydrodynamic forcing conditions, where the dominant water motion forced the development of bed-forms [Fredsoe and Deigaard, 1992]. However, although forcing templates are still being used to describe the development of rip channels [MacMahan et al., 2007], the self-organisation of the depth- and wave-averaged water motion and the bed evolution are now generally assumed to dominate the formation of these bed-forms [Falqués et al., 2008]. The stability analysis is a modelling technique to describe the development of rhythmic bed-forms as a result of free instabilities in the coupled system of water motion and bed evolution. Feedback between the bottom and the water motion is essential for the development of bed-forms [Dodd et al., 2003].

It can be said that two types of stability analysis exist, that were already introduced in section 2.1: the linear and non-linear stability analysis.

Both modelling techniques will be discussed in the following sections. A schematic description both a linear and a non-linear stability analysis can be seen in Table 2.1.

2.3.1 Linear stability analysis

The development of rhythmic features on the seabed form the main focus of many linear stability analyses. To investigate the initial development of these bed-forms, an initial depth- and wave-averaged time-invariant equilibrium state is considered, the basic state. This basic state is composed of a steady topography and water

motion. Instabilities, such as rhythmic bed patterns, are not present yet. These stable conditions, are computed as a result of offshore wave forcing conditions as well as the bed profile [Calvete et al., 2005].

The second step in a linear stability analysis is the introduction of rhythmic perturbations to the basic state. These perturbations are assumed to be small compared to the values of the basic state, and non-linear perturbation terms in the governing equations can therefore be excluded. The various different perturbation length scales result in different characteristics of the developing bed patterns. The linear growth rate of various initial length scales gives insight into the rate at which rhythmic features with different length scales will develop. A perturbation length scale that grows is called unstable, whereas a perturbation that decreases in height, in order for the basic state to re-establish, is called stable. It is assumed that the length scale that shows the biggest linear growth rate will dominate the development of other length scales. This dominant length scale is called the 'fastest growing mode' (*FGM*).

A linear model can describe the initial stages of development, within short computational times. It can give insight into the initial length scale, rate of development, alongshore migration rate and initial orientation of bed-forms. Linear growth occurs as long as perturbations are small. When bed-forms evolve beyond this point, non-linear terms become significant. The short computation times make this type of modelling a potentially interesting tool for coastal engineers if the limitations of a linear stability analysis can be accounted for. A linear stability analysis, Morfo60, will be introduced in section 2.4.

2.3.2 Non-linear stability analysis

A non-linear stability analysis can give insight into the long term development of bed-forms. This type of model is generally not designed as a stability analysis, but can be a depth- and wave-averaged full time-domain model used to examine morphodynamical instabilities. Alternatively, a weakly non-linear model can use a reduced system of equations to examine the non-linear behaviour of a short range of length scales around the linear *FGM* [Falqués et al., 2008] or to examine the finite amplitude behaviour of bed-forms, whose amplitude is still small compared to the basic state parameters [Dodd et al., 2003].

In section 2.5, the non-linear model Morfo55 will be introduced [Garnier, 2006]. This non-linear model forms an extension to an already existing model, Morfo50 [Caballeria et al., 2002]. This model uses the full non-linear equations to describe the temporal evolution of the surf and shoaling zone. The model is used as a stability analysis by implementing an undisturbed beach. This undisturbed beach is perturbed to give rise to the development of rhythmic bed patterns. The non-linear model describes how a wide range of length scales would initially develop, but that soon the fastest linear growing mode will dominate. Over time, non-linear effects will increase in importance, and the development of bed-forms slows down, until an equilibrium height is reached.

Fully non-linear equations

A full time-domain model

<p>Initial assumptions:</p> <ul style="list-style-type: none"> • Constant wave forcing H_{rms}, T_p, θ • Alongshore uniformity $\frac{\partial}{\partial y} = 0$ • Time invariance $\frac{\partial}{\partial t} = 0$ <p style="text-align: center;">⇓</p> <p style="text-align: center;"><i>Basic state</i></p>	<p>Initial assumptions:</p> <ul style="list-style-type: none"> • Constant wave forcing H_{rms}, T_p, θ • Alongshore uniformity $\frac{\partial}{\partial y} = 0$ <p style="text-align: center;">⇓</p> <p style="text-align: center;"><i>Start of run</i></p>
<p>Subsequent conditions:</p> <ul style="list-style-type: none"> • Sinusoidal perturbations $\frac{\partial}{\partial y} = ik$ • Exponential growth $\frac{\partial}{\partial t} = \omega_r$ • Linearisation 	<p>Subsequent conditions:</p> <p>Initial perturbation:</p> <ul style="list-style-type: none"> • Random perturbations • 'Dirac function'
<p>Linear stability analysis</p> <p style="text-align: center;"><i>Morfo60</i></p>	<p>Non-linear stability analysis</p> <p style="text-align: center;"><i>Morfo55</i></p>

Table 2.1: Model set-up for a linear and a non-linear stability analysis.

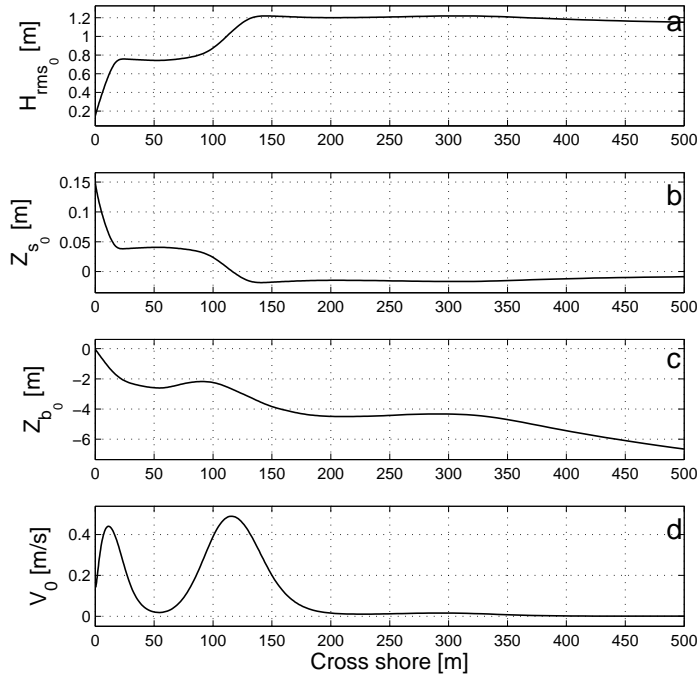


Figure 2.6: The basic state profiles of (a) the wave height, (b) the mean free surface elevation, (c) the bed level, and (d) the alongshore velocity, for the same moderate offshore wave conditions ($H_{rms} = 1.15$ m, $T_p = 7.6$ s and $\theta = 18.7^\circ$).

2.4 Morfo60

Morfo60 is a comprehensive morphodynamical linear stability model, describing the development of nearshore bed patterns as a free instability of the coastal system. The shallow water equations in combination with descriptions of the bed evolution, the wave phase and the energy density, form the model framework (see Calvete et al. [2005] for more details).

2.4.1 Basic state

The approach used in Morfo60 is standard for linear stability models, where a stability analysis determines if disturbances imposed on an equilibrium state grow or decay. In Morfo60 the equilibrium state represents the alongshore uniform solution of (2.7) - (2.11) for a given wave forcing (offshore wave height (H_{rms}), wave period (T_p) and offshore wave angle (θ)) and cross shore beach profile ($z_b = -Z_0(x)$), along with the resulting flow for $\theta \neq 0$: $\vec{v} = (0, V_0(x))$, free surface elevation ($z_s = \eta_0(x)$), wave energy ($E = E_0(x)$) and phase field ($\Phi = \Phi_0(x)$).

An example of the cross shore distributions of several variables is given in Fig. 2.6. The bed profile (Fig. 2.6(c)) originates from field measurements at Duck (see section 3.2.2) and shows two alongshore bars. A moderate wave height ($H_{rms} = 1.15$ m) is applied at the modelling boundary and wave energy dissipation occurs at the onshore bar and in front of the beach (see Fig. 2.6(a)). Fig. 2.6(b) depicts the mean free surface elevation of the basic state (Z_{s_0}). Offshore set-down can be observed, whilst when waves begin to break, set-up is predicted. The moderate wave angle ($\theta = 18.7^\circ$) at the modelling boundary results in a significant alongshore current at the onshore bar and in front of the shoreline, as can be seen in Fig. 2.6(d). Different offshore wave conditions will result in different basic state profiles, and therefore give rise to a different *FGM*.

2.4.2 Perturbations

The model introduces perturbations of arbitrary length scales ($\lambda = \frac{2\pi}{k}$) into the basic state:

$$u = u(x)e^{\omega t +iky} \quad (2.23)$$

$$v = V_0(x) + v(x)e^{\omega t +iky} \quad (2.24)$$

$$z_s = Z_{s_0}(x) + z_s(x)e^{\omega t +iky} \quad (2.25)$$

$$E = E_0(x) + e(x)e^{\omega t +iky} \quad (2.26)$$

$$\Phi = \Phi_0(x, t) + \phi(x)e^{\omega t +iky} . \quad (2.27)$$

$$z_b = -Z_0(x) + h(x)e^{\omega t +iky} \quad (2.28)$$

Substituting (2.23) - (2.27) into (2.7) - (2.11) results in a system of equations that defines an eigenvalue problem. Its solution determines the characteristics of each of the perturbation length scales. The growth rate (ω_r), the migration rate ($c_m = \frac{\omega_i}{k}$), where ω is composed of an imaginary and a real part ($\omega = \omega_r + i\omega_i$), and the eigenfunctions for each perturbation variable are obtained for each length scale (λ) in a range of physically plausible length scales ($\lambda \approx 50 - 6000$ m). It is assumed that the fastest growing perturbation length scale (λ_{FGM}) will dominate

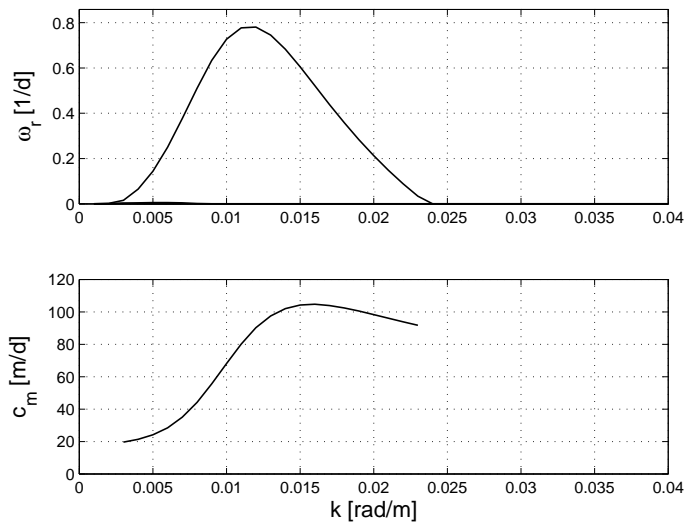


Figure 2.7: (a) The growth rate of various bed pattern length scales ($\lambda = \frac{2\pi}{k}$), and (b) the corresponding migration rate, for moderate offshore wave conditions ($H_{rms} = 1.15$ m, $T_p = 7.6$ s and $\theta = 18.7^\circ$).

the development of other length scales.

In a linear stability model, the equations are simplified by assuming that values of variables in the equilibrium state are significantly bigger than the perturbations and that non-linear terms of the perturbations can therefore be neglected. In reality, the effects of the non-linear terms in the equations become more important as the height of the perturbations increase, resulting in a reduction in the accuracy of the predictions of a linear stability analysis, as bed features evolve.

Fig. 2.7(a) depicts the initial linear growth rate for the range of physically plausible length scales under the same offshore wave conditions, as were applied in the basic state. λ_{FGM} is the length scale with the highest growth rate ($k = 0.012$

[rad/m], $\lambda = 523$ m). The migration rate (c_m) for growing bed pattern length scales, is depicted in Fig. 2.7(b).

The Morfo60 computer model solves the perturbed equations using a spectral method [Iranzo and Falqués, 1992]. The terms in the equations are expanded into polynomials. The different physical variables (u , v , e , z_s , z_b and ϕ) are expressed as a finite sum of $N + 1$ so-called basis functions, here Chebyshev polynomials of the first kind (N being the number of grid points). These are defined by: $T_k(x) = \cos(k \cos^{-1} x)$, for $k = 0, 1, 2, \dots$ [Canuto et al., 1988]. These expansions are substituted into the governing equations and a spectral method is used to solve the resulting equations.

The spectral method is chosen because it allows computational nodes to be distributed efficiently where variations are most rapid (generally close to the shoreline) [Calvete et al., 2005]. The method used here is a collocation method in which we insist that the equations are solved exactly at the computational nodes (i.e. collocation points). This, in combination with the boundary conditions, gives for each governing equation $N + 1$ equations with $N + 1$ unknowns, the unknowns being the ‘amplitudes’ or ‘weights’ of each Chebyshev polynomial. The number of collocation points is therefore critical for numerical convergence. Model runs with various numbers of collocation points have been carried out, and 300 points have been used throughout since they produced consistent results.

In the present study, both the perturbed effects of refraction over the current and the depth perturbation terms are excluded from (2.10), excluding perturbed

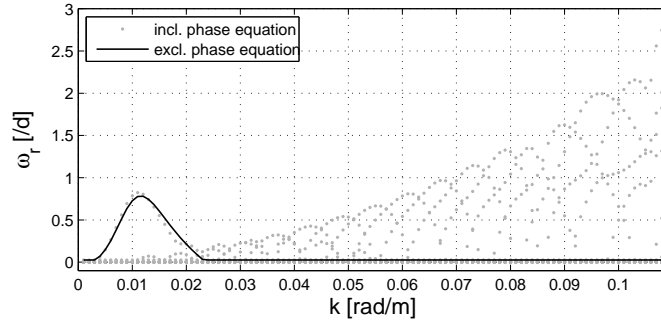


Figure 2.8: The effect of the inclusion of perturbed effects of refraction over the current and the depth perturbation terms on the growth rate curve.

terms in the wave phase equation. The influence of these terms on the physically accurate predictions of the growth rate and length scale of crescentic bed patterns is minor, as was shown in van Leeuwen et al. [2006] and can be seen in Fig. 2.8. However, especially smaller length scales ($k = \frac{2\pi}{\lambda}$) show a wide range of numerical results when these terms are included. These numerical results obscure the determination of a physically plausible fastest growing mode. These terms are therefore excluded from the perturbed part of the wave phase equation for all future runs made by the linear stability analysis.

The solution to the eigenvalue problem not only gives insight into the length scale, growth rate and migration rate of the perturbations, but can also give the cross- and alongshore distribution of the perturbations for different variables. These eigenfunctions show how the initial development of these variables will cause perturbations onto the basic state profiles. The eigenfunctions of the wave height (H_{rms}), mean surface elevation (z_s), bed level (z_b) and the alongshore velocity (v) are depicted in Fig. 2.9. The eigenfunctions are arbitrary in amplitude. The

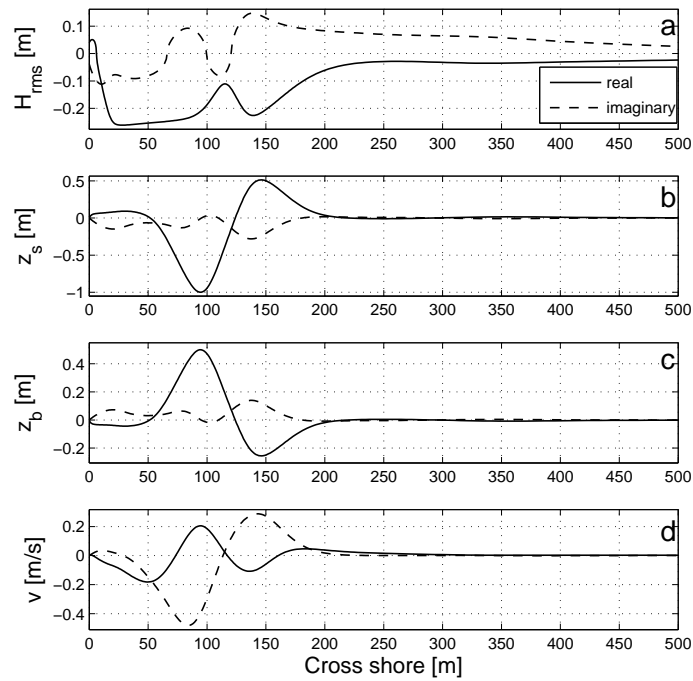


Figure 2.9: The real and imaginary part of the perturbation profiles of (a) the wave height, (b) the mean free surface elevation, (c) the bed level, and (d) the alongshore velocity, for the same moderate offshore wave conditions ($H_{rms} = 1.15$ m, $T_p = 7.6$ s and $\theta = 18.7^\circ$).

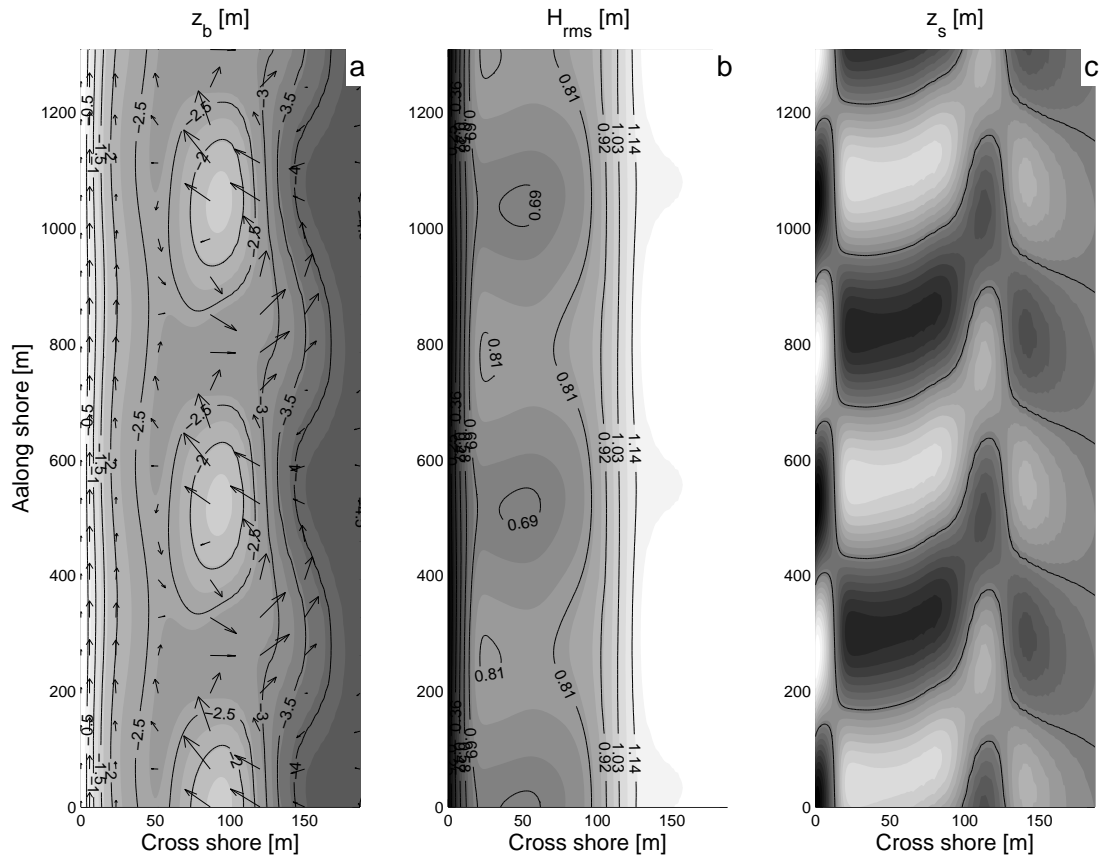


Figure 2.10: (a) The total bed profile (*contour*) and currents (*arrows*), (b) the total wave height distribution, and (c) the perturbed mean free surface elevation, for the dominant length scale (λ_{FGM}), for moderate offshore wave conditions ($H_{rms} = 1.15$ m, $T_p = 7.6$ s and $\theta = 18.7^\circ$).

eigenfunctions generally show a peak between 80 and 100 m offshore. This peak corresponds well with the location of the nearshore bar, since crescentic bed patterns mainly develop at this bar.

By applying an arbitrary amplitude (A) to these eigenfunctions (f'), the full alongshore distribution (F) of different variables can be obtained.

$$F(x, y) = F_0(x) + Af'(x)e^{iyk_{FGM}}, \quad (2.29)$$

where $f' = f'_r + i f'_i$ and F_0 is the basic state alongshore constant distribution of a variable. The cross and alongshore distribution of various characteristic variables under the previously presented offshore wave conditions, is shown in Fig. 2.10. The oblique wave angle results in a strong alongshore current, and the oblique orientation of especially the bed patterns (Fig. 2.10(a)) and the free surface elevation (Fig. 2.10(c)).

Settings used to describe the evolution of crescentic bed patterns at Duck are presented in Table 2.2. A wide range of different wave conditions will be examined. Therefore, both the description of the friction by Feddersen et al. [2000] and the dissipation formulation by Church and Thornton [1993] will be used to describe realistic circumstances for the evolution of bed-forms.

Name	Parameter	Unit	Value
General			
Gravitational acceleration	g	m/s^2	9.81
Offshore boundary	x_{max}	m	4000
Minimum depth at shoreline	D_{min}	m	0.2
Range of examined length scales	λ	m	57 – 6283
<i>Bed profile computed from measurements at Duck from August to November, 1998</i>			
Dissipation			
<i>According to Church and Thornton [1993]</i>			
Coefficient of wave dissipation	B^3	–	2.2
Breaking index	γ_b	–	0.42
Bed roughness length	z_{rl}	m	0.01
Reynolds stresses			
Turbulence parameter	M	–	1.0
Friction			
<i>According to Feddersen et al. [2000]</i>			
Friction coefficient	$a_{Fed.}$	–	1.16
Sediment			
Median grain size	d_{50}	m	2.0×10^{-4}
Kinematic viscosity	μ	m^2/s^2	1.3×10^{-6}
Sediment porosity	p	–	0.4
Relative sediment density	s_{rds}	–	2.65
Bedslope coefficient	γ	m^2/s	1.6
Sediment porosity	p	–	0.4

Table 2.2: Settings used in the linear stability analysis Morfo60.

2.5 Morfo55

The main objective of this research is to investigate to what extent a linear stability analysis can describe the development and evolution of bed-forms, as they are observed in reality. The limitations of a linear stability analysis make the accuracy of such a model doubtful for the prediction of the long term evolution of bed patterns under changing forcing conditions. To this end, a non-linear stability analysis is used to investigate to what extent a linear stability analysis can correctly describe circumstances that are originally beyond the capabilities of a linear stability analysis. The inability to accurately predict bed pattern evolution after the initial stages as well as the assumption of an alongshore constant bed profile are significant limitations. A non-linear stability analysis can describe the evolution of bed-forms from their beginnings until bed-forms reach their final height and this type of model can also describe pre-existing bed patterns.

Morfo55 is a full time-domain model that describes developments in the nearshore zone. The model uses the same depth- and wave averaged equations as Morfo60. However, these equations are not linearised, in order to preserve the complete description of the temporal evolution of perturbations (see Garnier [2006] for more details). This model is not designed solely as a non-linear stability analysis tool and has been used to investigate a much wider range of nearshore situations [eg. Garnier, 2006]. However, Morfo55 can be used to carry out a non-linear stability analysis. For this purpose, settings are restricted in order to investigate the stability of a certain nearshore system, of water motions and bed evolution (see Table 2.1).

The non-linear Morfo55 model uses a finite difference scheme to discretise the basic governing equations [Garnier et al., 2006]. The key difference between the spectral method used in the Morfo60 model and the finite difference method used in Morfo55 is that in the finite difference method the equations are approximated to obtain a solution, whereas in the spectral method the solution is being approximated. While a finite difference method replaces the continuum equation by an equation on grid points, the spectral method expresses the solution as a truncated expansion in a set of basis functions [Press et al., 1989].

A central finite-difference method on a regular rectangular grid is used for the spatial derivatives $((f_x)_{i,j} = \frac{f_{i+1,j} - f_{i-1,j}}{2\Delta x} + O((\Delta x)^2))$. The discretised variable f can be approximated at a half space step in each directions as:

$$f_{i\pm 1/2,j}^k = \frac{f_{i,j}^k + f_{i\pm 1,j}^k}{2}, \quad f_{i,j\pm 1/2}^k = \frac{f_{i,j}^k + f_{i,j\pm 1}^k}{2}, \quad (2.30)$$

where the discretised variable (f) at the central node at time k is defined as:

$$f_{i,j}^k = f(x(i), y(j), t(k)) \quad (2.31)$$

The grid distribution in the cross shore direction is set at $\Delta x = 2.5$ m to obtain numerical convergence. The grid distribution in the alongshore direction is set at $\Delta y = 10$ m, to ensure sufficient detail in the description of short crescentic bed patterns ($\lambda \geq 100$ m).

The explicit Adams–Bashforth scheme is used for the temporal derivatives.

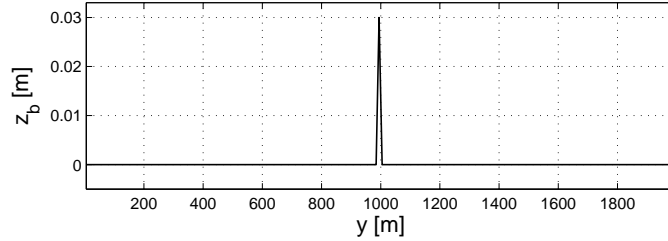


Figure 2.11: A numerical analogue of a Dirac-delta function with an amplitude of 3 cm, applied to excite all frequencies to the same extent.

The flux of different variables in time (Ψ_f) can be formulated as:

$$\frac{\partial f}{\partial t} = \Psi_f, \quad (2.32)$$

where f corresponds to any of the unknowns: D , u , v , E , Φ or z_b . The flux (Ψ_f) includes all the terms of the equation of f except the term of the temporal derivative. The temporal discretisation using the Adams-Basforth scheme subsequently becomes:

$$\frac{f_{i,j}^k - f_{i,j}^{k-1}}{\Delta t} = \frac{3}{2}\Psi_{f_{i,j}^{k-1}} - \frac{1}{2}\Psi_{f_{i,j}^{k-2}}, \quad (2.33)$$

where k is the time index: $k \in [2, N_t]$ (N_t representing the total modelled period), $k = 0$ corresponds to the initial conditions, while the value of the variables for $k = 1$ is obtained using the Euler first order scheme [Garnier, 2006].

Similar conditions are created as are implemented in the basic state of the linear stability analysis. An alongshore constant beach profile is implemented, along with constant wave forcing at the modelling boundary. Instead of investigating the characteristics of a wide range of perturbation length scales, as happens in a linear stability analysis, all perturbation length scales are excited simultaneously. This can be done by applying an initial perturbation to the system. Previously, small

scale random perturbations have been used. These perturbations subsequently excite a wide range of different length scales. However, random perturbations may not excite all length scales to the same extent, if they are not truly random. This means that some length scales will start with a bigger initial amplitude than other length scales. Alternatively, a numerical analogue of a Dirac-delta function can be introduced to the system. This derived 'Dirac function' is a spike in the cross- and alongshore distribution of a certain variable (here generally the seabed) (see Fig. 2.11). This spike excites all perturbation length scales to the same extent, resulting in the initial development of all these bed-forms.

Time-domain simulations can develop numerical instabilities. The model carries out an iterative process in time, where small fluctuations can quickly overwhelm any physical development of bed-forms. The sensitivity of the model to input settings, makes that a much narrower range of conditions can be applied than what is possible with a linear stability analysis. The settings used by Morfo60 (Table 2.2) are determined to give a physically accurate description of the physics involved, for the very wide range of wave conditions that occur at Duck. The settings used for the non-linear runs (Table 2.3) differ from the settings applied in Morfo60. The settings used in Morfo55 have been applied successfully previously [e.g. Garnier, 2006; Garnier et al., 2008] and have been shown to reduce the risk of the development of numerical instabilities. The main differences are the application of linear friction instead of Feddersen et al. [2000] friction and the dissipation function of Thornton and Guza [1983]. Both differences are of particular importance for the implementation of extreme wave conditions, when

Name	Parameter	Unit	Value
General			
Gravitational acceleration	g	m/s^2	9.8
Offshore boundary	x_{max}	m	250
Alongshore domain width	y_{max}	m	2000
Minimum bed level at shoreline	z_{min}	m	0.25
Range of examined length scales	λ	m	100 – 1000
Morphological time step	δt_{morph}	s	3.0
<i>Bed profile according to Yu and Slinn [2003]</i>			
Dissipation			
<i>According to Thornton and Guza [1983]</i>			
Coefficient of wave dissipation	B^3	–	1.0
Breaking index	γ_b	–	0.6
Bed roughness length	z_{rl}	m	0.01
Reynolds stresses			
Turbulence parameter	M	–	1.0
Friction			
<i>Linear friction is applied</i>			
Bottom friction coefficient	c_d	–	0.001 (constant)
Sediment			
Median grain size	d_{50}	m	2.5×10^{-4}
Kinematic viscosity	μ	m^2/s^2	1.3×10^{-6}
Sediment porosity	p	–	0.4
Relative sediment density	s_{rds}	–	2.65
Bedslope coefficient	γ	m^2/s	5
Sediment porosity	p	–	0.4

Table 2.3: Settings used in the non-linear model Morfo55.

waves approach the shore under a moderate to large oblique angle. However, the non-linear stability analysis will be used to investigate the capacities of a linear stability analysis in a non-linear regime, and forcing conditions will be mild, creating only minor differences between linear friction and Feddersen et al. [2000] friction, and between dissipation according to Thornton and Guza [1983] and Church and Thornton [1993].

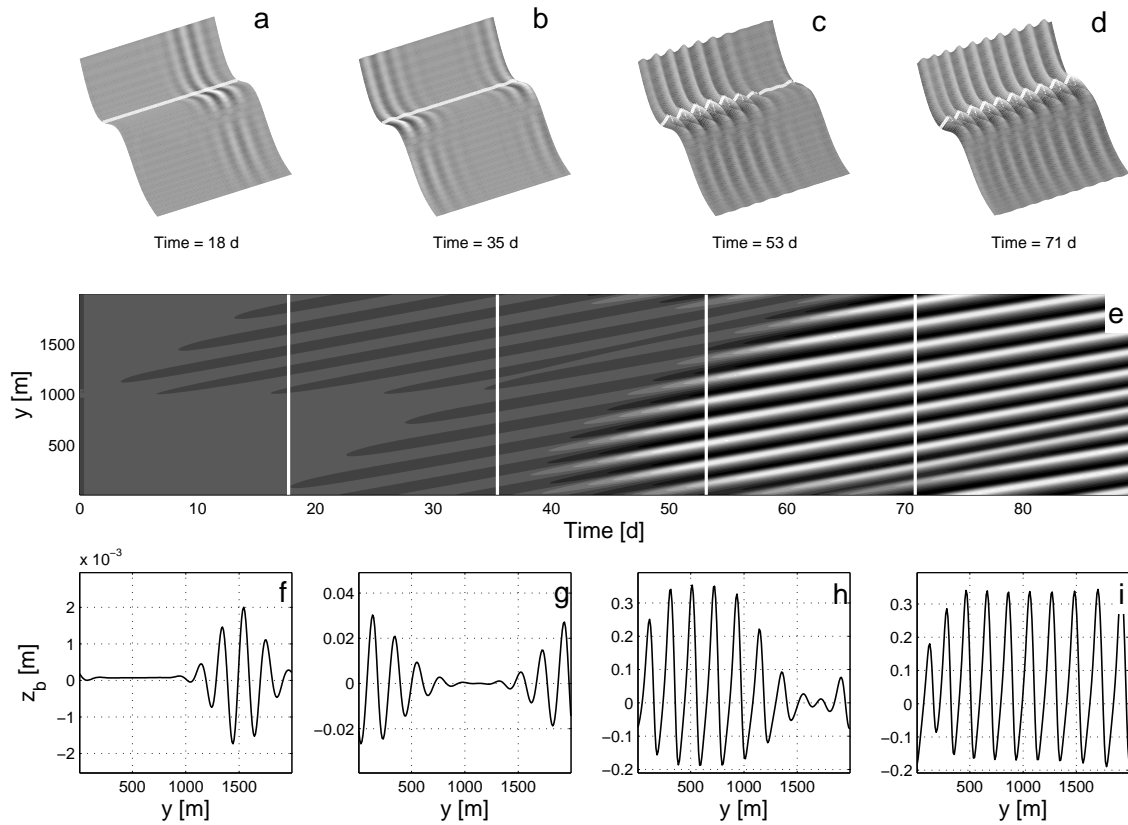


Figure 2.12: (a)-(d) The development of bed patterns at four moments in time under constant oblique wave forcing ($H_{rms} = 0.9$ m, $T_p = 7.5$ s and $\theta = 5^\circ$) at the modelling boundary ($x_{max} = 250$ m). (e) The continuous temporal evolution of one alongshore transect (white areas are crests, whereas black represents troughs). (f)-(i) The alongshore transect at each of the four moments in time.

The temporal evolution of the nearshore region can most easily be depicted by showing the evolution of the seabed (see Fig. 2.12). The top row of figures depict how bed-forms evolve, and migrate under mild oblique wave conditions ($H_{rms} = 0.9$ m, $T_p = 7.5$ s and $\theta = 5^\circ$). The initial bed profile is alongshore constant, derived by Yu and Slinn [2003], originally from Lippmann et al. [1999]. At the start of the run, a 'Dirac function' is placed in the centre of the domain, at the alongshore bar. This 'Dirac function' forms the starting point for the development of crescentic bed patterns. However, the oblique wave forcing causes the perturbation to migrate and so the first bed-forms (Fig. 2.12(a)) appear up-current from the original location of the 'Dirac function'. Also note that the periodic alongshore boundaries make migrating bed-forms re-appear at the down-current end of the modelling domain. Fig. 2.12(a)-(d) show not only how bed patterns migrate, but also that the area where bed patterns occur, expands in the alongshore direction. Whereas initially only one bed-form exists due to the 'Dirac function', this expands gradually towards the alongshore modelling boundaries. The white lines in Fig. 2.12(a)-(d) represent a specific alongshore perturbation profile. These alongshore transects are depicted in Fig. 2.12(f)-(i) for the same moments in time as Fig. 2.12(a)-(d). The continuous temporal evolution of this specific alongshore profile is depicted in Fig. 2.12(e). Not only expand the perturbations in alongshore direction, but the amplitude also increases, reaching a stable height after around 45 days.

Since the purpose of the non-linear results is to investigate to what extent a linear stability analysis can accurately describe field observations, characteristics

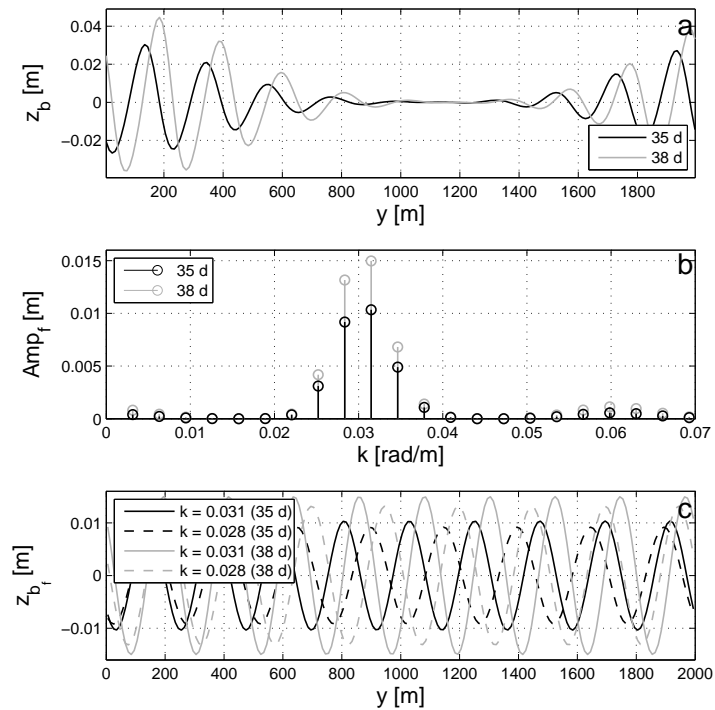


Figure 2.13: (a) The alongshore distribution of the bed perturbation after 35 d (*black*) and 38 d (*grey*). The Fourier analysis of the perturbation profiles after 35 and 38 d. (c) The reconstructed perturbation profiles as a result of the two most dominant frequencies of the Fourier analysis.

of the evolution of bed patterns from the non-linear model should be made comparable to the predictions by a linear stability analysis.

Argus field observations analysed by van Enckevort et al. [2004] give the observed bed pattern length scale in time. This length scale can be compared with λ_{FGM} of a linear stability analysis. A Fourier analysis is carried out to determine the dominant length scale of the output of Morfo55. A Fourier analysis attempts to express a signal (f) as a summation of periodic functions of different wave lengths.

$$f(y) = \frac{a_0}{2} + \sum_{n=1}^{\infty} [a_n \cos(ny) + b_n \sin(ny)] \quad (2.34)$$

Fig. 2.13(a) depicts the alongshore bed perturbation at 35 and 38 days from the start of the run. Fig. 2.13(b) subsequently depicts the Fourier analysis of either signal. The Fourier analysis suggests that the dominant length scale is 200 m ($k = 0.0314$ [rad/m]). The dominant length scale is assumed to correspond with λ_{FGM} of the linear stability analysis.

The number of length scales that can be observed in a run of Morfo55 is limited: The periodic boundaries at the alongshore ends of the domain force the variables at one end of the domain to be mirrored at the other end. This means that once the bed is covered with bed patterns, only a whole number of bed patterns with this periodicity can exist within the modelling domain. Secondly, the Fourier analysis can also only observe length scales that form a function of the total modelling width.

A second important variable that is of interest for the investigation of non-

linear effects, is the linear growth rate. A non-linear stability analysis describes the non-linear evolution, and therefore the growth rate is not linear for the entire period of development. However, linear growth occurs initially when the bed-forms start to develop. The determination of the linear growth rate is based on the change in amplitude of the length scales in the Fourier analysis (Amp_f) (see Fig. 2.13(b)). For each length scale, the amplitude can be determined at each time step ($Amp_f = \sqrt{a^2 + b^2}$). The change in amplitude is used to calculate the linear growth rate:

$$\omega_r = \frac{\ln(Amp_{f_{t=j+1}}/Amp_{f_{t=j}})}{\delta t} \quad (2.35)$$

When the linear growth rate is constant in time, for a specific length scale, this means that this length scale develops linearly, and only linear terms in the equations would be sufficient to describe the development of this length scale accurately.

Finally, the migration rate of bed-forms (c_m) can be determined by calculating the displacement in the periodic output of the Fourier analysis (see Fig. 2.13(c)). The displacement between the peaks in the curve of the dominant mode at day 35 (*black line*) and at day 38 (*grey line*) gives the migration of this length scale over these three days.

In the following chapter, linear stability results are compared with field observations by van Enkevort et al. [2004], using settings that closely represent the field conditions. Chapter 4 subsequently gives an analysis of the influence of pre-existing bed patterns on the development of bed patterns, using the non-linear stability analysis.

Chapter 3

A field test of a linear stability model for crescentic bars*

3.1 The Duck research facility

The Field Research Facility of the United States Army Corps of Engineers at Duck is used to collect numerous kinds of morpho-dynamical data. Duck is located at a barrier island in front of the American East coast (Fig. 3.1, [<http://www.frf.usace.army.mil/frf.shtml>]). Sediment sizes at Duck vary at different cross shore locations, coarser sand can be found at the breaker line ($D_{50} \approx 0.25$ mm), while fine sand can be found further offshore ($D_{50} \approx 0.125$ mm) [Stauble, 1992; Gallagher et al., 1998]. The offshore yearly averaged root mean square wave height (H_{rms}) in this area is 0.63 m and the averaged peak wave period (T_p) is 9.1 s [van Enckevort et al., 2004]. During storm surges the wave height

*The results from this chapter have been presented at the *River Coastal and Estuarine Management Conference*, (2007), Enschede, The Netherlands. The approach presented in section 3.5.2 has appeared in the conference proceedings under [Tiessen et al., 2007]. The other parts of this chapter will be published in *Coastal Engineering*, shortly.



Figure 3.1: The Duck research facility. The facility is located on a barrier island off the East coast of the United States. The pier is located in the middle of the research facility. The beaches around the pier are monitored for bathymetry measurements.

can increase to more than 3 m and the wave period can reach more than 15 s. The tidal variation at Duck is between 1 and 1.3 m. Over the years many researchers have used data from Duck [Lippmann and Holman, 1989; Stauble, 1992; Konicki and Holman, 2000; Elgar et al., 2001; Alexander and Holman, 2004; van Enckevort et al., 2004; Plant et al., 2006].

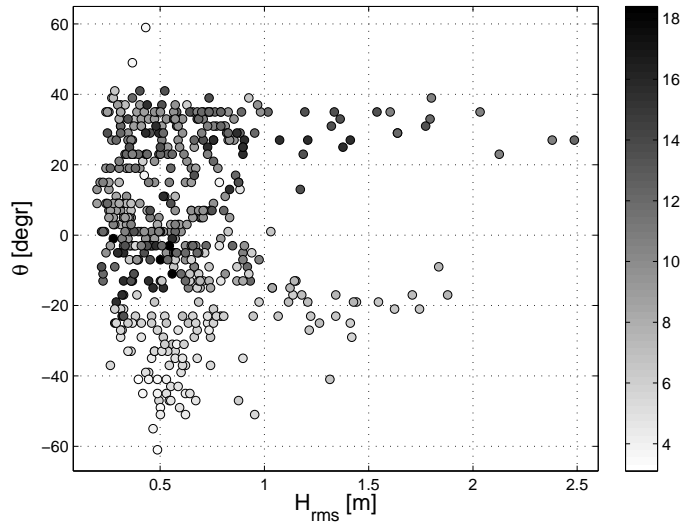


Figure 3.2: Wave conditions during the two month observation period at Duck at the 8 m water depth contour. The wave height (H_{rms}) is plotted versus the wave angle (θ), while the wave period (T_p [s]) is shown in the grey scale of the dots.

3.2 Field data

In this section a description of the data collected at Duck, which is used in this project will be introduced. The model uses wave, bathymetry and tidal data to create predictions of the occurrence and characteristics of crescentic bed patterns. These predictions will be compared with field observations (in section 3.3) that were obtained by van Enkevort et al. [2004] using the Argus imaging technique, which will also be briefly described in this section.

3.2.1 Wave conditions

The offshore wave conditions used in Morfo60 were recorded at Duck at about 8 m water depth, around 1000 m offshore. These wave conditions are refracted back

to the offshore modelling boundary at a water depth of around 35 m. Wave conditions were recorded at 3 hour intervals. Wave data recorded over a two month period in 1998, from August 20th (day 232) until October 22nd (day 294), are used to generate model predictions of the development of crescentic bed patterns at Duck, resulting in 500 different recorded wave conditions and model predictions. The wave angles were recorded from the North and are corrected to describe wave angles normal to the shoreline (the shoreline is determined to be orientated at a -19° angle from the North). Positive wave angles correspond with waves coming from the North to North-West, where negative wave angles correspond to waves coming from the West to South-West.

A wide range of wave angles were measured (Fig. 3.2), up to $\pm 60^\circ$. Large wave heights ($H_{rms} > 1$ m) generally occur for wave angles of approximately $\pm 20^\circ$. The wave period is shown in the grey scale of the dots. The distribution of the wave period shows a clear separation between positive and negative wave angles. Waves approaching the shore from the North to North-West only occur for short wave periods of less than 8 seconds. Large wave angles from the South-West are not restricted in the wave period, reaching up to 16 seconds.

To correctly calculate the wave conditions offshore, the bathymetry needs to be known. Two factors influence the bathymetry: firstly the variability of the seabed. Seasonal variation in the wave conditions causes differences in the bathymetry over time. Secondly, tidal variation causes variable water depths.

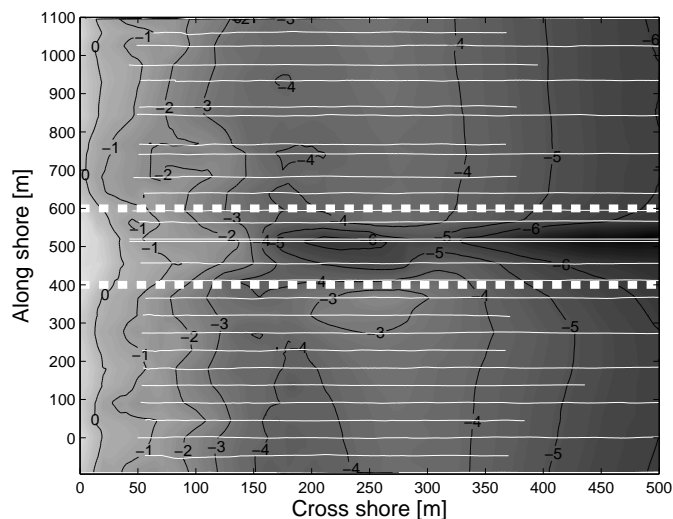


Figure 3.3: The measured bathymetry of the nearshore region at Duck at August 12th 1998. The white lines show the location of the measurements, the thick white dotted lines represent the area around the pier that is excluded from the analysis.

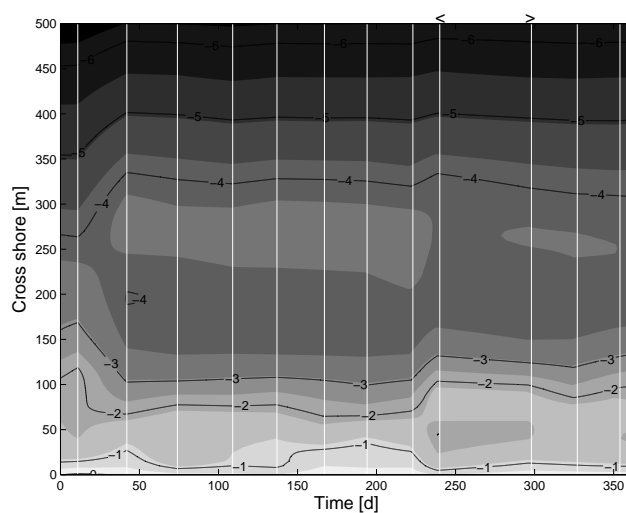


Figure 3.4: The evolution of the alongshore averaged bed profile over 1998. The vertical white lines represent dates when bathymetry surveys were carried out. '<' and '>' on the top of the figure represent the start and the finish of the observation period.

3.2.2 Bathymetry

An alongshore constant beach profile is used to describe the seabed. This beach profile is obtained using field measurements from Duck. Once a month the bed level was measured over a 1000 m wide stretch of beach (Fig. 3.3), out to water depths of about 8 m. Two alongshore bars exist, the nearshore bar is located around 80 m offshore at a depth of around 1.5 m, while an offshore bar is located around 250 – 300 m offshore, at a water depth between 3 and 4 m. Wave breaking generally occurs in front of the onshore bar, although during high wave conditions wave energy dissipation can also partially occur at the offshore bar. The pier, located in the middle of the scanned beach area, causes a significant disturbance in the formation of crescentic bed patterns (see Fig. 3.1). The impact on the water flow and wave propagation [Elgar et al., 2001], results in an increased water depth offshore, while close to the shore the water depth is generally less than the surrounding area (Fig. 3.3). The pier area was excluded from the analysis of the Argus images, presented by van Enckevort et al. [2004], and is also excluded in this research.

Apart from variation of the bar location in the alongshore and cross shore direction due to the presence of bed patterns, seasonal changes can also be observed. In this research, the profiles obtained during the monthly bathymetry surveys are averaged in the alongshore direction and subsequently smoothed using a cross shore weighted average to reduce fluctuations. A 200 m wide area around the pier is excluded from the calculation of the alongshore averaged beach profile (see Fig. 3.3). It is assumed that the bed changes linearly in between the cross shore profiles

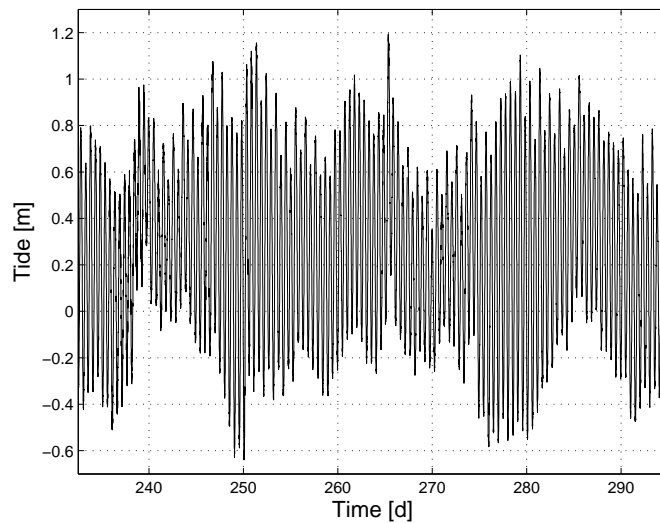


Figure 3.5: The tidal variation at Duck during the observation period.

created by the monthly surveys (Fig. 3.4). Prior to the observation period, a rapid change in the nearshore region occurred, when an onshore terrace deformed into an alongshore bar. Crescentic bed patterns are generally predicted by Morfo60 to develop around this onshore bar.

3.2.3 Tide

The mean water level variation at Duck was recorded at 6-minute intervals (see Fig. 3.5). This not only included the tidal variation, but also surges due to weather conditions. The sum of both the tidal variation and surge at Duck is generally between 1 and 1.5 m [van Enkevort et al., 2004]. This variation in water depth (the term tide subsequently refers to the total mean water level variation) is implemented in Morfo60 by shifting the bed profile. During high tides, the bed is moved downwards resulting in an increased water depth over the bar; at low tide the bed is moved up leading to a decreased water depth over the bar. The bed is



(a)

(b)

Figure 3.6: Argus imaging at Duck: (a) A snapshot of a beach section at Duck. (b) A time-averaged (timex) image of the same beach section, revealing the position of the alongshore bar.

also adjusted in the cross shore direction to account for the increased (decreased) distance between the bars and the shore line.

3.2.4 Argus images

Argus imaging data collected at Duck is considered although it does not form part of the analysis presented in this research; findings using this data were previously published by van Enckevort et al. [2004]. The Argus imaging system is based on wave breaking to determine the location of bed patterns [Lippmann and Holman, 1989]. Waves break when the water becomes shallow. If the water depth decreases very abruptly, more wave breaking will occur. An example of a steep reduction of water depth can be found at bars in front of the shore. Wave breaking produces foam and bubbles, which can be seen in a picture (Fig. 3.6(a), [<http://www.frj.usace.army.mil/frj.shtml>]). If the picture is taken over a longer period of time, more waves will break at different locations along the shore, creat-

ing a band of white foam and bubbles (Fig. 3.6(b)). If there are different cameras at different angles to the shore, these different images can be merged and rotated such that a 180° view can be obtained of bed patterns as they occur nearshore. Argus imaging is a new way of obtaining highly detailed and very frequent data of the nearshore seabed. This way of field observations is still in development and more and more applications are invented for this way of obtaining data [Holman and Stanley, 2007].

Apart from limitations of the photo analysis [Holman and Stanley, 2007], van Enckevoort and Ruessink [2001] showed that changes in wave height and water level can cause significant changes in the observed bar crest position. If there are no alongshore variations in the forcing conditions and the seabed, these effects are similar along a stretch of beach. However, the influence of the pier on the wave height (under oblique wave incidence) can result in local changes of the observed bar crest [Elgar et al., 2001]. In the results presented by van Enckevoort et al. [2004] a variable area around the pier is removed to exclude the local effects of the pier from their analysis.

3.3 Development over time

In order to examine to what extent a linear stability analysis can be used for the correct prediction of the development of crescentic bars, a comparison of model predictions and field observations in time is presented. Fig. 3.7 shows the measured wave and tidal data along with results of the Morfo60 experiments. In Fig. 3.7(a), several durations with large wave heights can be identified. The periods after three storms (day 237, day 264 and day 273) are subsequently examined in more detail. The first of these events is especially severe, when a hurricane makes landfall close to Duck.

Length scale predictions from Morfo60 (λ_{FGM}) immediately after a storm are significantly larger than those predicted in between storms. During and immediately after storms, length scales between 500 and 1000 m are predicted. In between storms, length scale predictions decrease to between 150 and 400 m, until new high wave conditions occur, and the length scale increases. A similar trend is evident in the field data: during the initial development after a storm, length scales ($\lambda_{obs.}$) between 500 and 800 m are observed, while in the ensuing days this decreases to typical values of around 300 m. This bed pattern length is observed until a new storm occurs [van Enckevort et al., 2004]. The relative error between the observed length scales and the predicted length scales ($\delta_{\lambda_{obs.}, \lambda_{FGM}} = \frac{1}{N} \sum_{j=1}^N \left| \frac{\lambda_{obs.j} - \lambda_{FGMj}}{\lambda_{obs.j}} \right|$) is 0.44.

Field observations show a more gradual bed pattern development after storms than the model predictions. Model predictions fluctuate more rapidly over time due to changing forcing conditions (wave and tide) and because the model does

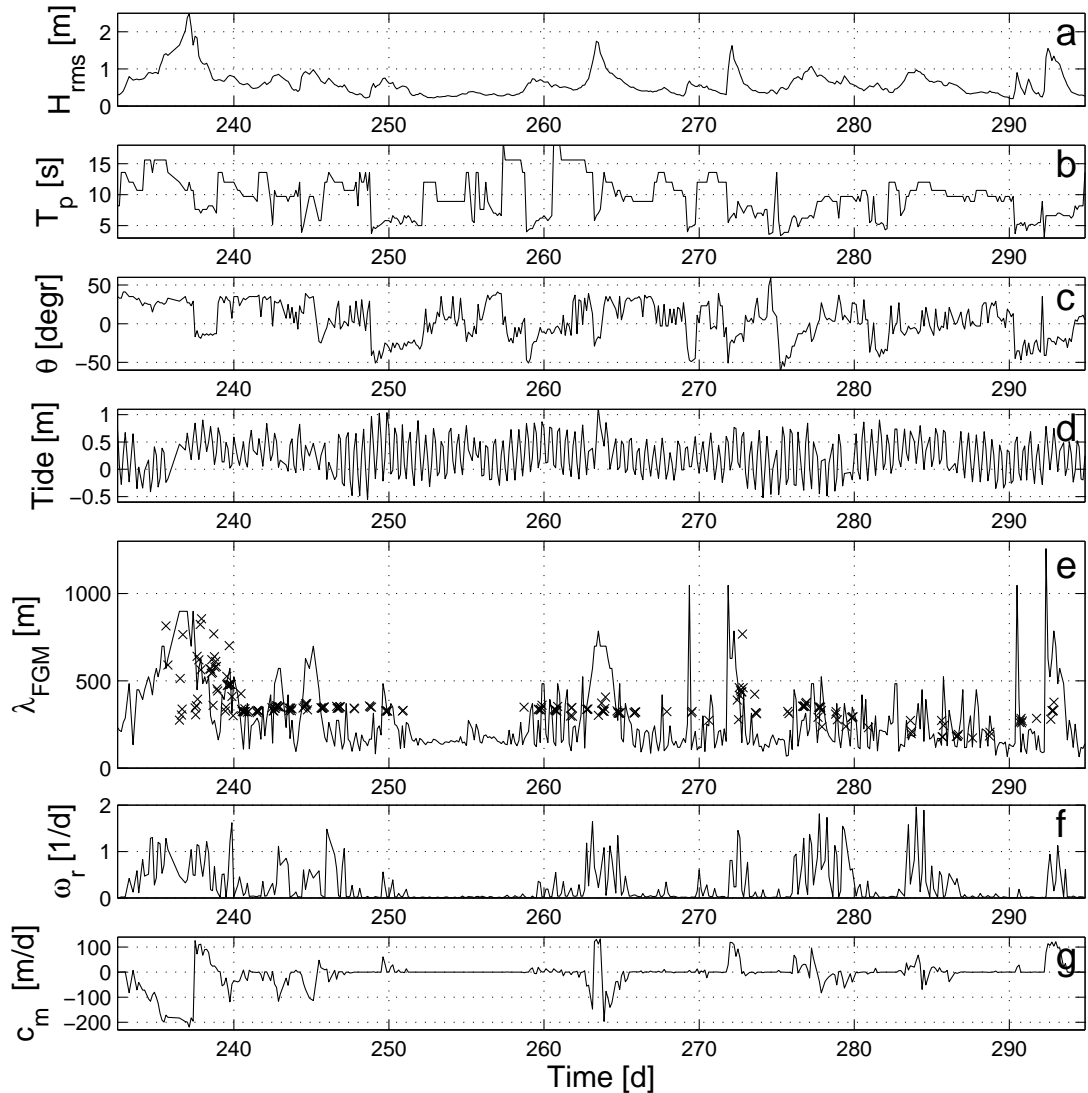


Figure 3.7: Morfo60 model predictions and corresponding wave conditions during the observation period. (a, b, c) depict the forcing wave conditions (wave height (H_{rms}), wave period (T_p) and angle of the incoming waves (θ)) as they were collected at the wave gauge in front of the Duck coast. (d) shows the tidal variation at the same time as the wave records, as it was recorded at the pier at Duck. (e, f, g) show the resulting bed pattern length (λ_{FGM}), growth rate (ω_r) and migration rate (c_m) as predicted by Morfo60. (e) shows both the predicted length scale (solid line) and the field observations (\times). The horizontal axis represents time in all graphs, from August 20th 1998 (day 232), until October 22nd 1998 (day 294).

not take pre-existing bed patterns into account. An algorithm to identify the more physically meaningful model predictions will be presented in section 3.5.

High wave conditions generally coincide with increased growth and migration rates. Predicted migration rates are generally small, but can be as big as 200 m/day during high wave conditions. In reality, migration rates of up to 60 m/day are observed at Duck during this period [van Enkevort et al., 2004], although at other locations migration rates up to 180 m/day occur [van Enkevort and Ruessink, 2003b].

A second major influence on the model predictions is the tidal level. Tidal variation strongly influences the growth rate. The growth rate decreases for increased tidal levels.

The effects of the wave angle and the wave period on the model predictions cannot be observed distinctly in these plots.

Fig. 3.8 shows the corresponding accumulated growth for each wave number ($k_{FGM} = \frac{2\pi}{\lambda_{FGM}}$) over the two month observation period. The accumulated growth is the sum of the predicted growths ($\sum \omega_r \Delta t$) for each length scale during the modelled period. Two length scales with significantly larger accumulated growths can be identified: $k_{FGM} = 0.011$ and 0.023 rad/m ($\lambda_{FGM} = 570$ and 273 m, respectively). These peaks roughly correspond to the length scales observed in the field [van Enkevort et al., 2004]: around 500 to 800 m (immediately after a storm), and around 300 m (in between storms).

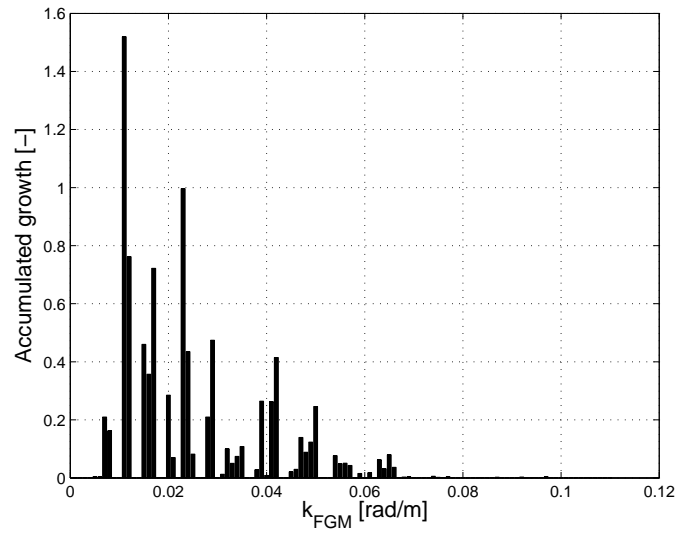


Figure 3.8: The accumulated growth ($\sum \omega_r \Delta t$) for each wave number ($k_{FGM} = \frac{2\pi}{\lambda_{FGM}}$) for all model predictions during the observation period.

Large variations occur in the model predictions due to the changing forcing conditions in combination with the assumed alongshore constant beach profile. Before these variations are addressed and a closer comparison between field observations and model predictions is presented, an analysis of the relationships between the different forcing conditions and crescentic bed pattern characteristics of the model predictions is given.

3.4 Relationships between input and output parameters

In using Morfo60 to reproduce the development of crescentic bed patterns over the 2-month period at Duck, changes in several parameters were implemented; i) changing wave conditions; ii) changing tidal levels; iii) gradual change in the beach profile. The impact of these different conditions on the model predictions (growth rate, migration rate and length scale) are examined.

3.4.1 Wave conditions

The effects of changing wave conditions on the development of crescentic bed patterns has been studied before (Deigaard et al. [1999], Calvete et al. [2005]). In these sensitivity analyses the effects of changes in individual wave parameters were investigated; the combined effects of actual wave data were not presented. Fig. 3.9 shows the effects of the different wave conditions recorded at Duck on all model predictions. The effect on the model predictions of reversing the sign of the incident wave angle whilst keeping other forcing conditions the same is limited to reversing the migration direction and orientation of the bed patterns. The reason for showing both negative and positive wave angles is to illustrate the potential range of different wave conditions and therefore model predictions for the different wave angles.

Calvete et al. [2005] presented a sensitivity analysis of the Morfo60 model for different wave conditions. It was observed that large wave heights or wave angles

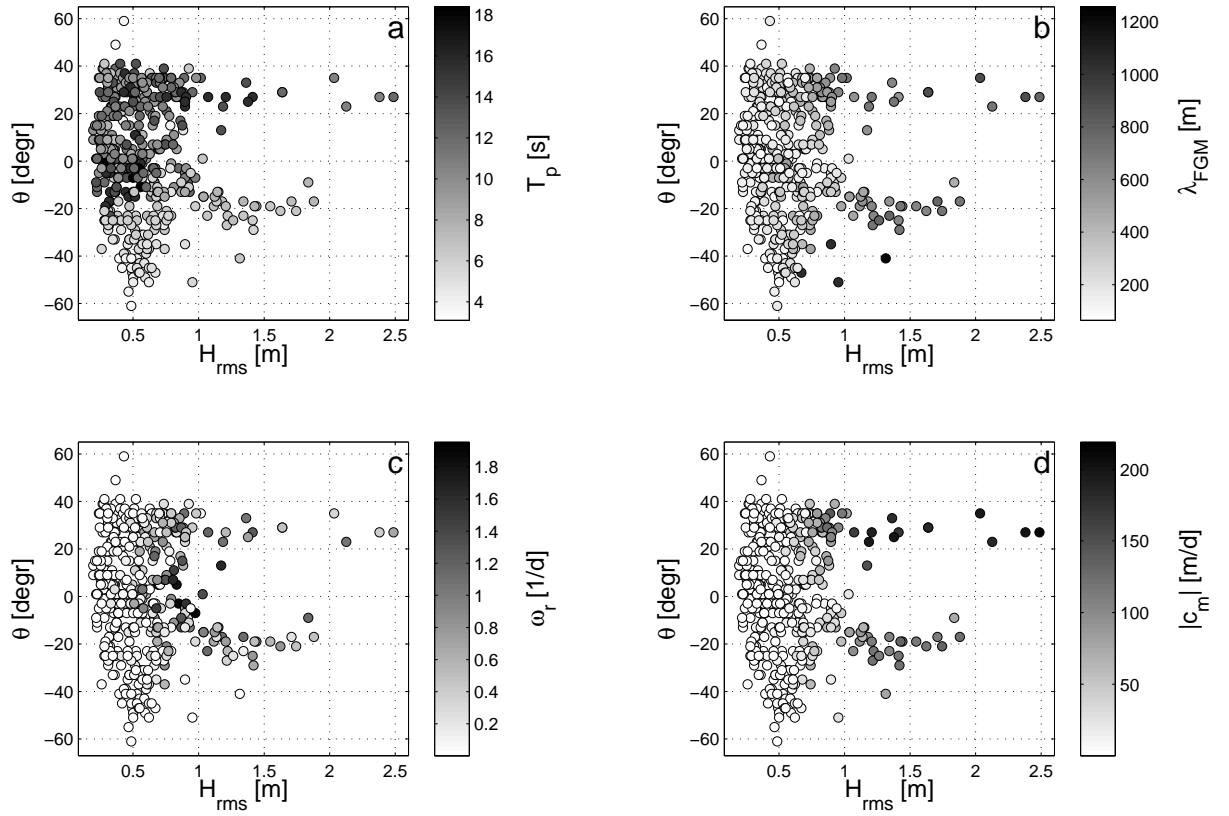


Figure 3.9: The distribution of the recorded wave conditions and model predictions.

The data is distributed between wave height (H_{rms}) on the x axis and wave angle (θ) on y axis. The grey scale of the dots depicts the value of (a) the wave period (T_p) and the output parameters: (b) λ_{FGM} , (c) ω_r , and (d) $|c_m|$.

resulted in increased length scales of crescentic bed patterns. The distribution of different wave conditions at Duck and the resulting predicted bed pattern lengths are shown in Fig. 3.9(b). The strong influence of the wave angle on the predicted length scale can also be observed in these results. Increased length scales are predicted for increased wave heights, although the largest length scales occur for moderate wave conditions ($0.6 < H_{rms} < 1.4$ m) and extreme wave angles ($\theta < -30^\circ$).

Calvete et al. [2005] also showed that increased wave heights or wave periods, or a decrease in wave angle would result in increased growth rates of the predicted bed pattern. The influence of the wave conditions at Duck on the growth rate (Fig. 3.9(c)) reveals that the highest growth rates do not, however, occur for the highest waves and greatest wave periods, but for more moderate conditions ($0.6 < H_{rms} < 1.2$ m and $8 < T_p < 12$ s). Large wave heights generally correspond with increased wave angles while increased wave periods correspond with small waves or increased wave angles, reducing the growth rate in both cases. The greatest growth rates occur for small wave angles ($|\theta| < 10^\circ$). These findings suggest that under field conditions growth rates and length scales may not exhibit the relationships generated in the reported sensitivity analyses, and that these characteristics depend on the range of occurring forcing conditions.

The influence of the wave conditions on the migration rate was not presented by Calvete et al. [2005]. The wave data distribution at Duck (Fig. 3.9(d)) shows that increased wave heights ($H_{rms} > 0.8$ m) together with moderate wave angles

($20^\circ < |\theta| < 40^\circ$) correspond with large migration rates. Wave angles that are larger still are not only accompanied by decreased wave heights, but also by a sharp decrease in wave periods, both resulting in decreased migration rates.

Finally, the distribution of the different crescentic bed pattern characteristics can be compared. Comparing the length scale and migration rates in Fig. 3.9(b) and 3.9(d) suggests that predictions of large length scale crescentic bed patterns ($\lambda_{FGM} > 800$ m) generally correspond with large migration rates ($c_m > 120$ m/day). Also interesting to note is that the greatest growth rates roughly correspond with more moderate length scales ($\lambda_{FGM} < 700$ m) and migration rates ($|c_m| < 100$ m/day).

3.4.2 Bed profile

Several bed profiles were investigated to study the effects of the changing along-shore constant bed profile. The bed profile at the start and at the end of the observation period are tested as well as the profile described by Yu and Slinn [2003] (see Fig. 3.10(a)). The Yu and Slinn [2003] profile is an approximated description of the beach profile measured at Duck in October 1990, and is used previously by Calvete et al. [2005]. The bed profiles at the start and the end of the observation period, both show two alongshore bars, while in the Yu and Slinn [2003] profile only the onshore bar occurs. The major difference between the profiles at the start and the end of the observation period is the lower (0.2 m) onshore bar at the start of the observation period. The onshore bar in the Yu and Slinn [2003] profile is more similar to the bar profile at the end of the observation period.

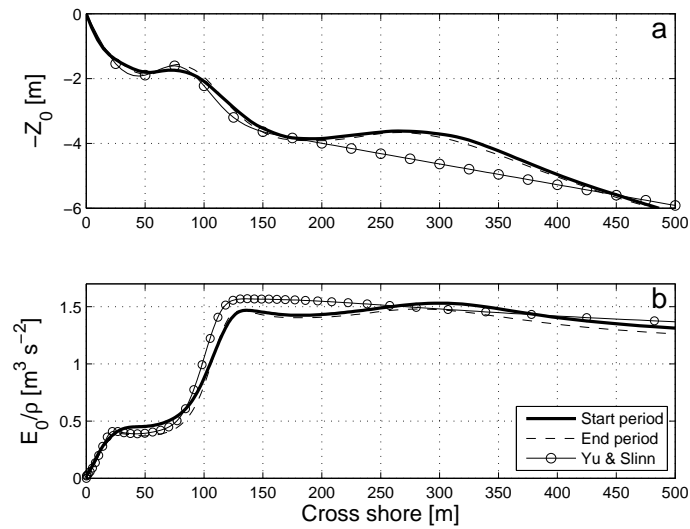


Figure 3.10: The different wave energy distributions for different bed profiles (at the start of the observation period, at the end and the Yu and Slinn [2003] profile).

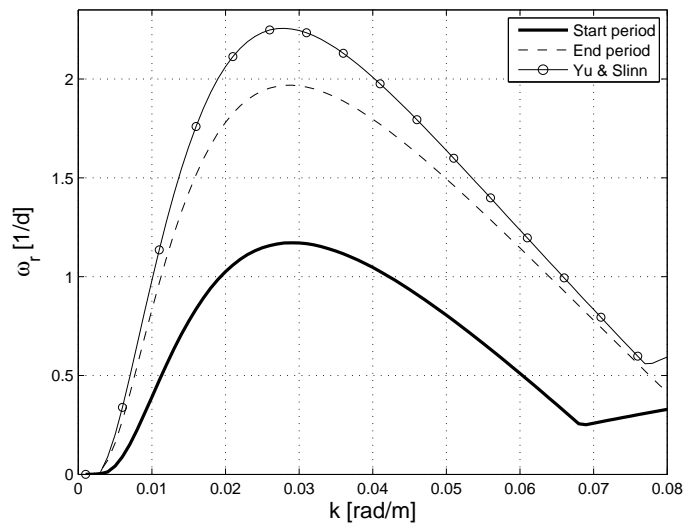


Figure 3.11: The growth rate (ω_r [1/d]) as a function of the wave number (k [rad/m]) for different bed profiles.

Moderate wave conditions ($H_{rms} = 1$ m, $T_p = 8$ s, $\theta = 3^\circ$) are applied at the modelling boundary and Morfo60 model output for the three different bed profiles results in three different wave energy distribution plots (Fig. 3.10(b)) and growth rate curves (Fig. 3.10). The reduction of the wave energy in front of the onshore bar gives an indication of the growth rate of crescentic bed patterns which form at this cross shore location. A growth rate curve depicts the predicted growth rate (ω_r) for each examined perturbation length scale ($\lambda = \frac{2\pi}{k}$), for a certain set of forcing conditions described in the basic state. The biggest growth rate within one curve represents the length scale that is assumed to dominate the other length scales (λ_{FGM}). The growth rate curves for the three different bed profiles show a similar shape, and the fastest growing mode is occurring for similar k values ($k \approx 0.029$ rad/m, $\lambda \approx 216$ m). However, the actual growth rate is different for the different cases; the occurrence of an offshore bar reduces the growth rate ($\omega_r = 2.3$ 1/d for the Yu and Slinn [2003] profile, compared to $\omega_r = 2.0$ 1/d for the profile at the end of the observation period), and a lower onshore bar also results in a decreased growth rate ($\omega_r = 1.2$ 1/d for the profile at the start of the observation period). The different growth rate curves correspond well with the observed reduction in the wave energy in front of the onshore bar. Due to the absence of the offshore bar, the wave energy plot for the Yu and Slinn [2003] profile depicts a higher energy level in front of the onshore bar. Whereas, energy is dissipated in front of the offshore bar for the other two bed profiles. The reduction in wave energy on and in front of the onshore bar is less for the bed profile with a lower onshore bar height, reducing the height of the growth rate curve for the profile at

the start of the observation period.

The results are consistent with findings of Calvete et al. [2007], concerning the height of the onshore bar; an increased bar height results in increased growth rates of the crescentic bed patterns. Secondly, the existence of an offshore bar results in a decrease of predicted growth rates (similar to Klein et al. [2003]).

In comparison with the influence of other input parameters, the effect of the gradual change in bed profile on the length scale, growth rate and migration rate of crescentic bed patterns is negligible. Changes in waves and the tide have a much stronger influence on the predicted bed pattern characteristics. Tidal variation results in significantly larger changes in the beach profile than the gradual change seen in the alongshore averaged beach profile itself. Tidal variation results in a bed height variation up to 2 m, whereas changes in the alongshore averaged seabed just result in a 20 cm difference between the start and end of the observation period. In the runs carried out to describe the development of crescentic bed patterns at Duck, both tidal variation and the alongshore averaged bed change over time. Since this change is mainly the result of the tidal variation, the effects of variation of the alongshore constant bed level are included in the following section, concerning tidal variation.

3.4.3 Tidal variation

Tidal variation has not been considered in previous research that uses a linear stability analysis to describe the development of crescentic bed patterns. Therefore

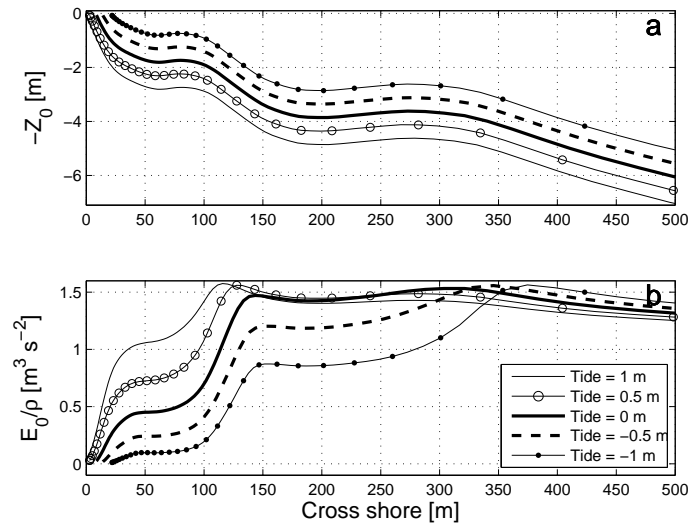


Figure 3.12: The cross shore bed profiles and wave energy distributions for different tidal levels (tide = -1 m, -0.5 m, 0 m, 0.5 m and 1 m). The location of the shoreline is varied for different tidal levels to ensure that the peak of the onshore bar occurs at the same location.

a more extensive analysis of the effects of tidal variation on the model predictions is presented here. The analysis comprises two kinds of results. First a sensitivity analysis is presented of the effects of variation of the tidal level on crescentic bed pattern characteristics. Secondly, the influences of the actual conditions at Duck on the model predictions are investigated.

Sensitivity analysis

Moderate wave conditions ($H_{rms} = 1$ m, $T_p = 8$ s and $\theta = 3^\circ$) are applied at the offshore modelling boundary, using the bed profile at the start of the observation period in order to represent characteristic post storm conditions. The effect of

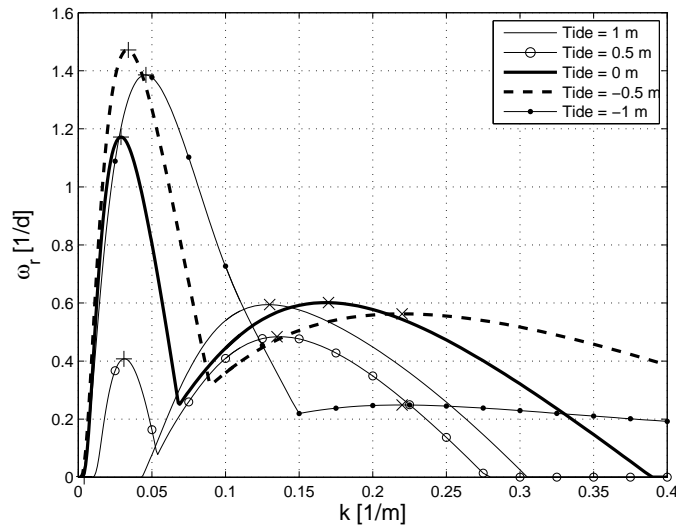


Figure 3.13: The growth rate (ω_r) as a function of the wave number (k) for moderate wave conditions ($H_{rms} = 1$ m, $T_p = 8$ s and $\theta = 3^\circ$) for different tidal levels (tide = -1 m, -0.5 m, 0 m, 0.5 m and 1 m). The fastest growing crescentic mode is shown with a +, while \times represents the *FGM* of transverse bars.

tidal variation on the model predictions of Morfo60 is examined using five different tidal levels (-1 m, -0.5 m, 0 m, 0.5 m and 1 m) (see Fig. 3.12).

The variation of the tidal level and the resulting change of water depth above the two bars (Fig. 3.12(a)) cause the wave energy to decrease at different cross shore locations for different tidal levels (Fig. 3.12(b)). The decrease in wave energy in front of the onshore bar is suggestive of the development of crescentic bed patterns at this location. At the highest tidal levels energy dissipation occurs mainly at the shoreline, and the decrease in wave energy on top of the onshore bar is limited, and non-existent on top of the offshore bar. However, the lowest

tidal levels cause waves to break already offshore, and to a limited extent at the onshore bar, with hardly any wave energy reaching the shoreline.

Fig. 3.13 shows the growth rate curves for the different tidal levels. The growth rate curves for each tidal level apart from the highest tide ($Tide = 1$ m) actually comprise two separate growth rate curves, which correspond to different bed patterns. The switch from one curve to the other is apparent in the abrupt change in $d\omega_r/dk$. The first curve (peak shown with a '+') occurs around $k \approx 0.02 - 0.05$ rad/m ($\lambda \approx 125 - 315$ m), and describes the development of crescentic bed patterns. The second curve (peak shown with 'x') occurs around $k \approx 0.1 - 0.25$ rad/m ($\lambda \approx 25 - 67$ m), and describes the development of a bed pattern previously described as transverse bars [Ribas and Kroon, 2007]. Therefore, as k is increased the fastest growing bed-form at that value of k switches from a crescentic to a transverse bar at some point (apart from for the highest tidal level, where only the development of transverse bars is predicted). The focus of this research lies with the development of crescentic bed patterns and so pattern length scales < 57 m ($k > 0.11$ rad/m) are not taken into consideration.

The growth rate of the crescentic bed patterns is strongly influenced by the tidal level, with predicted growth rates decreasing for larger tidal levels, and in fact for 1 m tidal level no growth is predicted. Increased growth rates for smaller tidal levels are the result of increased wave breaking on the nearshore bar (Fig. 3.12), and therefore more wave stirring and increased sediment transport rates [Falqués et al., 2000]. Also λ_{FGM} of the crescentic bed patterns decreases for low tidal levels.

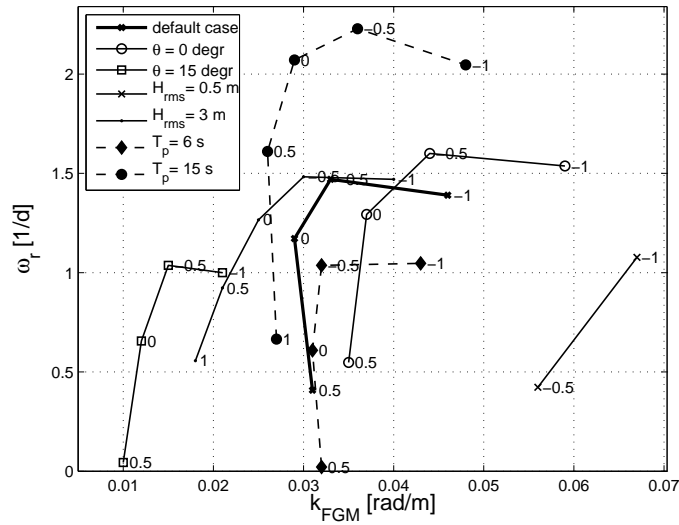


Figure 3.14: The wave number (k_{FGM}) and the growth rate (ω_r) of the fastest growing crescentic mode as a function of the tidal level (tide = -1 m, -0.5 m, 0 m, 0.5 m and 1 m) for different wave conditions (default case: $H_{rms} = 1$ m, $T_p = 8$ s, and $\theta = 3^\circ$, the legend shows which wave parameter is altered). The different wave conditions represent different circumstances at Duck. The tidal level is depicted next to each data point. In some cases no development of crescentic bed patterns is predicted for higher tidal levels, in which case the line is truncated.

The effects of the tidal level for different wave conditions are examined in detail in Fig. 3.14. A consistent relationship between tidal level and the growth rate and length scale of crescentic bed patterns can be observed. λ_{FGM} increases from lowest to highest tidal levels. This change in length scale is, however, mostly limited to the lowest tidal levels. Conversely, the growth rate decreases from lowest to highest tidal level, and the change is limited to the highest tidal levels.

This change in growth rate is the result of increased wave breaking on top of the onshore bar for low tidal levels. The highest tidal levels result in wave breaking at the shore and the development of transverse bars (see Fig. 3.13), as the peak in the transverse bar curve exceeds that for the crescentic bars. As the tidal level decreases, wave breaking shifts gradually to the onshore bar, resulting in increased stirring, sediment transport rates, and growth rates there [Falqués et al., 2000]. For the lowest tidal levels, wave breaking starts to occur on top of the offshore bar, with the beach being saturated further onshore, resulting in similar growth rates regardless of further reduction in tidal levels. The predicted migration rates of crescentic bed patterns are not presented in this figure, but this research showed that increased tidal levels generally result in increased migration rates. The reason for the increase in length scale of the crescentic bars at high tidal levels is not clear. It would be tempting to ascribe the decrease in length scale as tidal level falls to greater refraction before the waves break on the onshore bar, but a similar relationship is observed for normally incident waves.

As was shown by Calvete et al. [2007], small changes in bathymetry can significantly influence the length scale and in particular the growth rate of crescentic bars. Changes in bathymetry characteristics (crest height, trough depth, offshore beach slope etc.) all influence the growth rate and length scale. The tidal variation at Duck causes significant changes in most of these measures concurrently, however the observed relationships between the tidal level and the length scale and growth rate of crescentic bed patterns do not obviously correspond with the behaviours reported by Calvete et al. [2007]. It should also be noted that changes in the length and time scale in Fig. 3.14 greatly exceed those shown in Calvete et al.

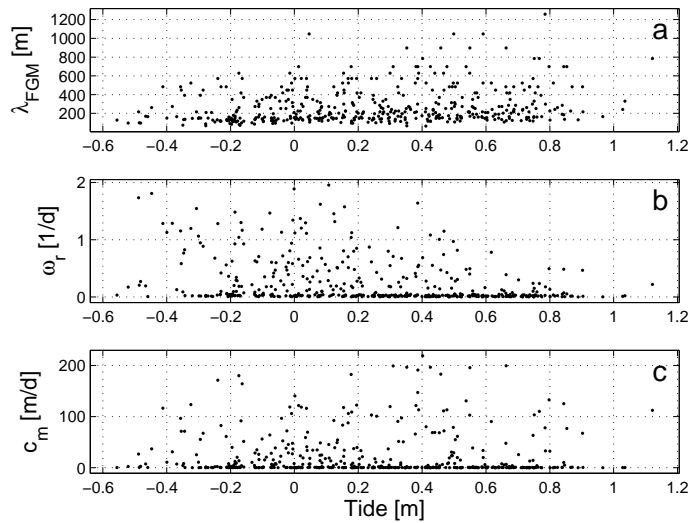


Figure 3.15: (a) The alongshore spacing (λ_{FGM}), (b) the growth rate (ω_r), and (c) the migration rate (c_m) of the fastest growing mode as a function of the tidal level, for all wave data recorded at Duck during the observation period.

[2007]. This is because the changes in beach profile (due to tidal level changes) greatly exceed those examined by Calvete et al. [2007], where, moreover, changes in only one part of the profile were examined in each experiment; here, the tidal changes affect all parts of the profile simultaneously.

Effects of the tide on the Duck results

In Fig. 3.15 the model predictions for Duck are plotted against the tidal level. There is some evidence that small tidal levels do indeed result in increased growth rate predictions, which is expressed in the moderate correlation coefficient ($\rho = \frac{\sum_{j=1}^N (A_j - \bar{A})(B_j - \bar{B})}{\sqrt{\sum_{j=1}^N (A_j - \bar{A})^2 \sum_{j=1}^N (B_j - \bar{B})^2}}$, where A and B represent different variables, and N is the number of field observations) between these two parameters: $\rho_{Tide, \omega_r} = -0.32$.

Changes in the predicted bed pattern length scale due to tidal variation are less clearly visible ($\rho_{Tide,\lambda} = 0.22$). The largest λ_{FGM} predictions occur for larger tidal levels, but a shift in length scale due to changes in tidal level is not visible in this graph. Fig. 3.15(c) depicts the effects of changes in the tidal level on the migration rate of the predicted bed patterns. No clear relation between the two parameters can be identified ($\rho_{Tide,|c_m|} = -0.02$) since changes in the migration rate are strongly influenced by changing wave conditions (see section 3.4.1).

3.5 Physically significant developments algorithm

3.5.1 Introduction

As mentioned in section 3.3, the Morfo60 predictions of the crescentic bed pattern length scale can vary widely from one wave record to the next. This variation suggests frequent changes in the development of crescentic bed patterns, whilst in reality a gradual development is observed in between storms. These model variations are, in fact, the direct result of changing tidal and wave conditions recorded at Duck and applied in Morfo60. Linear stability analyses have a significant limitation in that they do not take into account the pre-existing bed patterns, which may influence the subsequent morphological evolution.

The discrepancy between the fluctuating nature of the model predictions and the more gradual development in the field observations makes it challenging to apply knowledge obtained from a linear stability analysis of the development of crescentic bed patterns for engineering or management purposes. Similarities between predictions and field observations can nonetheless be observed. For instance both show large crescentic bed pattern length scales after storms and more moderate length scales in between storms. Secondly, Fig. 3.7 and Fig. 3.8 show that the λ_{FGM} -values over the two month period are similar to corresponding $\lambda_{obs.}$ -values after and in between the storms.

If a linear stability analysis is to be of use for engineers and managers in describing the development of crescentic bars or the occurrence of rip channels, an approach must be developed whereby physically more significant information can

be extracted. Correspondingly, the goal is to develop a physically based algorithm that can extract the physically more meaningful model predictions.

Differences between field observations and model predictions suggest that the influence of antecedent model predictions is necessary for the correct description of the development of crescentic bed patterns. Fig. 3.8 shows that the fastest growing length scales are similar to the observed length scales. This suggests that if the growth rate of the model predictions is taken into account, the predicted fastest growing length scales during the 2 month observation period will be similar to field observations.

One limitation of a stability analysis cannot be implemented in the physically significant developments algorithm (the *PSD* algorithm). The linearised equations reduce the capabilities of such a model to only the initial development of bed patterns. The linear stability model should therefore specifically be orientated at periods when initial developments of bed patterns occur in the field. In other words, the main strength of this algorithm lies in the prediction of physically meaningful model predictions post-storm.

In the following section several versions of the algorithm are presented and examined. The results from the most suitable algorithm are compared with the field observations, and determined is the extent to which this algorithm improves the prediction of observed length scales, compared with the original Morfo60 results.

3.5.2 Testing different algorithms

The algorithm is based on two assumptions. (1) It is more likely that a certain length scale will be observed at a certain time, if prior to this moment, the model has predicted similar length scales (λ_{FGM}) of crescentic bed patterns. (2) The growth rate (ω_r) of the bed pattern is a measure of the “importance” of the prediction. In other words, model predictions with larger growth rates are more likely to be observed.

The algorithm is designed to show when a significant event occurs. These significant events are periods when the predicted length scale of crescentic bed patterns (λ_{FGM}) and the field observations ($\lambda_{obs.}$) are likely to show similarities. A significant development is defined as a period of time when both the bed-form grows by a significant factor and consistent length scales (λ_{FGM}) are predicted. In the determination of physically significant events only the fastest growing mode at each time step is taken into consideration.

The cumulative growth factor describes the amount of change in the height of a bed pattern (h) from one time to another (see also Falqués [2006]), and is given by:

$$\frac{h_{j=m}}{h_{j=n}} = \exp \left[\sum_{j=n}^m \omega_{r_j} \Delta t \right] \quad (3.1)$$

where the duration over which the accumulated growth ($\sum \omega_{r_j} \Delta t$, see section 3.3) is determined, is between $t = n\Delta t$ and $t = m\Delta t$ and Δt is the time between the field measurements (3 hours). n increments between the model predictions at the start and at the end of the observation period ($n = 1 \rightarrow 500$). For each value

Table 3.1: The characteristics of the *PSD* algorithm for the three different cases.

	$\lambda_{sig.} [m]$	$(\lambda^+ [m], \lambda^- [m])$	Significance*
Case 1	λ_n	$\lambda_{sig.} - 100, \lambda_{sig.} + 100$	$\sum_{j=n}^m \Pi_j < 0.5 \sum_{j=n}^m (1 - \Pi_j)$
Case 2	$\frac{\sum_{j=n}^m \lambda_j}{m-n}$	$(1 - \frac{1}{4})\lambda_{sig.}, (1 + \frac{1}{4})\lambda_{sig.}$	$\sum_{j=n}^m \Pi_j < 0.5 \sum_{j=n}^m (1 - \Pi_j)$
Case 3	$\frac{\sum_{j=n}^m \omega_{r_j} \lambda_j}{\sum_{j=n}^m \omega_{r_j}}$	$\frac{2\pi}{10\Delta k + k_{sig.}}, \frac{2\pi}{-10\Delta k + k_{sig.}}$	$\sum_{j=n}^m \Pi_j \omega_{r_j} < 0.5 \sum_{j=n}^m (1 - \Pi_j) \omega_{r_j}$

* "Significance" stands for the determination of the maximum number of results outside the bandwidth, which is still allowed within a significant event.

of n, m increments between n and the moment when a threshold minimum of cumulative development is reached. The minimum cumulative development is set at 50 % of the initial bed pattern height ($\frac{h_{j=m}}{h_{j=n}} = 1.5$); thus for this period of time to be identified as a significant event we must have growth by a factor of 1.5 or more. Further, model predictions must show consistent length scales over time. This is quantified using a constant bed pattern length scale ($\lambda_{sig.}$).

Different versions of the algorithm defining physically significant developments have been developed. Here, three different cases will be presented (see table 3.1).

Case 1

The most basic version of the *PSD* algorithm consists of the initial value ($j = n$) of λ to be used as the constant bed pattern length ($\lambda_{sig.} = \lambda_n$). Consistency in length scale is assumed if $\lambda^- < \lambda_{sig.} < \lambda^+$. This band width (λ^-, λ^+) is set at 100 m around $\lambda_{sig.}$. Finally, an event is only assumed to be significant if the number of length scale predictions outside the band width is limited. The number of bed pattern length scales outside the band width (λ^-, λ^+) is compared to that of those inside this range:

$$\sum_{j=n}^m \Pi_j < 0.5 \sum_{j=n}^m (1 - \Pi_j), \quad (3.2)$$

where $\Pi_j = 0$ when λ_j is inside the band width, and $\Pi_j = 1$ for length scales outside the band width.

The results of the first version of the *PSD* algorithm are shown in Fig. 3.16. The algorithm observes physically significant developments during most of the observation period. Instead of emphasising the more important model predictions, the main effect is the dampening of fluctuations in the original predictions of Morfo60.

The focus of this research is on post storm conditions. The current settings of the *PSD* algorithm do not specify these conditions clearly, though. The significant developments seem to occur during periods in between storms, when low wave conditions occur. For these periods, the model predicts small bed pattern lengths and growth rates. For low wave conditions, the bed pattern length predictions are rather constant. Due to the fixed value of (λ^-, λ^+), these slow growing bed patterns can become physically significant developments. In regions of longer

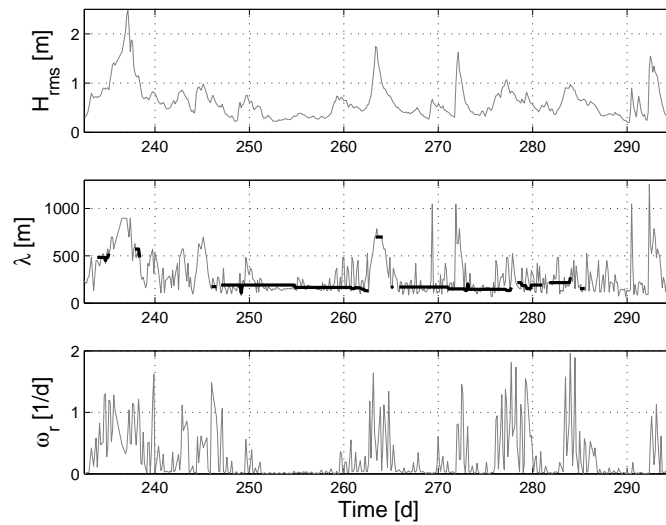


Figure 3.16: The *PSD* algorithm results for case 1: (a) the measured wave height in time, (b) the predicted length scale along with the *PSD* algorithm results, (c) the predicted growth rate. The grey line depicts the normal Morfo60 results, while the thick grey line represents the moments where physically significant events occur ($\lambda_{sig.}$).

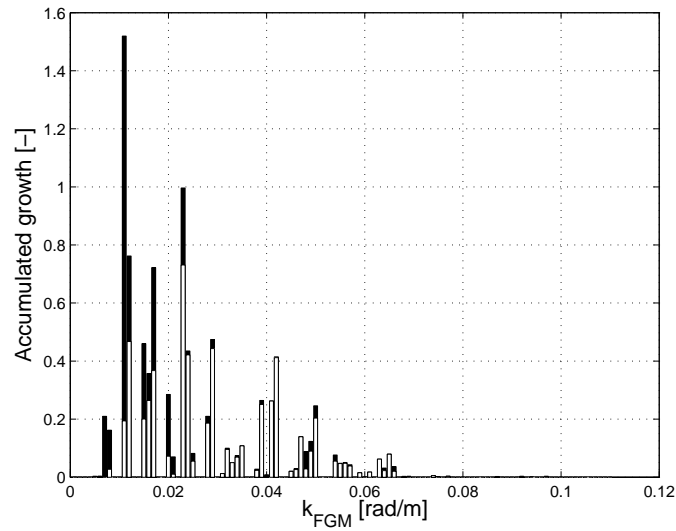


Figure 3.17: The accumulated growth for each wave number for the modelled period of time. The total length of the bars represent the total accumulated growth, while the white part of each bar represents the growth during *PSD* periods.

bed pattern length predictions, few periods with significant developments are observed, due to the increased spacing between adjacent length scales ($\lambda = \frac{2\pi}{k}$, $\Delta k = 0.001$ rad/m).

Fig. 3.17 shows which part of the accumulated growth is covered by the *PSD* algorithm. The fastest growing length scales according to the model predictions are hardly included in the *PSD* algorithm results. Since under low wave conditions, more constant bed pattern length scale predictions occur, the *PSD* algorithm is most suitable for shorter length scales ($k > 0.02$ rad/m).

Case 2

A more sophisticated formulation of the *PSD* algorithm quantifies the consistency in the predicted length scales differently. Instead of using a fixed value for the constant bed pattern length ($\lambda_{sig.}$), in the second case the value of $\lambda_{sig.}$ is determined as an average of the bed pattern lengths included.

$$\lambda_{sig.} = \frac{\sum_{j=n}^m \lambda_j}{m - n} \quad (3.3)$$

While the number of included model results (m) increases, the average will be composed of more bed pattern length predictions. Due to different spacings between adjacent length scales ($\lambda = \frac{2\pi}{k}$), the use of a constant value for the margin for constant wave length predictions (λ^-, λ^+) is not optimal. In this case, $\Delta\lambda$ is a fraction of $\lambda_{sig.}$, and is chosen to produce significant developments during post-storm periods. These settings are case sensitive, and will change for different locations and forcing conditions.

$$\lambda^+ = (1 - \frac{1}{4})\lambda_{sig.}, \quad \lambda^- = (1 + \frac{1}{4})\lambda_{sig.} \quad (3.4)$$

The number of bed patterns that is allowed outside this range is set as in case 1.

The physical developments determined for the second case (see figure 3.18), focus more around the high wave conditions. The *PSD* algorithm identifies periods with predictions of fast growth rates. These periods correspond with high wave conditions and generally longer bed pattern predictions. In this case, the value of (λ^-, λ^+) is dependent on $\lambda_{sig.}$, which results in the exclusion of most small bed pattern lengths as physically significant developments. The settings used in case 2 exclude most periods, for not showing consistency in length scale in combination

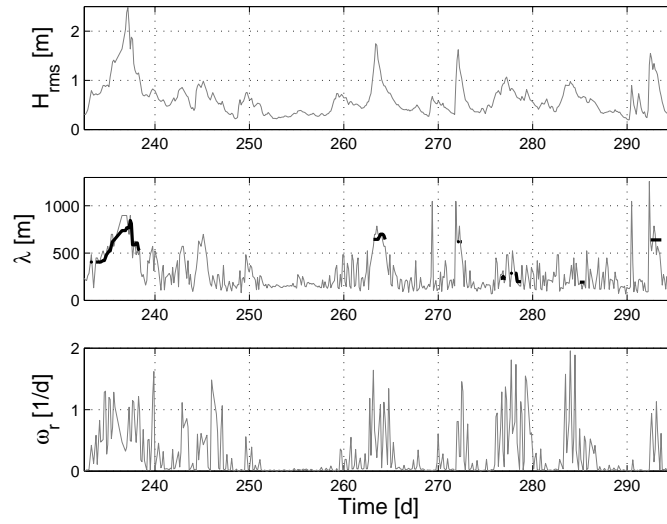


Figure 3.18: The *PSD* algorithm results for case 2. The grey line depicts the normal Morfo60 results, while the thick grey line represents the moments where physically significant events occur ($\lambda_{sig.}$).

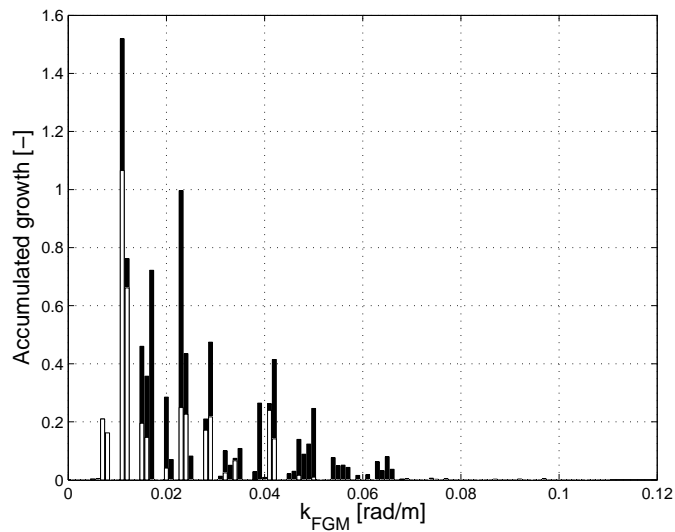


Figure 3.19: The accumulated growth for each wave number for the modelled period of time. The total length of the bars represent the total accumulated growth, while the white part of each bar represents the growth during *PSD* periods.

with significant growth. The algorithm focuses at high wave conditions during storms, and does not describe the post storm periods. As can be seen in Fig. 3.19, the algorithm focuses on the fastest growing bed pattern length scales, but only a limited part of the development of the fastest growing bed pattern length scales is captured by the applied version of the *PSD* algorithm.

Case 3

In the final case it is assumed that faster growing bed pattern lengths will dominate slower growing length scales. To express this assumption in this *PSD* algorithm, the constant bed pattern length scale is quantified using a weighted, averaged bed pattern length scale ($\lambda_{sig.}$):

$$\lambda_{sig.j} = \frac{\sum_{j=n}^m \omega_{r_j} \lambda_j}{\sum_{j=n}^m \omega_{r_j}}. \quad (3.5)$$

The band width within a constant bed pattern length scale is assumed (λ^-, λ^+), is given by:

$$\lambda^+ = \frac{2\pi}{10\Delta k + k_{sig.}}, \quad \lambda^- = \frac{2\pi}{-10\Delta k + k_{sig.}} \quad (3.6)$$

where Δk represents the step size in which length scales are examined in the linear stability analysis ($\Delta k = 0.001$ rad/m) and the significant wave number $k_{sig.} = \frac{2\pi}{\lambda_{sig.}}$. Finally, an event is only assumed to be significant if the amount of growth of length scale predictions outside the band width is limited. The accumulated growth of the bed pattern length scales outside the band width (λ^-, λ^+) is compared to that of those inside this range:

$$\sum_{j=n}^m \Pi_j \omega_{r_j} < 0.5 \sum_{j=n}^m (1 - \Pi_j) \omega_{r_j} \quad (3.7)$$

Thus, the threshold for a significant event to occur is met when more than 67 % of the accumulated growth occurs in the range (λ^-, λ^+).

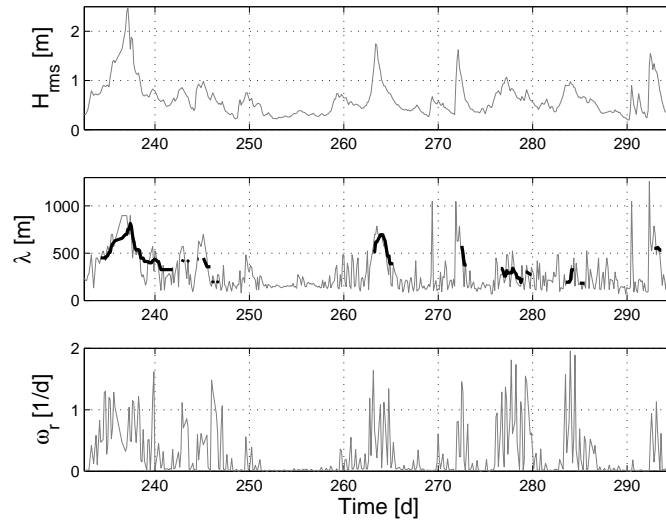


Figure 3.20: The *PSD* algorithm results for case 3. The grey line depicts the normal Morfo60 results, while the thick grey line represents the moments where physically significant events occur ($\lambda_{sig.}$).

The use of a band width (λ^- , λ^+) that is dependent on the $k_{sig.}$, results in a bandwidth that is related to the distance between adjacent length scales. This means that for short length scales (λ^- , λ^+) is small, whereas for longer bed pattern lengths this increases. The use of the growth rate (ω_r) for determining whether a development is significant or not (3.7), results in more specific significant developments for fast growth rates. The results for this case, shown in Fig. 3.20, indicate that the *PSD* algorithm has now focused only on high wave conditions and post storm periods, that correspond with fast growth rate predictions.

Fig. 3.21 shows the Morfo60 predictions of the cumulative growth for each length scale ($\lambda = \frac{2\pi}{k_y}$) for the full two-month period, along with the significant cumulative

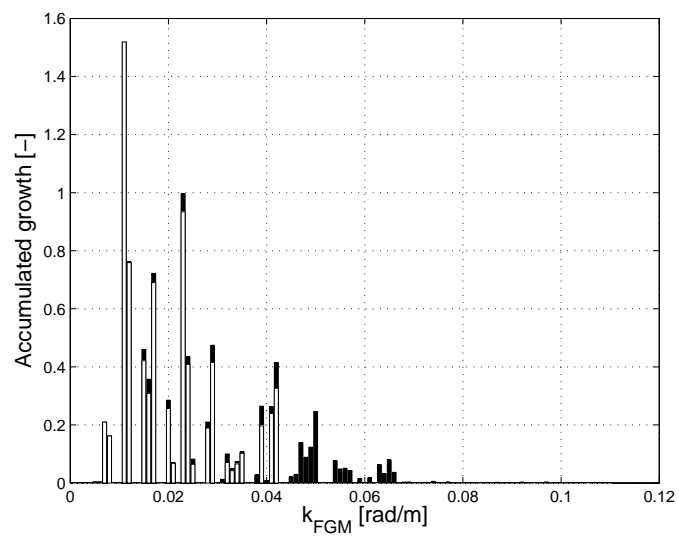


Figure 3.21: The accumulated growth for each wave number for the modelled period of time. The total length of the bars represent the total accumulated growth, while the white part of each bar represents the growth during *PSD* periods.

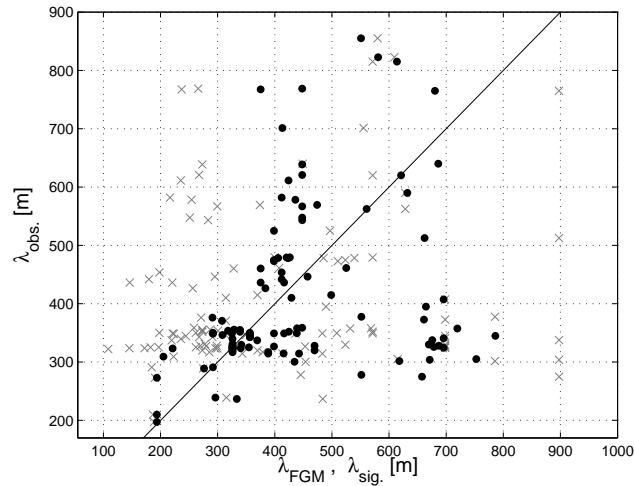


Figure 3.22: Predicted length scales (λ_{FGM} : \times) and length scales according to the *PSD* algorithm ($\lambda_{sig.}$: \bullet), versus the observed length scales ($\lambda_{obs.}$) of the crescentic bed patterns. The solid line represents perfect correspondence between predicted length scales and those from field observations.

growth as it is determined in the third case. The significant developments algorithm can identify the fastest growing length scales, and these correspond with length scales observed directly after high wave conditions [van Enkevort et al., 2004].

3.5.3 Comparison with field observations

The final version of the *PSD* algorithm described the post-storm periods to the fullest extent, but does not include mild wave condition periods where development of bed patterns is small. This version of the *PSD* algorithm will be further examined, by comparing its predictions of bed pattern length scales with field observations, and by comparing its predictive skills with those of the original linear stability model results.

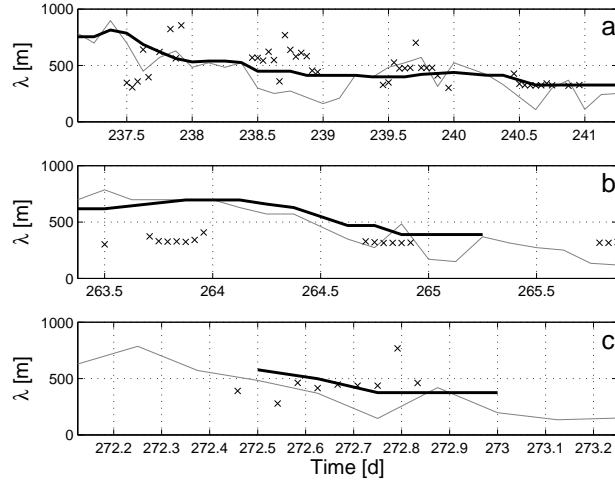


Figure 3.23: Significant developments after (a) the first, (b) second, and (c) third storm. Shown are the evolution of the observed bed pattern length: λ_{obs} . (\times), the model predictions: λ_{FGM} (*grey line*), and the outcome of the significant developments algorithm: λ_{sig} . (*thick black line*).

In Fig. 3.22 λ_{FGM} and the length scale according to the *PSD* algorithm (λ_{sig}) are compared with λ_{obs} . The predicted length scales are both significantly bigger and smaller than the observed length scales due to the models sensitivity to changes in wave conditions. Especially during low wave conditions, the model predicts smaller length scales than are observed in reality, although the effect of this is not shown in full in this figure since during this time field observations of the bar position were not available due to lack of wave energy dissipation on top of the bar. λ_{sig} shows a closer correspondence with λ_{obs} than does λ_{FGM} : $\delta_{\lambda_{obs}, \lambda_{FGM}} = 0.44$, while $\delta_{\lambda_{obs}, \lambda_{sig}} = 0.29$. Note that for $\lambda_{sig} > 350$ m there is a large scatter in λ_{obs} ; during post storm periods a wide range of bed pattern length scales was

observed along the beach (ranging from 300 to 1000 m) by van Enckevoort et al. [2004]. In the comparison presented here only alongshore-averaged $\lambda_{obs.}$ -values are plotted, creating discrepancies between predicted and observed length scales. In reality, most $\lambda_{sig.}$ -values will be observed at some point along the coast during post storm periods.

It is assumed that immediately after storms pre-existing bed patterns are removed, so that the assumption of quasi-alongshore uniformity is valid, thus allowing for a better comparison with linear stability predictions. Therefore we now examine these post-storm periods, when new crescentic bed patterns are, in theory, evolving. The duration of these post-storm periods is set between the peak in the wave height during the storm and the moment when the wave height (H_{rms}) becomes less than 0.5 m. This time corresponds roughly with the moment in time when field observations do not show significant changes in the bed pattern length scale until a new storm occurs [van Enckevoort et al., 2004].

In these periods $\lambda_{sig.}$ corresponds better with $\lambda_{obs.}$ than does λ_{FGM} : see Fig. 3.23. The *PSD* algorithm has an averaging effect on the length scale model predictions. In particular during the first days after the first storm (Fig. 3.23(a)), but also to a lesser extent after the third storm (Fig. 3.23(c)), the *PSD* algorithm describes increased length scales, similar to the field observations, which gradually decrease to more moderate length scales. After the second storm period (Fig. 3.23(b)), $\lambda_{sig.}$ increases compared to earlier values, but $\lambda_{obs.}$ shows no significant increase. This may be due to pre-storm bed-forms still being present after this

particular storm, preventing the evolution of new patterns.

The assumption that the original raw model predictions correspond better with field observations during post-storm periods can be examined by calculating the relative error between the λ_{FGM} and $\lambda_{obs.}$ for these periods and comparing this with the relative error over the entire observation period. However, the relative error for only post-storm periods increases, compared to the relative error over the entire observation period. ($[\delta_{\lambda_{obs.}, \lambda_{FGM}}]_{post\ storm} = 0.46$, while $[\delta_{\lambda_{obs.}, \lambda_{FGM}}]_{entire\ period} = 0.44$). Also the relative error between the $\lambda_{sig.}$ and $\lambda_{obs.}$ increases if only post-storm periods are taken into account: $[\delta_{\lambda_{obs.}, \lambda_{sig.}}]_{post\ storm} = 0.35$, while $[\delta_{\lambda_{obs.}, \lambda_{sig.}}]_{entire\ period} = 0.29$. This increase can be attributed to the incorrect predictions after the second storm, when we have reason to believe that the pre-existing bed-forms are not removed completely. These pre-existing bed patterns cause the development of crescentic bed patterns to be different from that predicted by a linear stability analysis. If only the first and third post-storm period would be taken into account, the relative errors would be: $[\delta_{\lambda_{obs.}, \lambda_{FGM}}]_{post\ storm\ 1\ \&\ 3} = 0.39$, while $[\delta_{\lambda_{obs.}, \lambda_{sig.}}]_{post\ storm\ 1\ \&\ 3} = 0.25$. This shows that the linear model (and the *PSD* algorithm) can predict the initial development of crescentic bed patterns more accurately than the periods in between storms. The difference is limited though, since most field observations occur during post-storm periods.

3.6 Discussion

The previous sections show that a linear stability analysis can be used to describe the actual development of crescentic bed patterns with some success. It also highlights limitations in the use of a linear stability analysis, and it shows that the subsequent application of an algorithm to emphasise the physically more meaningful model predictions can yield predictions closer to observations.

An alongshore uniform beach profile is assumed as the initial profile in the Morfo60 runs. This profile is assumed to occur after storms, when it has been assumed that all pre-existing bed patterns are removed [Komar and Holman, 1986]. In reality, alongshore variations occur. Existing bed patterns may not only influence the subsequent development of bed patterns and cause changes in growth rate and length scale from those predicted, but may also grow themselves, in a way that does not necessarily correspond with the predictions of the development of crescentic bed patterns according to a linear stability analysis.

A phase or response time difference occurs between the Argus observations analysed in van Enckevort et al. [2004] and the Morfo60 model predictions. The Argus images depict developed bed patterns, where Morfo60 predicts initial development. In other words, a linear stability analysis results in a bed pattern growth rate and spacing that are expected to develop, based only on the wave data, the alongshore uniform bathymetry and the tidal records at one instance. Previous predictions may bear little relation to these. On the other hand observed bed-forms must already have been growing for some time. This response time dif-

ference between field observations and model predictions is unaccounted for. The time necessary for the Argus system to detect a bed pattern depends not only on the growth rate, but also on the height and shape of pre-existing bed patterns, the overall bathymetry, the tidal level and the wave conditions. Argus images will only reveal the existence of crescentic bed patterns if wave breaking occurs on top of these features. The *PSD* algorithm partially addresses this response time difference by identifying periods of time with consistent length scale predictions.

The post-storm period of time when field observations are compared with results of the *PSD* algorithm is determined using the wave height. When the wave height falls below 0.5 m, a stable situation has generally developed. After this point observed length scales of the crescentic bed patterns do not change significantly, until the next storm occurs. The period of time when a linear stability analysis can produce valid bed pattern length predictions is unknown, but is likely to be linked to the accumulated growth ($\sum \omega_r \Delta t$) of consistent bed patterns, as is assumed in the *PSD* algorithm.

The alongshore constant beach profile used by Morfo60 changes linearly in between field measurements. In reality, changes in the quasi-alongshore constant profile may occur abruptly during storm periods. Changes in the beach profile are small but can have a significant effect on the model predictions [Calvete et al., 2007]. Calvete et al. [2007] note that an increase in shore-to-bar-crest distance results in an increased length scale of predicted crescentic bars. It is therefore possible that (abrupt) bar movement not recorded in bathymetric measurements

for the observation period might also be resulting in length scale differences between model and observations.

The influence of the pier at Duck on the developing bed patterns is only partially accounted for. The pier is located in the middle of the observations area, and causes a depression of the seabed underneath the pier. This depression was excluded from the field observations made by van Enckevort et al. [2004] and is also excluded from the model calculations (as was mentioned in section 3.2.2). A second effect of the pier structure is the influence on the wave climate [Elgar et al., 2001]. Wave conditions and currents can be altered when passing through the pier structure, causing locally different circumstances for the development of crescentic bed patterns. Spatial variation of the bed pattern length scales are observed by van Enckevort et al. [2004], especially post storm. The causes of these variations are not specified, though. A linear stability analysis assumes an alongshore homogeneous wave field. Where a wave field varies on the spatial and temporal scale there is some evidence that bed-form spacings can correlate with this modulation [Reniers et al., 2004].

The accuracy of Argus field observations is not discussed in this paper (see Lippmann and Holman [1989]). Apart from limitations of the photo analysis [Holman and Stanley, 2007], van Enckevort and Ruessink [2001] showed that changes in wave height and water level can cause significant changes in the observed bar crest position and that the evolution of the bar crest cannot be observed during low wave conditions [van Enckevort et al., 2004]. The influence of the pier on

the wave height (under oblique wave incidence) can result in local changes of the observed bar crest [Elgar et al., 2001], and consequently in the results presented by van Enkevort et al. [2004]. Lastly, but very significantly, the field observations show a wide spread of observed length scales immediately after storms (ranging from 300 to 1000 m); this variation is not taken into account in the comparison with the the model predictions, where only the alongshore averaged wave length is considered.

3.7 Conclusions

A linear stability analysis can predict the regeneration of crescentic bars at Duck after storms to a moderate degree of accuracy ($\delta_{\lambda_{obs.}, \lambda_{FGM}} = 0.44$). The linear stability model results (Morfo60) show increased length scale predictions after storms, similar to what is observed in field measurements after the first and third storm [van Enckevort et al., 2004]. Field observations after the second storm do not show increased length scales immediately after the storm, possibly due to the existence of pre-existing bed patterns. Within a couple of days after a storm, the length scale of the crescentic bed patterns gradually decreases in both the observations and the predictions of the linear stability analysis. The model predicts length scales that are of the same order as the observed length scales. Immediately after the first and third storm length scales between 500 and 800 m can be observed. Also in between storm periods, length scales similar to those predicted are observed; observed and predicted length scales vary between 150 and 400 m.

Tidal variation strongly influences the growth rate of bed patterns. Small tidal levels result in increased growth rates, as stirring and sediment transport rates increase for smaller tidal levels. The tidal level also affects the length scale and migration rate. An increase in tidal level results in bigger bed pattern lengths and migration rates, although the effect of the tidal level on the length scale and migration rate are minor compared to the influence of wave conditions. Although high tidal levels during storms are causing the greatest damage to coastal defences, our research suggests that lower tidal levels cause increased development of nearshore crescentic bed-forms.

Observations show the gradual development and change of the crescentic bed patterns, while a linear stability analysis always assumes an alongshore uniform beach and is therefore more affected by changes in the wave conditions and the tidal variation. Predicted bed patterns show much more variability in time than field observations. These fluctuations obscure a direct comparison of field observations with model predictions (although these do indicate the range of possible responses to the wave conditions). To overcome this a physically significant development (PSD) algorithm was developed, which can identify the more physically relevant model predictions with respect to growth rate and consistent length scale. This algorithm applied to the linear stability analysis results shows closer agreement with the observed bed patterns for the entire observation period ($\delta_{\lambda_{obs.}, \lambda_{sig.}} = 0.29$) and yields post-storm model predictions of length scales that are more similar to observed length scales in two of the three post-storm periods examined. This, therefore, partially addresses the limitations inherent in a linear stability analysis, producing more physically meaningful predictions. The conclusion is that a linear stability analysis can be a useful tool for coastal engineers, although further work on refining the algorithm and its limitations is required, as well as investigations on bathymetries that are more regularly measured.

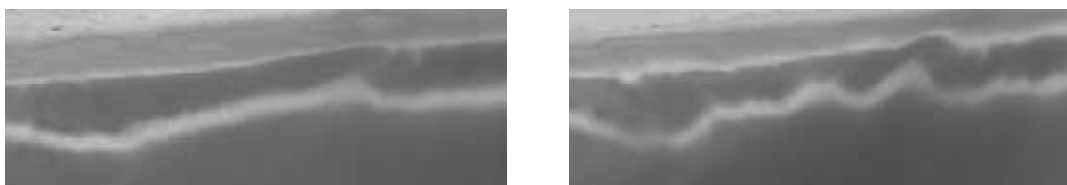
The *PSD* algorithm can identify similar length scales of crescentic bed pattern as are observed in reality, to a moderate degree of accuracy. Limitations of the use of a linear stability analysis still exist, though. A linear stability analysis is

quick in generating results using only limited amounts of input data, compared to traditional time-domain models. However, the linearised equations create a situation where only the initial development of bed perturbations can be predicted. Secondly, the assumption of a alongshore constant beach profile is possibly valid immediately post-storm, but not suitable for all wave data (as is done so far). As mentioned before, the *PSD* algorithm was designed to emphasise the more physically significant model predictions. The algorithm partially compensates the effects of the assumed alongshore constant bed profile, in that it excludes short-term insignificant model predictions, whose length scales do not correspond with previous predictions. However, the *PSD* algorithm is not intended to address the limitations of a linear stability analysis. In the next part of this thesis, a first step will be made to mitigate the limitations of a linear stability analysis by investigating the effects of pre-existing bed-forms on the development of crescentic bed patterns. Where so far linear stability analysis predictions were mainly compared to field observations during the early stages of post-storm redevelopment, the next part of this thesis is aimed at investigating to what extent linear stability predictions can still be of value after this initial period.

Chapter 4

Non-linear analysis of pre-existing crescentic bed patterns

A linear stability analysis predicts the initial development of rhythmic features, starting from an alongshore constant beach. In the previous chapter, it was shown that a linear stability analysis can describe the evolution of crescentic bed patterns from an alongshore uniform beach, that is assumed to occur after a storm, with reasonable accuracy. However, the linear model predicted less well when the bed already showed pre-existing bed-forms. When wave conditions change, a



(a)

(b)

Figure 4.1: Two Argus images of a crescentic bar, showing how, starting from (a) a crescentic bed pattern with a big length scale, a bed-form breaks up (b) due to a change in wave conditions [van Enckevort et al., 2004].

linear stability analysis describes significantly different behaviour from that observed in reality. During higher waves immediately after a storm peak, crescentic bed patterns with big length scales are generally observed [van Enckevort et al., 2004]. When the wave conditions settle down, a gradual decrease in length scale is observed by van Enckevort et al. [2004]. This breaking up of bed patterns (see Fig. 4.1) cannot be described correctly by Morfo60, which shows more rapid changes in the predicted length scale, due to changing wave conditions. Klein and Schuttelaars [2006] previously studied the effects of pre-existing bed-forms on the evolution of the nearshore seabed using a non-linear model. However, these results were limited in range and focused on the differences in evolution of the nearshore and offshore bar. The decay of pre-existing bed patterns was presented. However, the long term development and rise to dominance of a bed pattern with a different length scale could not be determined due to limitations in the modelled period.

The goal of this part of the research is to investigate to what extent pre-existing bed-forms interact with the evolution of crescentic bed-forms, and to what extent these bed-forms negate the predictions made by a linear stability analysis. To this end, a non-linear stability analysis is undertaken, using a fully non-linear finite difference model: Morfo55 [Caballeria et al., 2002; Garnier, 2006] (introduced in section 2.5). This non-linear stability analysis can describe a wide range of initial conditions, including alongshore variability of the bed. This model can therefore include pre-existing bed-forms and calculate the effects of these initial disturbances on the natural evolution of crescentic bed-forms.

Firstly, a comparison between the linear stability analysis used in the previous sections (Morfo60) and the non-linear model (Morfo55) is presented. Secondly, the non-linear evolution of an alongshore uniform undisturbed nearshore bed is investigated. Thereafter, a wide range of pre-existing bed-forms is implemented into the model to see to what extent the development of crescentic bed patterns is affected by this. A closer look at various characteristics of the bed pattern evolution is presented.

4.1 Linear compared to non-linear results

The non-linear stability analysis, used to investigate the effects of pre-existing bedforms, and the linear stability analysis, used for the prediction of length scales of crescentic bars that were compared with the Duck field observations in chapter 3, describe the same processes using the same equations. However, differences also exist (see section 2.3 for more details). In order to examine to what extent results from the non-linear stability analysis can improve the predictive skills of the linear stability analysis in describing the temporal evolution of crescentic bed patterns, a comparison between the linear and non-linear model is carried out.

The various physical parameters are set to the same values for both the linear and non-linear model. In general, settings of the linear stability analysis were adapted to correspond better with the settings applied in the non-linear stability analysis (presented in Table 2.12). Where the linear stability analysis only describes the initial evolution, a full non-linear model describes the long term temporal evolution. This makes the non-linear model more prone to develop numerical instabilities and therefore more sensitive to the model settings than a linear model. Settings that were altered in either the linear model, or the non-linear model, which do not correspond with the settings presented in Table 2.12, will be discussed below.

The basic state bed profile from Morfo60 is used as initial bed profile in Morfo55. This option in Morfo55 was, however, implemented incorrectly. The bed level (z_b) was calculated as the sum of the water depth (D) and the free sur-

face elevation (z_s), where the opposite should be applied. The description of the bed profile in Morfo55 is altered to give the correct interpretation

The second discrepancy between the input bed profile originating from the linear model and the reproduced description by Morfo55 was due to application of an initial bed level at the shoreline ($z_{b_{min}}$). Morfo60 applies a boundary condition at the shoreline for the total depth (D_{min} , where $D = z_b + z_s$) while Morfo55 uses a boundary condition for the bedlevel ($z_{b_{min}}$). In Morfo55, this minimum bed level was added to the overall bed level, which originated from the linear model. This meant that the entire bed profile was shifted downwards, to create a minimum bed level at the shoreline. Morfo60, on the other hand, determined at what location the minimum depth (D_{min}) would be reached, and set this at the minimum cross shore location. This, in effect, results in the removal of the part of the bed profile closest to the shore but, apart from this alteration, retains the original profile and therefore stays closer to reality than the non-linear model. The boundary condition applied in the non-linear model is altered to represent the boundary condition of the linear model.

Another significant difference between Morfo55 and Morfo60 is the different shoreward boundary condition for the velocity profile. Both models assume $v_i(x = 0) = 0$ m/s. However, where Morfo60 assumes the shoreline to be where the water depth is zero ($D = 0$), Morfo55 assumes that the shoreline is where the bed level reaches the minimum value ($z_b = z_{b_{min}}$). At the onshore modelling boundary ($D = D_{min}$) of Morfo60 does the velocity not reach zero, since only

assumed is that $v_i \rightarrow 0$ at $D = 0$. In Morfo55, the alongshore velocity is forced to zero at the minimum bed level by applying a different boundary condition. Here it is assumed that $v_i(x_1) = \frac{1}{3}v_i(x_2)$. The discrepancy between both models' application of this boundary condition results in the velocity profiles showing significant differences near the shore. This affects the predicted characteristics of the evolving bed-forms, and therefore obscures a comparison between both models. To make the applied boundary conditions match more closely, several solutions have been tested. The presented results are created using a different boundary condition for Morfo55, based on the velocity profile in Morfo60: $v_i(x_1) = 0.93v_i(x_2)$.

To get the closest correspondence between Morfo60 and Morfo55, different offshore wave conditions are applied due to the different locations of the offshore boundary of Morfo60 and Morfo55. The applied wave conditions correspond with moderate conditions at Duck, occurring in between storm periods. For Morfo60 (at $x = 1000$ m): $H_{rms} = 0.85$ m, $T_p = 7.5$ s and $\theta = 9^\circ$, while for Morfo55 (at $x = 250$ m): $H_{rms} = 0.88$ m, $T_p = 7.5$ s and $\theta = 5^\circ$. Shoaling forces the wave height at 250 m offshore to be slightly higher than at 1000 m offshore, while the different wave angle is the result of refraction of waves while approaching the shore [Dean and Dalrymple, 1984]. Finally, both models apply a minimum water depth at the shoreline. For Morfo55, the minimum bed level (z_{min}) is set at 0.15 m, while the minimum water depth (D_{min}) is set at 0.1 m. Both minimum depths are reduced compared to standard runs, to reduce differences in the nearshore zone.

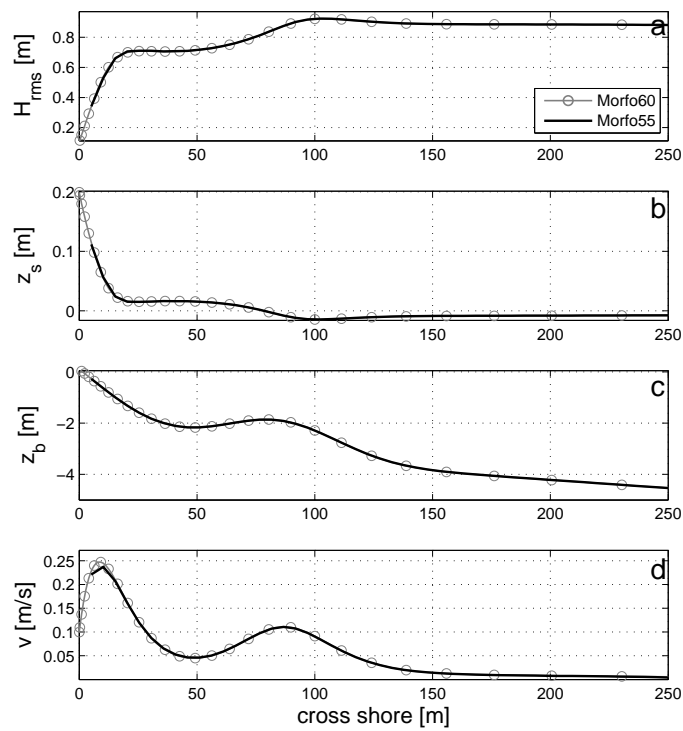


Figure 4.2: A comparison between the basic state profiles of Morfo55 and Morfo60. Shown are the basic state profiles of (a) the wave height, (b) the mean free surface elevation, (c) the bed level, and (d) the alongshore velocity.

4.1.1 Basic state

Fig. 4.2 shows a comparison between the basic state cross shore profiles of some characteristic model variables for Morfo60 and Morfo55. The basic state profiles of the non-linear model show the cross shore distribution of the amplitude of each variable at 3.5 days from the start. The model has a brief start-up period, when the wave conditions build up and a stable cross shore distribution of wave energy, as well as various other processes is established. This start-up period is finished after 3.5 days and the evolution of bed-forms has not yet started in earnest at this moment.

The bed profiles of Morfo55 and Morfo60 match very well, as can be seen in Fig. 4.2(c). However, the difference in minimum onshore water depth as well as the fact that the furthest onshore grid point is located at 2.5 m offshore in the Morfo55 run, mean that the Morfo60 results progress further onshore. Fig. 4.2(a) and 4.2(b) show the basic state profile of the wave height (H_{rms} [m]) and free surface elevation (z_s [m]) for both Morfo55 and Morfo60. Both models show near-perfect agreement for both variables, even though different onshore and offshore conditions are applied. Fig. 4.2(d) shows the alongshore basic state velocity (V_0 [m/s] in Morfo60). The newly applied boundary condition for Morfo55 means that the velocity profile close to the shore closely reproduces the Morfo60 results; the minor differences in this graph are due to the limited number of gridpoints nearshore in Morfo55, compared to Morfo60.

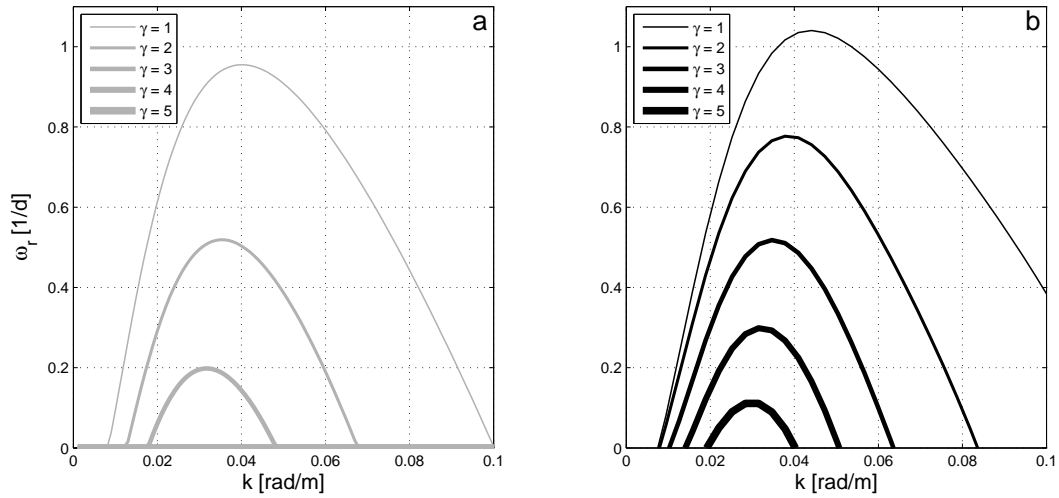


Figure 4.3: (a) The growth rate curves for different γ -values for Morfo60. (b) The calculated equivalent growth rate curves for different γ -values for Morfo55 at day 3.5. The growth rate curve of Morfo55 for $\gamma = 1.0$ [m^2/s] is unstable in time, indicating that for this value of γ linear growth might not occur.

4.1.2 Perturbations

The evolution of bed-forms in Morfo60 and the comparison between field observations and model predictions, presented in chapter 3, focused around the length scale of the bed-forms ($\lambda = \frac{2\pi}{k}$) and the growth rate (ω_r). It is therefore of importance to analyse the similarities and differences in the linear growth rate curves of the linear and non-linear models. To this end, the linear growth of different length scales is calculated using a Fourier analysis of Morfo55 output, 3.5 days from the start. At this moment, the different γ values show the most stable linear development and therefore the most complete linear growth rate curve (see also Fig. 4.6).

Fig. 4.3 shows the growth rate curves for different values of the downslope term

(γ [m^2/s]) for Morfo60 (a) and Morfo55 (b). The γ -value represents to what extent bed-forms experience downslope movement of sediment. This term counteracts the sediment accumulation at the location of bed patterns, and causes saturation of the development when bed-forms reach their final height. A high γ -value results in increased downslope movement of sediment, and therefore a slower evolution of bed-forms. Generally, a value of $\gamma = 1.6$ [m^2/s] is used [Soulsby, 1997], to describe physically plausible evolution of bed-forms (this value was used to reproduce the evolution of bed-forms at Duck by Morfo60). For Morfo55 runs that show temporal evolution over long periods of time, a bigger γ -value is used ($\gamma = 5$ [m^2/s]). This value reduces the speed at which bed-forms evolve, and results in a more gradual evolution of the seabed.

The growth rate curve of Morfo60 (Fig. 4.3(a)) clearly shows the sensitivity of ω_r to various γ -values, with decreasing growth rates for increasing γ -values. For $\gamma > 3$, no growing bed-forms are predicted. The results from the non-linear model show similar behaviour (Fig. 4.3(b)), where increasing values of γ also result in decreasing growth rate curves. There is good agreement between the shape of the linear and non-linear curves, resulting in very similar length scales of the fastest growing modes. However, Morfo55 predicts significantly bigger growth rates than Morfo60 for the same value of γ . Differences in the growth rate curves are investigated, but have not been resolved. The difference is not the result of variations in the number of grid points, in either Morfo55 or Morfo60. Furthermore, although the growth rate curves calculated from the non-linear model results change in time, these changes are minor; differences generally occur outside the physical domain

($\lambda < 100$ m), and the growth rate of the fastest growing mode does generally not alter during the linear growth period. The reason for the difference in the growth rate curves of Morfo55 and Morfo60 could be the result of a different application of the downslope term. Large γ -values result in a bigger difference between either growth rate curves than small γ -values. However, a small γ -value or even a non-existent downslope term generally results in a crash of the Morfo55 model and otherwise the growth rate curve is very instable in time, complicating the comparison between Morfo55 and Morfo60 results.

Nonetheless, the shape of the growth rate curve is strikingly similar and corresponding fastest growing length scales are predicted by both models. The similarities suggest that bed-forms with the same length scale will initially develop under the same circumstances for both models, although at different evolution rates, depending on the value of γ .

The different migration rates of Morfo55 and Morfo60 for various γ -values during the initial development of various length scales are presented in Fig. 4.4. The results only show the physically plausible results. Migration rates for length scales that do not grow are excluded for Morfo60, and Fig. 4.4(b) only depicts migration rates that are reasonably consistent in time. Similar to the growth rate curves in Fig. 4.3, the migration rate increases for smaller γ -values. The non-linear model predicts smaller migration rates than the linear model, but the shape and peak of the migration rate curves of Morfo55 and Morfo60 are similar.

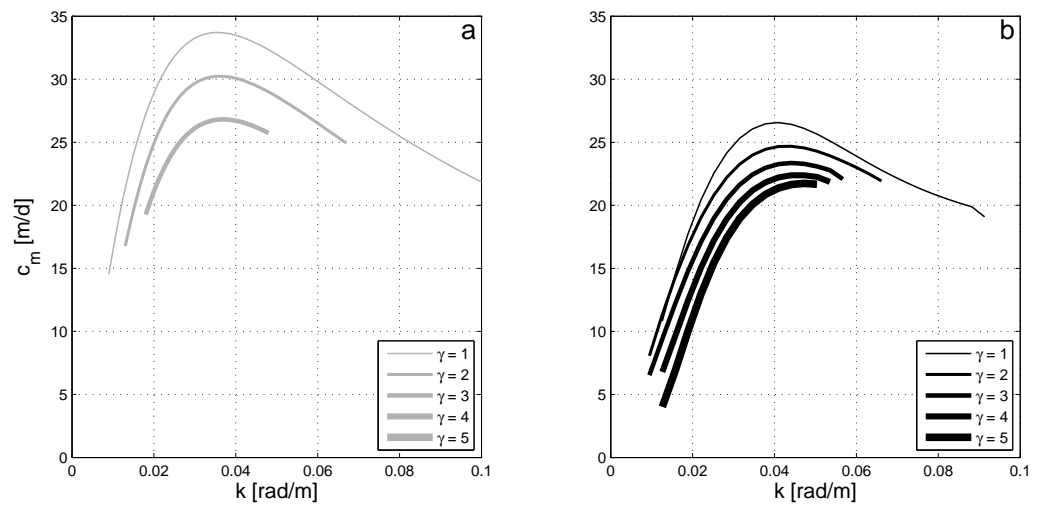


Figure 4.4: (a) The migration rate curves for different γ -values for Morfo60. (b) The calculated migration rate curves for different γ -values for Morfo55 at day 3.5. The number of plotted results is reduced and only include the physically plausible results.

For a further analysis of the development of perturbations in Morfo60 and Morfo55, a comparison of the eigenfunctions of the *FGM* is presented (see Fig. 4.5). The eigenfunctions of the non-linear stability results are created using the cross- and alongshore output at day 14. It was decided to display the eigenfunctions at this moment because the perturbation profiles already display a significant amplitude, even though linear growth is still being predicted for the dominant mode. At each cross shore location, a Fourier transformation is taken of the alongshore profile, for various perturbed variables. For each cross shore location only the output of the Fourier analysis for the dominant length scale is taken into account, creating a cross shore eigenfunction of the fastest growing mode of various variables. The amplitudes of the eigenfunctions in Morfo55 are dimensional and,

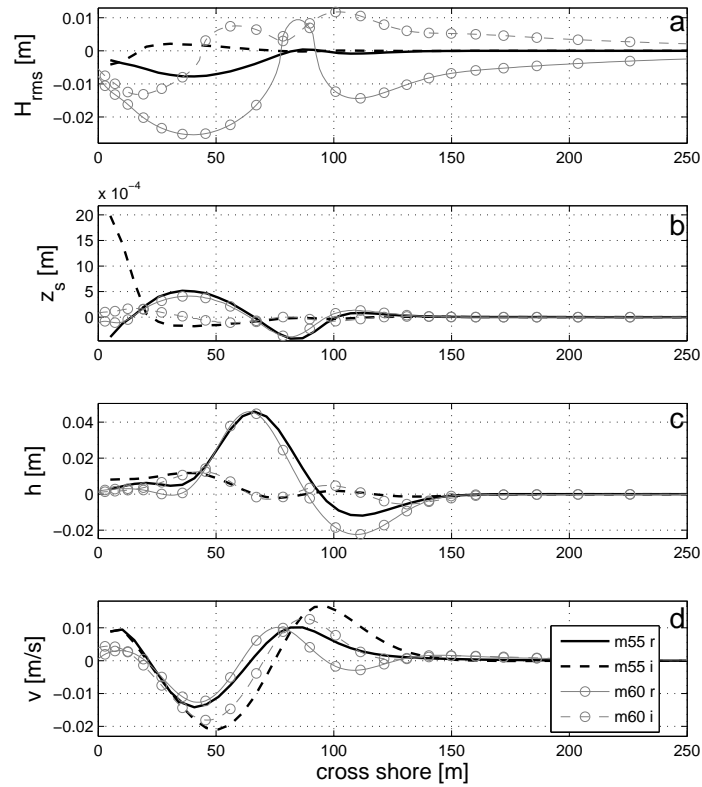


Figure 4.5: The real and imaginary parts of the eigenfunctions for both Morfo55 and Morfo60, for $\gamma = 3.0 [m^2/s]$. The eigenfunctions are phase shifted, to synchronise the phase of the Morfo55 and Morfo60 results. Secondly, Morfo60 results are non-dimensional and are therefore scaled to fit the amplitude of the Morfo55 results.

in principle, physically meaningful. In Morfo60, perturbations are assumed to be small and amplitudes are arbitrary, the amplitudes of eigenfunctions of different variables are proportional to each other, however. The maximum amplitude of the eigenfunction of the bed perturbation in Morfo55 is therefore taken as a measure for the Morfo60 eigenfunctions; all eigenfunctions are scaled to make the maximum amplitude of the bed perturbation the same as in Morfo55:

$$f_j = \epsilon f_j^*, \quad \epsilon = \frac{\max |z_{b_{pb}}(\text{Morfo55})|}{\max |z_{b_{pb}}(\text{Morfo60})|}, \quad (4.1)$$

where $j = 1, 2 = \text{real, imaginary}$, f_j^* represents the original Morfo60 eigenfunctions, f_j are the scaled eigenfunctions, and ϵ is the scaling factor, defined as the fraction of the maximum bed pattern perturbation height in Morfo55 over that of Morfo60.

Results show very similar behaviour for the bed level ($z_b [m]$), free surface elevation ($z_s [m]$) and the alongshore velocity ($v [m/s]$) for the linear and non-linear model. Slight differences can be observed, due to different boundary conditions. The alongshore velocity (v), for instance, shows a different distribution close to the shoreline for Morfo55, compared to Morfo60. Other minor differences are due to the fact that what is shown as eigenfunction of Morfo55 is the dominant length scale of a Fourier analysis of the perturbation distribution at this time, which can already be affected by non-linear effects. The eigenfunctions of z_b , η and v of the non-linear model show very similar behaviour to that of the linear model. However, the wave height eigenfunction (H_{rms}) of Morfo55 shows very different behaviour from the Morfo60 eigenfunction as well as a much smaller amplitude. An explanation for this difference has not been found during the research carried

out in this project, and could be addressed in the future.

The results presented in this section show that a non-linear model can describe the implementation of forcing conditions in terms of basic state cross shore profiles that are nearly the same as those of a linear stability model. Similar results are also predicted for the perturbed state, although here differences become apparent. Differences between the output of the linear and non-linear evolution of perturbations are, however, limited. Conclusions drawn from research carried out with a non-linear model can, therefore, be applied to improve the understanding and application of linear stability analysis results, and to improve the interpretation of linear results with regard to reality. Future research can be carried out to further investigate and address the differences between linear and non-linear model results.

4.2 Undisturbed evolution

To understand the impact of pre-existing crescentic bed-forms on the formation and evolution of these bed-forms, understanding of undisturbed evolution is necessary. The plain alongshore bed is initially perturbed by a 'Dirac function', a 0.03 m high spike in the middle of the modelling domain at 50 m from the shoreline. This spike excites all bed pattern length scales to the same extent, and forms the focus point of the initial development of bed-forms. The applied physical parameter settings used for these runs fit within a range of settings that have been applied before with success [Garnier et al., 2008]. These settings are very similar to those used in the previous section and give rise to crescentic bed-forms with very similar characteristics. The wave height is slightly higher than the previously applied wave height ($H_{rms} = 0.9$ m) and the original boundary condition for the alongshore velocity is applied. A big downslope term is applied ($\gamma = 5$ [m^2/s]) to create circumstances where bed-forms form and develop gradually in time, making it easier to observe the different stages of development. The minimum bed level at the shoreline is increased to 0.25 m. The model cannot describe bed-forms that exist above the waterline. The minimum nearshore bed level is increased to avoid nearshore perturbations evolving at this location to become too big. The increased bed level at the shoreline causes differences in the development of bed patterns at the shoreline, however, the focus of this research is the analysis of the development of crescentic bed-forms that occur further offshore. The minimum bed level is implemented in the original way by moving the bed downwards. This change in $z_{b_{min}}$ does not have significant impacts on the bed evolution, while it expands the time domain over which bed patterns develop.

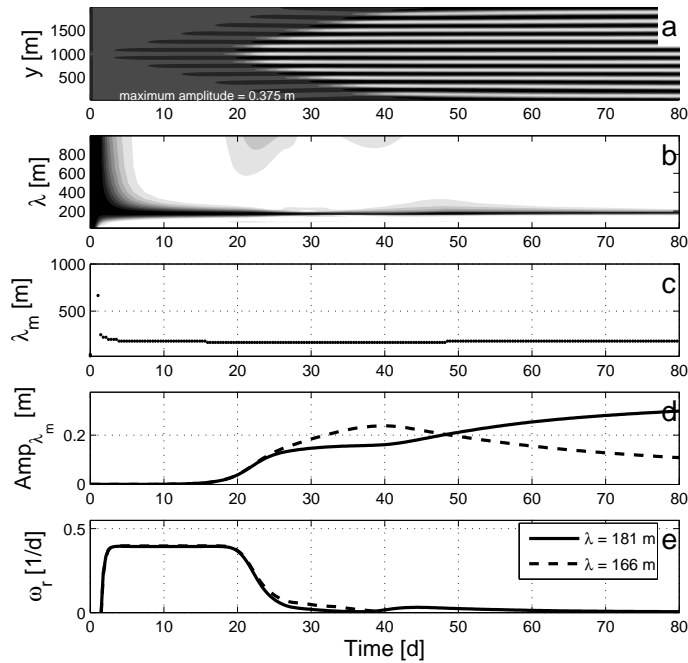


Figure 4.6: The evolution of the bed under normal wave incidence. (a) The evolution of the alongshore bed profile at 50 m offshore (white areas are crests, whereas black represents troughs), (b and c) the dominant length scale at each time step, (d) the development in height of various characteristic length scales, including the finally dominant mode, and (e) the linear growth rate of each of these length scales.

Normally incident waves are applied in Fig. 4.6, to study the natural evolution of crescentic bed-forms. Evolution of crescentic bed-forms starts from the centre, and gradually expands towards the longshore boundaries of the modelling domain due to the position of the 'Dirac function' (Fig. 4.6(a)). After the initial stages when no dominant length scale exists, two length scales quickly become significant (Fig. 4.6(c)); $\lambda = 166$ and 181 m, ($k = 0.038$ and 0.035 rad/m, respectively).

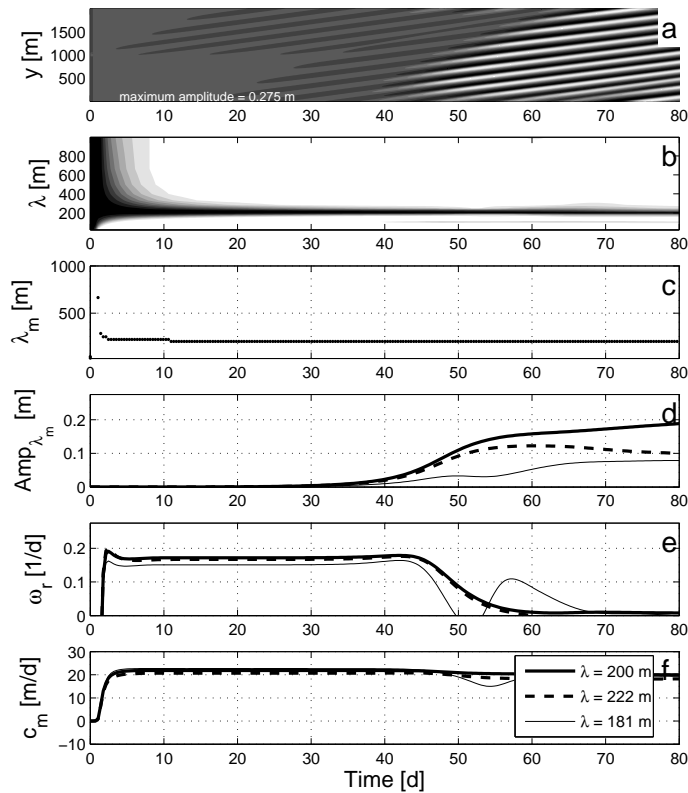


Figure 4.7: The evolution of the bed under oblique wave incidence forcing ($\theta = 5^\circ$).

Results are presented in the same way as in Fig. 4.6. (f) is added to this figure describing the migration rate of various characteristic length scales.

Although $\lambda = 166$ m initially shows the fastest development, $\lambda = 181$ m is the final dominant mode (Fig. 4.6(d)). Fig 4.6(e) depicts the linear growth rate for these dominant length scales. Constant linear growth rates can be observed for both length scales from around the third day until day 20, when non-linear effects cause a more gradual evolution of the bed patterns. The linear growth rate is very similar for both length scales, since both length scales correspond to the peak in the growth rate curve (see Fig. 4.8).

The undisturbed development of crescentic bed-forms under oblique wave forcing ($\theta = 5^\circ$) is shown in Fig. 4.7. The initial formation of bed patterns starts at the centre of the domain, however, by the time the bed patterns becomes visible in Fig. 4.7(a), it has migrated toward the upper end of the domain. Bed-forms that migrate out of the top of the modelling domain, reappear at the bottom end, due to the application of alongshore periodic boundaries. The dominant length scale stabilises around $\lambda = 200$ m ($k = 0.031$ rad/m) (Fig. 4.7(b)), with a final amplitude of around 0.28 m. Length scales around this dominant length scale also evolve, but show smaller linear growth rates (Fig. 4.7(e)). The migration rate of the developing bed-forms is very constant at 21.8 m/d (Fig. 4.7(f)). Migration rates of other significant length scales ($\lambda = 181$ and 220 m) are similar to this value; for $\lambda = 181$ m, the migration rate is 22.7 m/d, while for $\lambda = 222$ m, $c_m = 20.7$ m/d. Fig. 4.9 shows the migration rate curve at the same time as when the growth rate curves were determined. The migration rates observed over time in Fig. 4.7(f) correspond well with the initial migration rate curve.

Although slight changes in the dominant length scale occur over time, it can be concluded that under these circumstances undisturbed morphological evolution can be correctly predicted by a linear stability analysis, as long as the amplitude of the perturbations is small. The finally dominant length scale corresponds with fastest growing modes of the linear growth rate curve and although non-linear effects end the linear evolution and cause the further development of bed-forms to be non-linear, the bed-form characteristics do not significantly change.

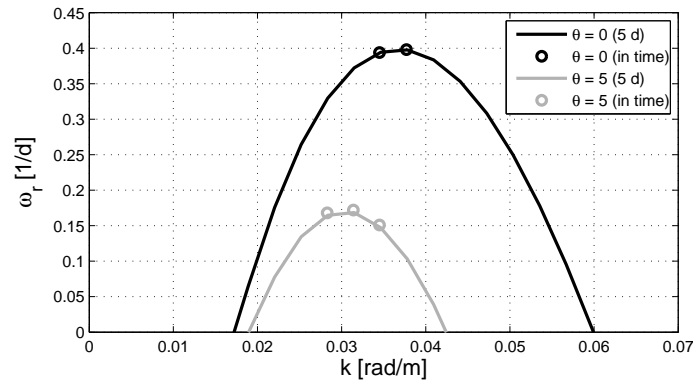


Figure 4.8: The growth rate curves for both normal wave incidence (*black line*) and waves approaching the shore under an oblique angle ($\theta = 5^\circ$) (*grey line*) after 5 days. The circles represent the average linear growth rates for various characteristic length scale, over the periods in time when constant linear growth is predicted: For normal wave incidence: Day 3 to 20, see Fig. 4.6(e) and for oblique wave incidence: day 5 to 43, see Fig. 4.7(e).

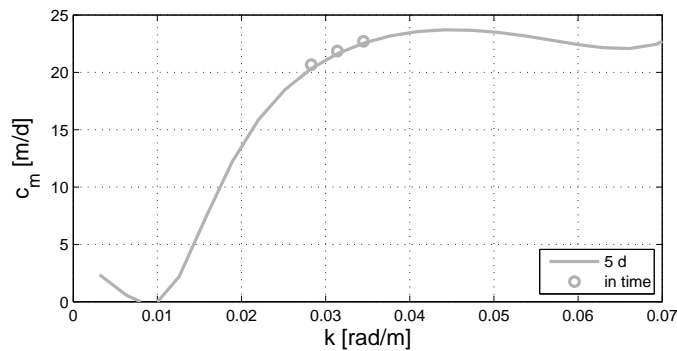


Figure 4.9: The migration rate rate curve for waves approaching the shore under an oblique angle ($\theta = 5^\circ$) after 5 days (*grey line*). The circles represent the average migration rates in time for some characteristic length scales (see Fig. 4.7(f)).

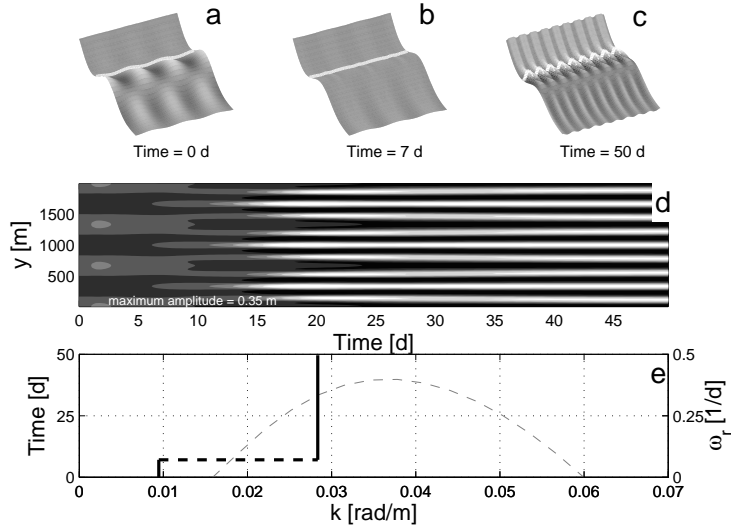


Figure 4.10: The evolution of the bed under normal wave incidence when long pre-existing bed patterns are implemented. (a) the bed profile at the beginning of the run, (b) the bed-forms breaking up, and (c) the bed profile at the end of the run. (d) the evolution of one transect (at 50 m offshore) of the perturbation distribution in time, (e) The evolution of the dominant length scale (*thick black line*, scale on left) and the growth rate curve for the undisturbed bed (*dashed grey line*, scale on right).

4.3 Evolution of pre-existing bed patterns

To study the effects of pre-existing bed-forms on the (linear) evolution of crescentic bed-forms under constant wave forcing, a wide range of bed patterns are applied. Two types of moderate wave conditions are applied ($H_{rms} = 0.9$ m, $T_p = 7.5$ s, $\theta = 0^\circ$ and $H_{rms} = 0.9$ m, $T_p = 7.5$ s, $\theta = 5^\circ$), whose undisturbed evolution was presented in the previous section. Pre-existing bed-forms are implemented using output from Morfo60. Eigenfunctions of length scales that are not the fastest growing mode are used to construct realistic bed pattern profiles as initial con-

ditions for each run. Various length scales and amplitudes have been studied; twelve pre-existing length scales have been investigated, ranging from 100 m to 1000 m in length. The range of examined pre-existing bed-forms exceeds the linear growth range for the applied moderate wave conditions, however. The effects of, in particular, pre-existing length scales that show no initial linear development are of interest for this research. Bigger wave conditions ($H_{rms} = 1.5$ m, $T_p = 7.5$ s and $\theta = 0^\circ$) are applied in the linear stability analysis to determine physically plausible descriptions of the bed perturbations for this wide range of bed patterns, since the model can only give physically accurate predictions of bed pattern length scales that show positive linear growth. Three amplitudes were applied for each of these initial bed patterns ($Amp_{ini.} = 0.05, 0.15$ and 0.25 m). However, for the examination of the effects of various initial amplitudes, a wider range of initial amplitudes has been applied for a single length scale ($\lambda_{ini.} = 500$ m). Three types of evolution can be determined: breaking up of bed-forms, merging of bed-forms and bed-forms undergoing further growth.

An example of the effects of pre-existing bed-forms is presented in Fig. 4.10, where 1000 m long bed-forms with an amplitude of 0.25 m were implemented under normal wave forcing. The dominant length scale for undisturbed development (λ_{FGM}), is significantly smaller (181 m) than the initial pre-existing length scale ($\lambda_{ini.} = 1000$ m). The three plots of the bed profile (Fig. 4.10(a), (b) and (c)) show the breaking up of pre-existing bed-form, and the formation of bed patterns that are closer to λ_{FGM} . The full temporal evolution of one alongshore transect is depicted in Fig. 4.10(d). This graph clearly shows how the initial bed-form first

decreases in amplitude, before a new bed-form arises. The change of the dominant length scale in time, along with a growth rate curve of the undisturbed evolution of bed-forms under the same wave forcing is depicted in Fig. 4.10(e). This figure shows that although the bed-form breaks up, the linear *FGM* length scale does not arise. The final length scale (λ_{final}) is, however, significantly closer to λ_{FGM} and the maximum growth rate than λ_{ini} .

The plotted dominant length scale over time (Fig. 4.10(e)) forms a slightly schematic description of what is being predicted by the model. The plot is derived from 4.10(d), using the Fourier analysis. This means that only one alongshore transect is selected for the analysis of the dominant length scale. The cross shore location of this alongshore profile is at 50 m offshore, which is where the 'Dirac function' is applied in the undisturbed evolution case. However, this location is not at the top of the alongshore bar and not necessarily the location of the maximum crescentic bed pattern amplitude. The first signs of a changing perturbation profile could therefore develop at a different location than that analysed in this figure, since the cross shore location where the pre-existing bed-form breaks up is dependent on the pre-existing bed-form characteristics and the applied forcing conditions. Secondly, the development of the new bed patterns can result in locally and temporarily different dominant length scales. As can be seen in Fig. 4.10(d) around day 7, the crests of the new bed-form interrupt the pre-existing troughs before the original crests break up. This means that for a short period of time a bed pattern will be observed that differs from either the pre-existing or final length scales. This is, however, a local phenomenon, which might not be observed at the bar crest. It can, therefore, be assumed that although the original and

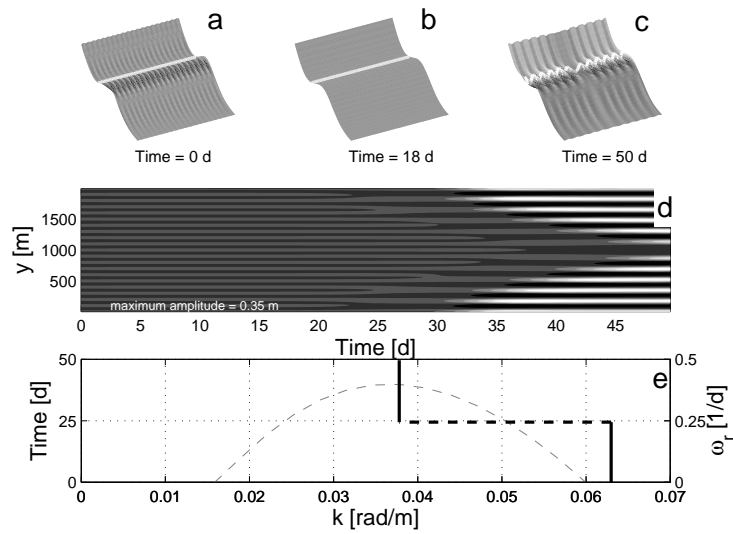


Figure 4.11: The evolution under normal wave incidence of the bed when pre-existing bed patterns are implemented that have a length scale that is significantly shorter than λ_{FGM} . The results are presented in the same way as in Fig. 4.10.

finally dominant length scale observed in Fig. 4.10(d) are a correct representation of the overall behaviour, the observed breaking up of bed-forms at this location is only a limited representation of the overall processes. The point in time when the dominant bed-form changes at this location only forms a measure for the speed at which this change occurs. It was therefore decided to plot only the initial and finally dominant length scales. The point in time when the dominant length scale changes in Fig. 4.10(e) is determined to be the last point in time when the initial length scale is still dominant, indifferent of previous or subsequent changes in the dominant length scale.

When $\lambda_{ini.} \ll \lambda_{FGM}$ similar behaviour to $\lambda_{ini.} \gg \lambda_{FGM}$ can be observed (Fig.

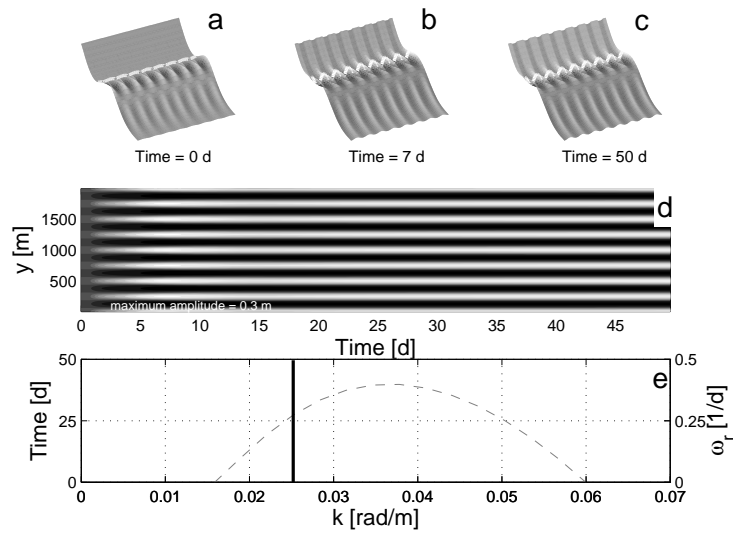


Figure 4.12: The evolution under normal wave incidence of the nearshore seabed when the pre-existing bed patterns have a length scale that is close to the optimum length scale in the undisturbed development. The results are presented in the same way as in Fig. 4.10.

4.11). The disappearance of a short pre-existing bed-form is however more extensive and the development of the final bed-form takes longer, compared to a bed-form that breaks up. It seems that the pre-existing bed-form is wiped-out more extensively, before a new bed-form arises, compared to $\lambda_{ini.} \gg \lambda_{FGM}$ (see Fig. 4.10). The length scale of the newly developing bed-form is, for this case, the same as for the undisturbed development (Fig. 4.6(e)).

For $\lambda_{ini.} \approx \lambda_{FGM}$ different behaviour can be observed (see Fig. 4.12). The pre-existing bed-form remains and does not break up to form shorter bed patterns. The pre-existing bed-form undergoes further growth, and quickly reaches its maximum amplitude of 0.3 m. This amplitude is slightly less than the final

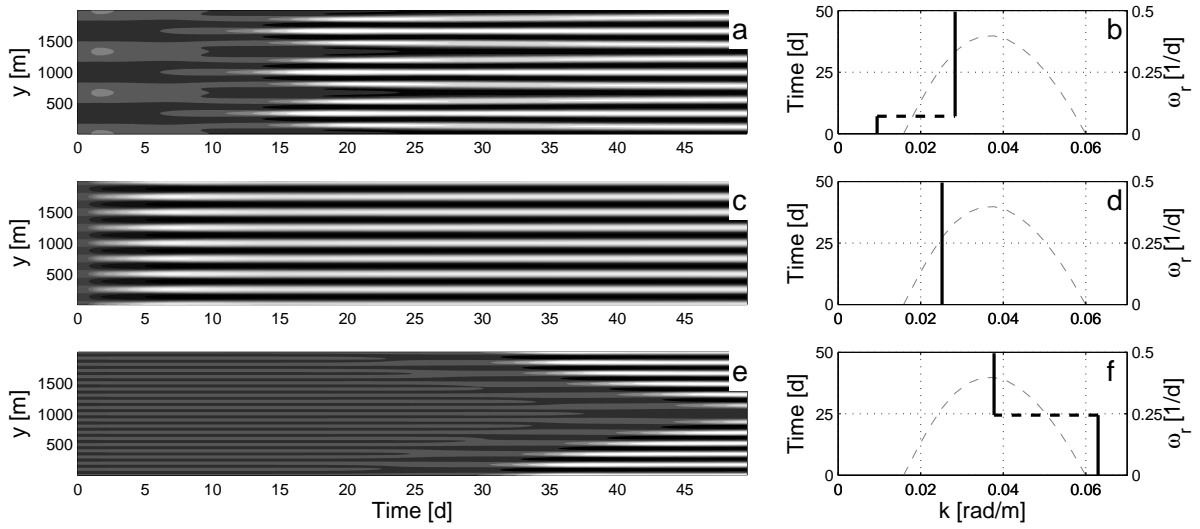


Figure 4.13: Examples of the evolution of the nearshore seabed when pre-existing bed patterns are implemented, under oblique wave incidence ($\theta = 5^\circ$). The results are presented in the same way as in Fig. 4.10(d, e).

amplitude of λ_{FGM} ($\max(\text{Amp}(\lambda_{FGM})) = 0.35$ m).

The way in which oblique waves interact with pre-existing bed-forms was also investigated. To this end, the same (shore normal) pre-existing bed-forms were applied. Three examples of the evolution of crescentic bed patterns under oblique wave incidence, for a rhythmically disturbed initial bed are shown in Fig. 4.13. Similar results as for normal wave incidence can be observed. Long initial bed-forms break-up, short bed-forms merge, and a pre-existing bed-form with a length scale close to λ_{FGM} undergoes further growth. The development of λ_{final} to its final height generally takes longer than for the normal wave incidence due to the lower linear growth rate. Furthermore, whereas bed patterns under normal wave incidence remain stationary, oblique wave angles cause migration of the bed-forms. For instance, Fig. 4.13(e) only shows the initial stages of development of the finally

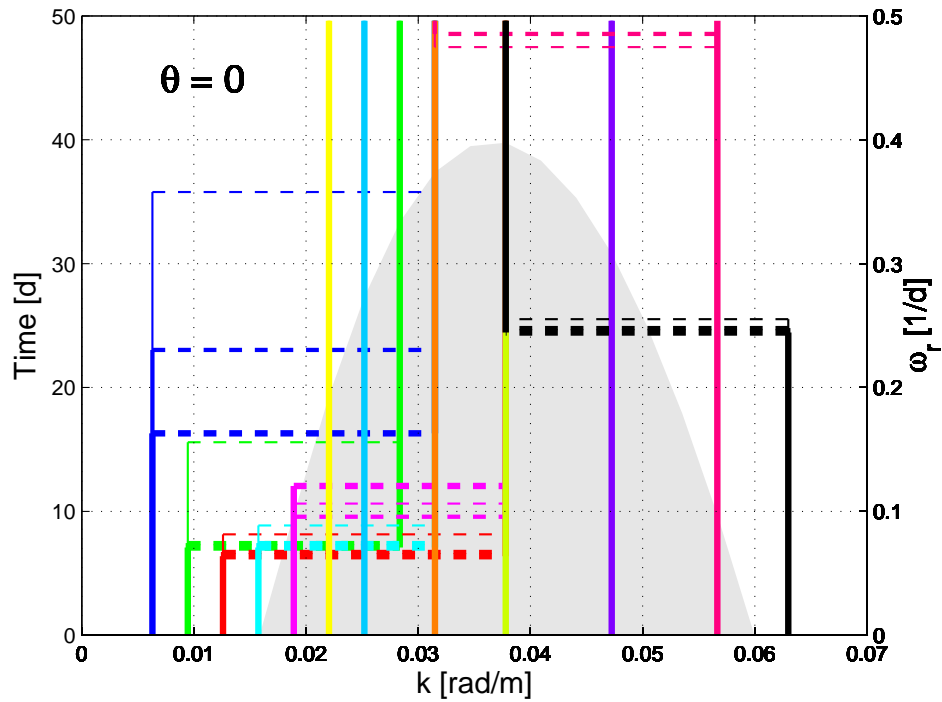


Figure 4.14: The evolution of various pre-existing bed pattern length scales (*colour*) and amplitudes ($Amp_{ini.} = 0.05, 0.15$ and 0.25 m) (*thickness*) and the development of new bed patterns under normal wave incidence, in comparison with the growth rate curve for undisturbed development (*grey field*).

dominant length scale. The oblique wave incidence causes the final bed-forms to migrate. The initial bed-forms in Fig. 4.13(c, e) migrate as well, but the initial bed-form for $\lambda_{ini.} \gg \lambda_{FGM}$ does not seem to migrate (Fig. 4.13(a)).

A wide range of different pre-existing bed-forms is examined, to study their effects on the evolution of crescentic bed-forms under normal and oblique wave incidence. For each pre-existing length scale, three pre-existing amplitudes are examined ($Amp_{ini.} = 0.05, 0.15, 0.25$ m). To present the outcomes of all pre-existing

bed-forms, for normal or oblique wave incidence, a plot similar to Fig. 4.13(b, d, f) is selected. Fig. 4.14 and 4.15 show the outcomes of various different length scales in the colour of the lines, and the thickness of the lines represents the initial amplitude, where the thinnest line represents the smallest initial amplitude. The period of dominance of the pre-existing and final length scale is shown in the left y-axis. The grey field in the background represents the growth rate curve for the undisturbed development, while the scale of the growth rate curve is shown on the right y-axis.

Fig. 4.14 shows the results for normal incidence wave forcing. The results show a clear relationship between the initial length scale and the final length scale, which depends on the difference between the initial length scale and λ_{FGM} of the undisturbed case.

It is noteworthy, that $\lambda_{ini.} = 333, 500$ and 100 m ($k_{ini.} = 0.019, 0.012$ and 0.063 rad/m, respectively) become $\lambda_{FGM} = 166$ m, ($k_{FGM} = 0.038$ [rad/m]), while $\lambda_{ini.} = 1000, 400$ and 111 m ($k_{ini.} = 0.006, 0.016$ and 0.057 rad/m, respectively) become $\lambda_{final} = 200$ m ($k_{final} = 0.031$ rad/m). Finally, for $\lambda_{ini.} \approx \lambda_{FGM}$ ($133 < \lambda_{ini.} < 286$ m ($0.022 < k_{ini.} < 0.047$ rad/m)), the pre-existing bed patterns remain and undergo further growth.

Whether bed patterns break up or undergo further growth seems to be closely related to the position of various initial length scales along the linear growth rate curve. Length scales that show significant linear growth in the undisturbed case remain when implemented as pre-existing bed-forms, while bed-forms that are outside the linear growth rate curve disappear when introduced to the system as

a pre-existing bed-form.

The finally dominant length scale that develops when the initial bed-forms break up or merge, is not always λ_{FGM} but can also be a length scale that is close to this dominant length scale (Fig. 4.14). For instance, $\lambda_{ini.} = 1000$ m ($k_{FGM} = 0.006$ [rad/m]) breaks up into a length scale that is not the dominant length scale, but much closer to it than the pre-existing length scale ($\lambda_{final} = 200$ m, $k = 0.031$ [rad/m]). The effect of the different initial amplitudes seems to be limited, appearing to influence only the duration until the dominant length scale changes; a bigger initial amplitude generally increases the rate of change and forces a more rapid development towards the finally dominant length scale than smaller amplitudes. However, this is not consistent for all $\lambda_{ini.}$ values, which might reflect the limitations inherent to the choice of cross shore location for which the temporal evolution is determined. The evolution of $\lambda_{ini.} = 111$ m ($k_{ini.} = 0.057$ [rad/m]) takes much longer than for the other initial length scales. The runs for this initial length scale were continued beyond the period shown in Fig. 4.14, and the pre-existing bed-form with the largest initial amplitude merges to become $\lambda_{final} = 200$ m ($k_{final} = 0.031$ [rad/m]) within the following days. Finally, the results presented so far suggest that there can be a long period of time before a bed-form breaks up or merges. In reality, these changes occur more quickly. New bed-forms generally arise within several days of the moment when new wave conditions occur. However, these runs were carried out using a very high value of γ . This creates circumstances that result in numerically stable model runs, but do not necessarily describe accurately the speed at which bed patterns form. Model

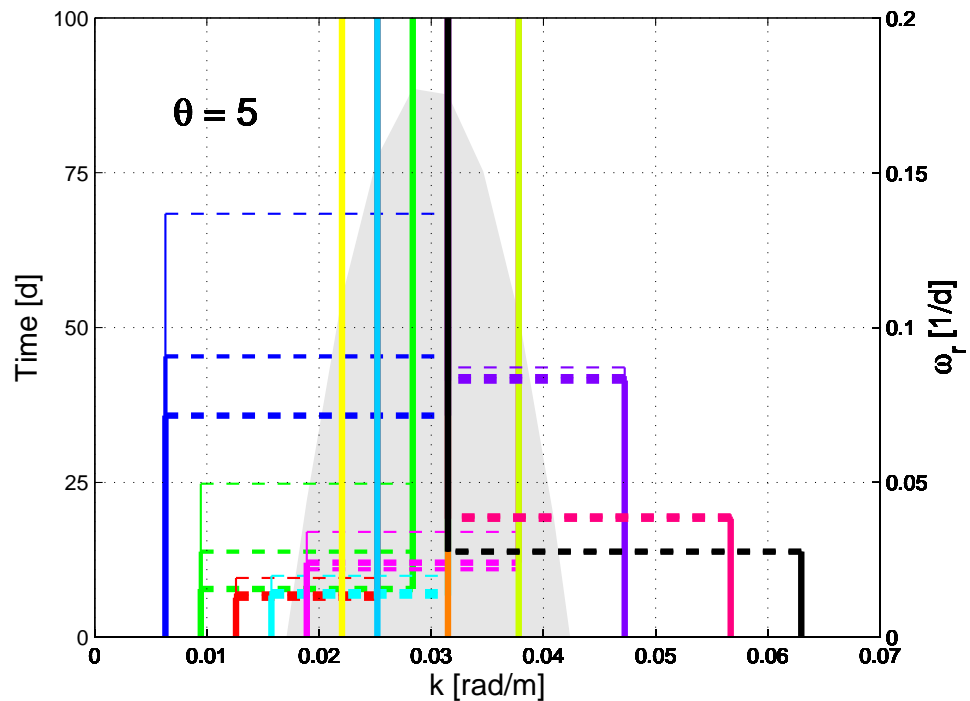


Figure 4.15: The development of various pre-existing bed pattern length scales (*colour*) and amplitudes (*thickness*) and the evolution of new bed patterns under oblique wave incidence, in comparison with the growth rate curve for undisturbed development (*grey field*).

results show, therefore, a much more gradual development than would be observed in reality.

Waves approaching the shore at an oblique angle show similar behaviour as observed with normal wave incidence (Fig. 4.15). However, the range of remaining bed-forms and the linear growth rate curve of the undisturbed development are shifted, due to the changed wave conditions. Under these conditions, fewer pre-existing bed-forms remain and develop, due to the limited range of linear growth rate curve.

It is noteworthy that $\lambda_{ini.} = 286, 250, 200$ and 166 m ($k_{ini.} = 0.022, 0.025, 0.031$ and 0.038 rad/m, respectively) remain and undergo further growth, while the other length scales break up or merge: $\lambda_{ini.} = 1000, 400, 166, 133$ and 100 ($k_{ini.} = 0.006, 0.016, 0.047, 0.057$ and 0.063 rad/m, respectively) break up or merge to become $\lambda_{final} = \lambda_{FGM} = 200$ m ($k_{FGM} = 0.031$ rad/m). $\lambda_{ini.} = 500$ ($k_{ini.} = 0.0013$ rad/m) breaks up to become $\lambda_{final} = 250$ m ($k_{final} = 0.025$ rad/m), and 333 m ($k_{ini.} = 0.019$ rad/m) breaks up to become $\lambda_{final} = 166$ m ($k_{final} = 0.038$ rad/m). The relationships between settings are similar to the relationships observed with the normal wave incidence. The time domain was extended for the oblique wave incidence case, since the linear growth rate is significantly smaller. However, most bed-forms break up or merge in the early stages of development.

Results presented so far show that the development of bed patterns when pre-existing bed-forms are present is significantly influenced by these initial perturbations. However, the behaviour predicted by the non-linear model suggests that although a linear model describes the evolution of the nearshore seabed when pre-existing bed-forms are implemented incorrectly, the non-linear development can be related to the linear growth rate curve. When a length scale of the pre-existing bed-form shows significant linear growth, this bed-form will remain and develop, while a bed pattern with a length scale outside the linear growth rate curve will break-up or merge to become the fastest growing length scale, or a length scale close to this. The evolution of bed-forms, even for changing wave conditions and with pre-existing bed-forms, therefore, seems to be closely related to the (linear) development of bed-forms at an undisturbed beach.

4.4 Output analysis of pre-existing bed-forms

The results presented in the previous section contain a large amount of data, which gives more insight into the linear and non-linear evolution of crescentic bed-forms, as well as the interaction with pre-existing bed-forms. The following section is an analysis of the effects of various pre-existing bed pattern characteristics on the evolution of crescentic bed-forms. The focus is on characteristics that are also described in a linear stability analysis.

4.4.1 Length scale

The effect of various initial length scales on the evolution of crescentic bed patterns is presented in Fig. 4.14 and 4.15. For a pre-existing length scale to persist, its undisturbed (linear) growth rate seems to be critical. When bed-forms break up or merge, λ_{final} is not always the λ_{FGM} . For $\lambda_{ini.} \gg \lambda_{FGM}$, the original bed patterns break up and split into a factor of the original length scale: Thus e.g. $\lambda_{ini.} = 1000$ m, under both normal and oblique wave incidence, splits into $\lambda_{final} = 200$ m. This applies to more initial length scales (see Table 4.1).

Values of $\lambda_{ini.}$ that are significantly smaller than λ_{FGM} decrease in height for a prolonged period, before giving rise to new bed-forms (see Fig. 4.11). The newly arising length scale is, in this case, not a whole-number factor of the original length scale. These shorter pre-existing bed-forms disappear almost completely from the Fourier analysis before giving rise to λ_{FGM} .

Finally, a clear relationship between the initial length scale and the rate of change is not apparent; the duration before a bed-form breaks up decreases with a

$\theta = 0^\circ$			$\theta = 5^\circ$		
$\lambda_{ini.}$	λ_{final}	$factor$	$\lambda_{ini.}$	λ_{final}	$factor$
1000 m	200 m	5	1000 m	200 m	5
666 m	222 m	3	666 m	222 m	3
500 m	166 m	3	500 m	250 m	2
400 m	200 m	2	400 m	200 m	2
333 m	166 m	2	333 m	166 m	2
286 m	286 m	—	286 m	286 m	—
250 m	250 m	—	250 m	250 m	—
200 m	200 m	—	200 m	200 m	—
166 m	166 m	—	166 m	166 m	—
133 m	133 m	—	133 m	200 m	0.67
111 m	200 m	0.56	111 m	200 m	0.56
100 m	166 m	0.60	100 m	200 m	0.50

Table 4.1: The initial and finally dominant length scales for normal and oblique wave incidence, as well as the factor by which the number of bed-forms along a certain beach width increases.

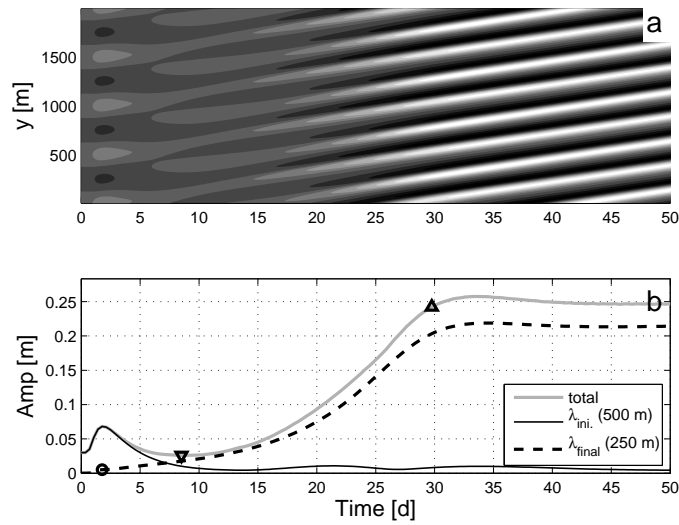


Figure 4.16: (a) The evolution of the seabed when bed patterns pre-exist for oblique wave incidence ($\lambda_{ini.} = 500$ m, $Amp_{ini.} = 0.15$ m). (b) The development of the amplitude of the initial pre-existing bed patterns is depicted as a solid black line in graph, while the final length scale is depicted as a dashed black line and the total amplitude evolution is depicted by a grey line.

decreasing length scale, for most $\lambda_{ini.} \gg \lambda_{FGM}$. However, $\lambda_{ini.} = 333$ m ($k = 0.018$ [rad/m]) is not consistent with this theory. For $\lambda_{ini.} \ll \lambda_{FGM}$ a similar relationship can be observed, but the duration before the length scale changes is much longer for these cases.

4.4.2 Amplitude

The evolution of the amplitude of the bed patterns can give information concerning the speed at which bed-forms reach their final height and the time at which the dominant length scale changes. Fig. 4.16 shows an example of the evolution of the

alongshore seabed (Fig. 4.16(a)) as well as the total amplitude and the development of the amplitude of the pre-existing and final length scale at this cross shore location, for oblique wave incidence (Fig. 4.16(b)). The results created under normal wave incidence show similar behaviour to those of oblique wave incidence. However, oblique waves result in a more gradual evolution of the seabed and a later change of the dominant bed pattern length scale and therefore display the processes involved more clearly.

The initially implemented length scale is 500 m, and $Amp_{ini.} = 0.15$ m. This length scale is longer than λ_{FGM} and breaks up. The new dominant length scale is 250 m. The total amplitude describes very closely the demise of the initial perturbation and consequently the rise of the final bed pattern. ' ∇ ' represents the time when the total amplitude is minimal, and roughly corresponds to the location where the dominant length scale changes from $\lambda_{ini.}$ to $\lambda_{final.}$ ' Δ ' depicts the first time when the total amplitude is within 95 % of the final total amplitude (from now on called Amp_{end}). This measure is chosen in preference to the time that the maximum total amplitude is reached, since the bed is generally still in development at this moment in time. ' \circ ' depicts the amplitude of the finally dominant length scale at the time when the pre-existing bed-form is at its maximum height ($Amp_{min}(\lambda_{final})$). This is assumed to be the starting point of the evolution of this length scale and gives insight into the duration and speed at which λ_{final} develops.

After 1.8 days, a peak in the bed pattern height can be observed. This peak is not the result of physical growth of the initial bed-form, but due to a shift in

the cross shore location of this bed pattern. The implemented pre-existing bed patterns were obtained by the linear stability analysis, using more extreme wave conditions than are applied here. An increased wave height gives rise to a higher and wider growth rate curve and, therefore, to a wider range of physically plausible predictions of crescentic bed pattern length scales. However, different wave conditions cause the predicted cross shore location of bed-forms to vary. The increased wave height, used to create all the pre-existing bed patterns, predicts the maximum height of the pre-existing bed-forms to be further offshore than would be the case for the current wave conditions. When more moderate wave conditions are applied, a shoreward shift of the pre-existing bed pattern occurs during the first couple of days. Since both graphs only depict the evolution of an alongshore transect that is located rather close to the shore, this shift of bed pattern location is observed as a rise in amplitude. Bed evolution up until this moment is therefore due to this change in offshore location of the bed-form, and does not necessarily describe the development of, or response to, pre-existing bed-forms which forms the focus of this research. Behaviour of the pre-existing bed-forms, as well as the newly developing final bed pattern up until this point in time (the first 1.8 days), are therefore not analysed further.

To investigate the effects of various initial amplitudes, a wide range of initial amplitudes has been examined using only one pre-existing bed pattern length scale ($\lambda_{ini.} = 500$ m). The effects of the initial amplitude of the pre-existing bed pattern on the time and level of the minimum and final total amplitude are presented in Fig. 4.17(a, b, c). The time at which the minimum total amplitude

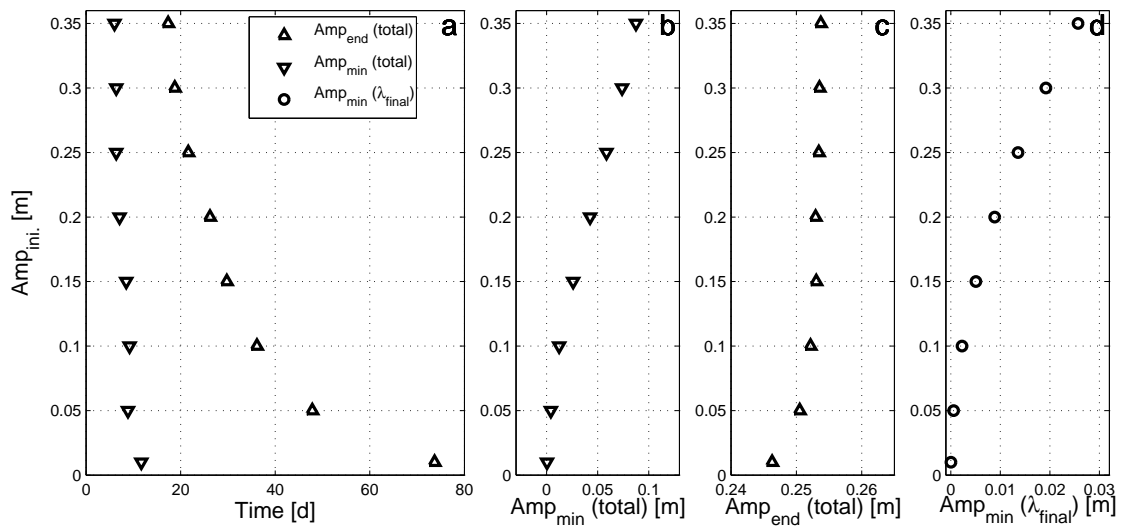


Figure 4.17: The time at which the minimum amplitude (Amp_{min}) is reached as well as when 95 % of the amplitude at the end of the modelling period (Amp_{end}) is surpassed, for (a) various initial amplitudes, (b) the minimum final amplitude, (c) final total amplitude, and (d) the minimum amplitude (after 1.8 days) of the finally dominant length scale ($Amp_{min}(\lambda_{final})$).

occurs decreases with increasing initial amplitudes. For $Amp_{ini.} = 0.01$ m this point is reached after around 12 days, whilst for $Amp_{ini.} = 0.35$ m $Amp_{min}(total)$ is reached after 6 days. Correspondingly, the time when 95 % of Amp_{end} is reached decreases also for increasing amplitudes. When $Amp_{ini.} = 0.01$ m, it takes over 70 days before 95 % of the final amplitude (Amp_{end}) is reached. For bigger values of $Amp_{ini.}$ this decreases to less than 20 days for $Amp_{ini.} = 0.35$ m. The height of Amp_{end} is reasonably constant for various $Amp_{ini.}$ (see Fig. 4.17(c)), while $Amp_{min}(\lambda_{final})$ (Fig. 4.17(b)) significantly increases for increasing $Amp_{ini.}$.

A possible reason for the increasing value of the minimum total amplitude ($Amp_{min}(total)$) for increasing values of $Amp_{ini.}$ is the minimum amplitude of the finally dominant length scale ($Amp_{min}(\lambda_{final})$) (see Fig. 4.17(d)). $Amp_{min}(\lambda_{final})$ is determined at the time when the pre-existing bed pattern amplitude is at its maximum (after 1.8 days). The development of bed-forms is generally assumed to be a function of the amplitude (for instance for linear growth rate), and a small value of $Amp_{min}(\lambda_{final})$ will result in a longer period of development than a higher value of $Amp_{min}(\lambda_{final})$, resulting in a longer period of time before 95 % of Amp_{end} is reached, as can be seen in Fig. 4.17(a). Assuming that the growth rate of λ_{final} and the decrease rate of $\lambda_{ini.}$ are both linear (which will be discussed in the following section), an explanation can be derived for the changing time when $Amp_{min}(total)$ is reached. The linear increase of $Amp_{ini.}$ corresponds roughly in an exponential increase of $Amp_{min}(\lambda_{final})$ (Fig. 4.17(d)). An increase of $Amp_{ini.}$ would result in a longer period of dominance of $\lambda_{ini.}$, however the corresponding exponential increase of $Amp_{min}(\lambda_{final})$ results in an even more rapid increase to

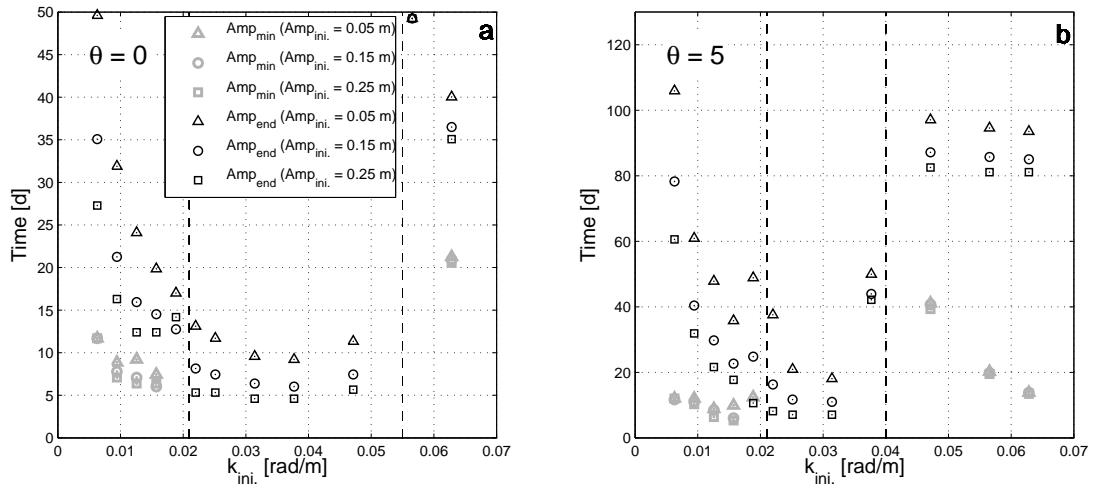


Figure 4.18: The time at which the minimum total amplitude of the bed perturbations occurs (*grey*) as well as the time when 95 % of the total final amplitude is reached (*black*), for various initial amplitudes ($Amp_{ini.} = 0.05$ m (' Δ '), 0.15 m (' \circ ') and 0.25 m (' \square ')) for both (a) normal, and (b) oblique wave incidence. The dashed vertical lines represent the range within the initial length scales which do not break up or merge, but undergo further growth.

dominance of λ_{final} , and therefore a shorter period of time before $Amp_{min}(total)$ is reached.

For various initial length scales, the same relationships between the initial amplitude and the time of the minimum and final amplitude can be observed as for $\lambda_{ini.} = 500$ m. Fig. 4.18 demonstrates the effect of the various initial bed pattern length scales on the times at which $Amp_{min}(\lambda_{final})$ and 95 % of the amplitude at the end of the modelling period (Amp_{end}) are reached for both normal and oblique wave incidence. The changes due to the initial length scale are significantly larger than the effects of the initial amplitude. Where, for normal wave incidence, a pre-

existing length scale of 1000 m with an initial amplitude of 0.25 m takes around 27 days to reach 95 % of its final amplitude, a pre-existing length scale of 333 m reaches this point within 15 days. The bed for both $\lambda_{ini.} = 1000$ and 111 m ($k_{ini.} = 0.006$ and 0.057 [rad/m], respectively) ($\theta = 0^\circ$, $Amp_{ini.} = 0.05$ m) is still in development when the runs finish and the amplitude is therefore still increasing. The time when 95 % of Amp_{end} is reached is therefore at the end of the modelling period.

A minimum amplitude is not shown for length scales that do not break up, but undergo further growth (shown between the dashed lines), since these length scales only increase in amplitude. In this context, the length scales just outside this region are striking (for $\theta = 0^\circ$: $k_{ini.} = 0.019$ and 0.057 [rad/m], and for $\theta = 5^\circ$: $k_{ini.} = 0.019$ [rad/m], in particular). These initial length scales do not persist but break up or merge to form a different final length scale. However, these initial length scales possess positive linear growth rates, as can be seen in Fig. 4.14 and 4.15. The development of crescentic bed patterns is different for these initial length scales, since these pre-existing length scales grow initially but then become dominated by a length scale closer to λ_{FGM} . Most of these initial bed-forms do not display a local minimum amplitude, as a result of this.

The difference between the normal wave incidence scenario and that when $\theta = 5^\circ$ is mainly an increase in time before 95 % of the final amplitude is reached. This is due to the reduced linear growth rate of the undisturbed development for $\theta = 5^\circ$ (see Fig. 4.8).

If $\lambda_{ini.} \ll \lambda_{FGM}$, significantly larger periods occur before $Amp_{min}(total)$ and 95 % of Amp_{final} are reached, for both normal and oblique wave incidence. An explanation for this behaviour can be seen in Fig. 4.19. Results show both the different initial length scales and initial amplitudes that break up or merge. The length scales that undergo further growth are not included in these figures since these do not show a minimum length scale.

Both normal wave incidence and oblique wave incidence results show that both $Amp_{min}(total)$ and $Amp_{min}(\lambda_{final})$ increase for increasing values of $Amp_{ini.}$ and $k_{ini.}$, for $k_{ini.} < 0.035$ [rad/m]. A possible reason for this is the increased steepness of the pre-existing bed patterns. Both an increase in $k_{ini.}$ as well as an increase in $Amp_{ini.}$ result in an increased steepness of the bed profile and, therefore, a more non-linear regime, causing $Amp_{min}(\lambda_{final})$ to increase.

For $k_{ini.} > 0.035$ rad/m, the results are less clear. A very limited number of data points are available for the normal wave incidence scenario, however, for oblique wave incidence a bigger number of results is available. Fig. 4.19(d) depicts increasing values of $Amp_{min}(\lambda_{final})$ for increasing $k_{ini.}$ values, while the value of $Amp_{min}(total)$ decreases under oblique wave incidence. While for $k_{ini.} < 0.035$ rad/m, an increase in $Amp_{min}(\lambda_{final})$ generally results in an increased $Amp_{min}(total)$, the opposite seems to happen for $k_{ini.} > 0.035$ rad/m. The reason for this seems not to be with the rise of the finally dominant bed-form, but with the demise of the pre-existing bed-form.

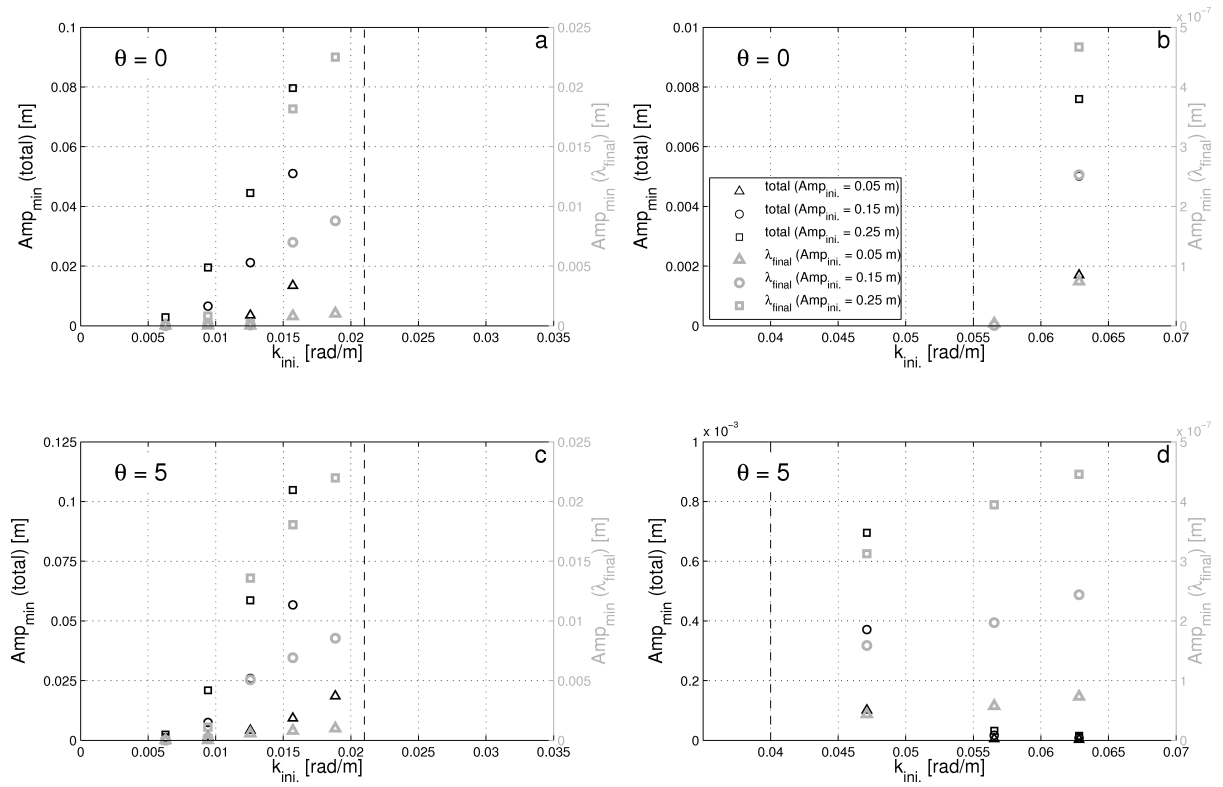


Figure 4.19: The minimum total amplitude of the bed perturbations, for various initial amplitudes (*black*) and the corresponding minimum values of the amplitude of the final length scale (*grey*) are plotted using different scales on the y-axis, for (a, b) normal, and (c, d) oblique wave incidence. The amplitudes for $k_{ini} < 0.035$ [rad/m] are plotted in a separate graph (a, c), since these are significantly bigger than those of $k_{ini} > 0.035$ [rad/m] (b, d)). The different initial amplitudes are depicted using different markers.

So far, it is unknown why and how $Amp_{min}(\lambda_{final})$ is dependent on $\lambda_{ini.}$. At the start of the run all length scales, apart from $\lambda_{ini.}$, are undisturbed, but within the first couple of time steps length scales that form a factor of $\lambda_{ini.}$ start to develop. In the following days, λ_{final} shows the most rapid development and dominates the other length scales. A possible explanation might be that the non-linear solution to the system of equations consists of higher harmonics of the original bed pattern length scale, but not of the lower harmonics [Schielen et al., 1993]:

$$\begin{aligned} \psi(x, y, t) = & \psi_0 + \epsilon^2\psi_{02} + \epsilon^3\psi_{03} + \dots \\ & + E_c[\epsilon\psi_{11}\epsilon^2\psi_{12} + \epsilon^3\psi_{13} + \dots] + c.c. \\ & + E_c^2[\epsilon^2\psi_{22} + \epsilon^3\psi_{23} + \dots] + c.c. \\ & + E_c^3[\epsilon^3\psi_{33} + \dots] + c.c. \\ & + \dots, \end{aligned}$$

where ψ stands for the solution of the system of equations and $E_c^j = e^{jk_c x + \omega_c t}$ [Schielen et al., 1993].

The time for the finally dominant bed-form to develop is not the main focus of this research. The increased γ -value in the sediment transport causes a much more gradual development than what would be expected in reality. The focus of this research lies in the processes involved in the occurrence of a changing dominant length scale and the influence of pre-existing bed-forms on the characteristics of finally dominant bed-forms, and not on the specific characteristic moments in time. The conditions simulated here are highly idealised since only one pre-existing length scale is implemented for each case. In reality, a wider range of pre-existing bed-forms will exist at any time, resulting in a wider range of length scales being

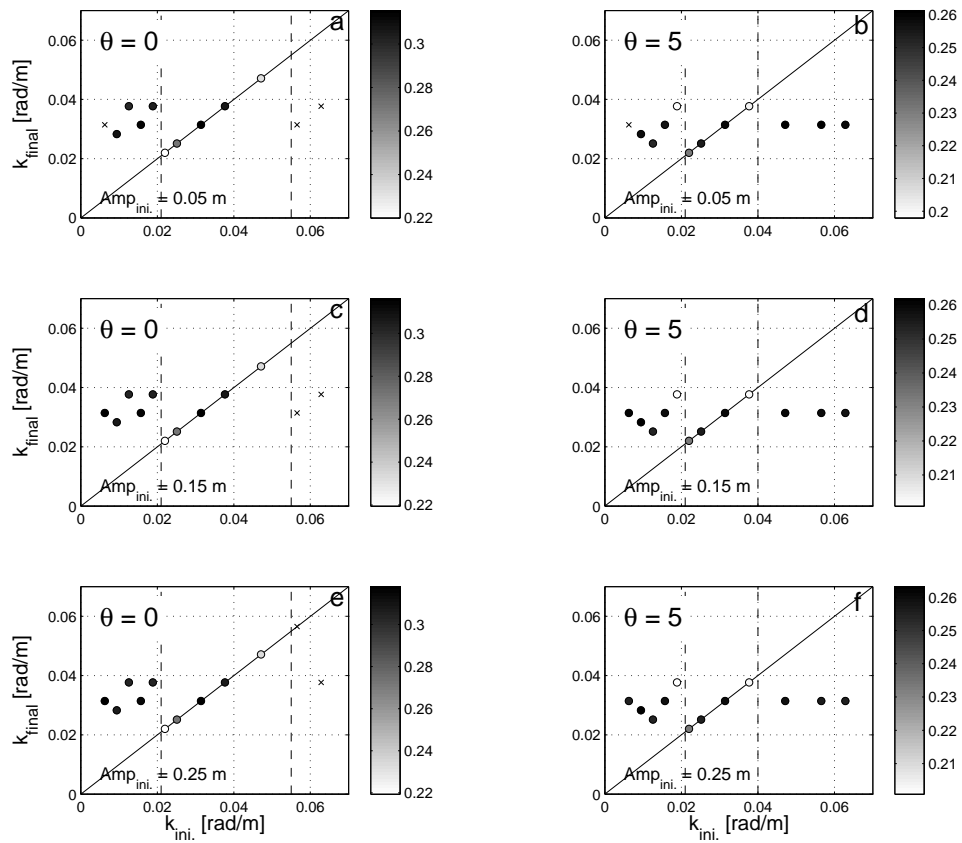


Figure 4.20: The final total amplitude of the bed perturbations, for various initial amplitudes for (a, c, e) normal, and (b, d, f) oblique wave incidence. The value of Amp_{end} is shown in the grey scale of the dots, the crosses represent model runs where the bed patterns are still in development at the end of the model run.

excited when changing wave conditions cause the dominant length scale to change.

The amplitude at the end of the modelling period (Amp_{end}) of the bed-forms that break up or merge shows remarkable correspondence with Amp_{end} of bed patterns that remain and undergo further development (see Fig. 4.20). An example of this behaviour can be seen for $\lambda_{ini.} = 500$ m ($k_{ini.} = 0.013$ [rad/m]) ($\theta = 5^\circ$), this initial length scale breaks up into $\lambda_{final} = 250$ m ($k_{final} = 0.035$ [rad/m]) and the amplitude of a fully developed bed pattern is around 0.25 m. This is the same value as Amp_{end} , for $\lambda_{ini.} = 250$ m, suggesting that a pre-existing pattern does not affect the final amplitude.

4.4.3 Growth rate

The *PSD* algorithm used in section 3.5 determines the physically most likely dominant length scale at different moments in time using the linear growth rate as well as the length scale from linear stability model predictions. This linear growth rate gives information about the initial evolution of bed-forms. It was assumed that when the model predicts significant growth over a period of time for similar length scales, this was more likely to correspond with real physical growth, than when either the model predicts small growth rates, or variable length scales. However, the linear growth rate, in theory, only describes the development of bed-forms accurately when non-linear effects are negligible. This means that the model predictions only form an accurate representation of the evolving bed for a period of time when bed patterns are small. Pre-existing bed patterns cause uncertainty

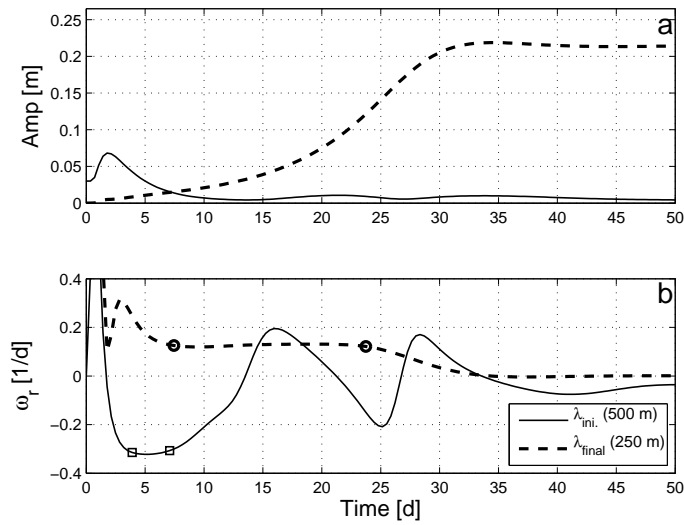


Figure 4.21: The evolution of (a) the amplitude, and (b) the linear growth rate, for oblique wave incidence, and initial conditions $\lambda_{ini.} = 500$ m and $Amp_{ini.} = 0.15$ m. The initial pre-existing length scale evolution is depicted as a solid line, while the final length scale is depicted as a dashed line.

in the accuracy of predictions made by a linear stability analysis, since it is not known to what extent linear growth dominates the evolution of bed-forms at this stage. The current model results, using a non-linear model, can give insight into the range of the linear regime in predicting the evolution of bed-forms accurately, when pre-existing bed-forms exist.

Linear growth rates can be calculated by determining the rate of change in the amplitude of various length scales, using Fourier analysis (see section 2.5). Fig. 4.6(e) and 4.7(e) depict the linear growth rate for the undisturbed development of bed-forms under normal and oblique wave incidence. The graphs show that

constant linear growth occurs from day 3 to 20 for normal wave incidence and between day 3 and 45 for oblique wave incidence. A constant linear growth rate suggests that the development of bed-forms can be described accurately by linear terms alone. After these constant linear growth periods, non-linear terms increase in importance and cause the growth to slow down. The period of linear growth for the undisturbed cases suggests that a linear stability analysis can accurately describe the development of crescentic bed patterns during this period.

Fig. 4.21(a) depicts the evolution of the amplitude of the initially and finally dominant length scale, for the case of $\lambda_{ini.} = 500$ m and $Amp_{ini.} = 0.15$ m, for oblique wave incidence. The linear growth rate of the finally dominant mode as well as the linear decay rate of the initial bed pattern are depicted in Fig. 4.21(b).

The first couple of days show non-linear behaviour, when the amplitude of the perturbations in this alongshore profile increase due to a cross shore shift of the peak of the pre-existing crescentic bed-form (see section 4.4.2). The development of λ_{final} shows a clear linear growth period ('o'), from this moment onwards. Also, the disappearing pre-existing bed pattern shows a brief period of linear decay ('□'). The behaviour of the decreasing pre-existing bed-form beyond this period becomes fluctuating. The amplitude of the pre-existing bed-forms is very small, and the dominant mode has shifted to λ_{final} , making the linear decay rate of $\lambda_{ini.}$ from this moment onwards, the result of other effects.

Linear growth and decay only occur when the linear growth and decay rate are

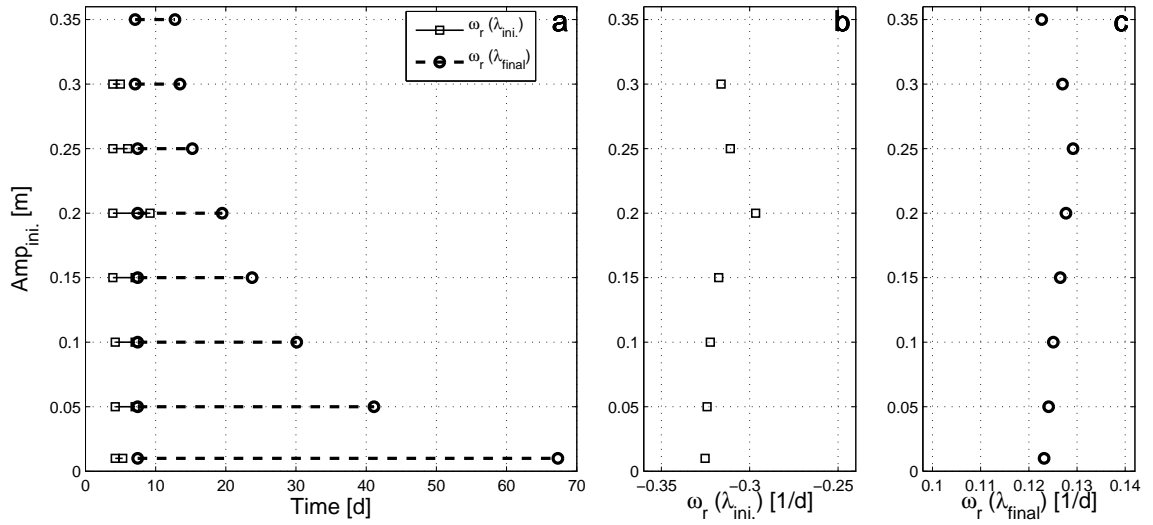


Figure 4.22: (a) The periods of linear growth and decay of the initial perturbation (*solid*) and the final length scale (*dashed*) in time, for various initial amplitudes ($\lambda_{ini.} = 500$ m). (b) The mean value of the growth and decay rate for the initial length scales, and (c) the final length scales.

constant; this is quantified as a change of $< 2\%$ in between two time steps (0.35 days). Another requisite is that the minimum period of linear growth is at least a day (4 time steps). For decaying pre-existing bed patterns, a third criteria is that the amplitude of the bed patterns should be bigger than a certain value. This value is set at 0.002 m. This is because the actual linear decay of the pre-existing bed-form prior to this point is interesting, while the fluctuations afterwards are the result of non-linear effects, due to the interference and dominance of λ_{final} .

The effects of different initial amplitudes on the linear growth rate are presented in Fig. 4.22 ($\theta = 5^\circ$, $\lambda_{ini.} = 500$ m). The period of linear growth of λ_{final} reduces for increasing $Amp_{ini.}$ (see Fig. 4.22(a)). This is due to the increasing value of $Amp_{min}(\lambda_{final})$ for increasing values of $Amp_{ini.}$ (see Fig. 4.17(d)). A

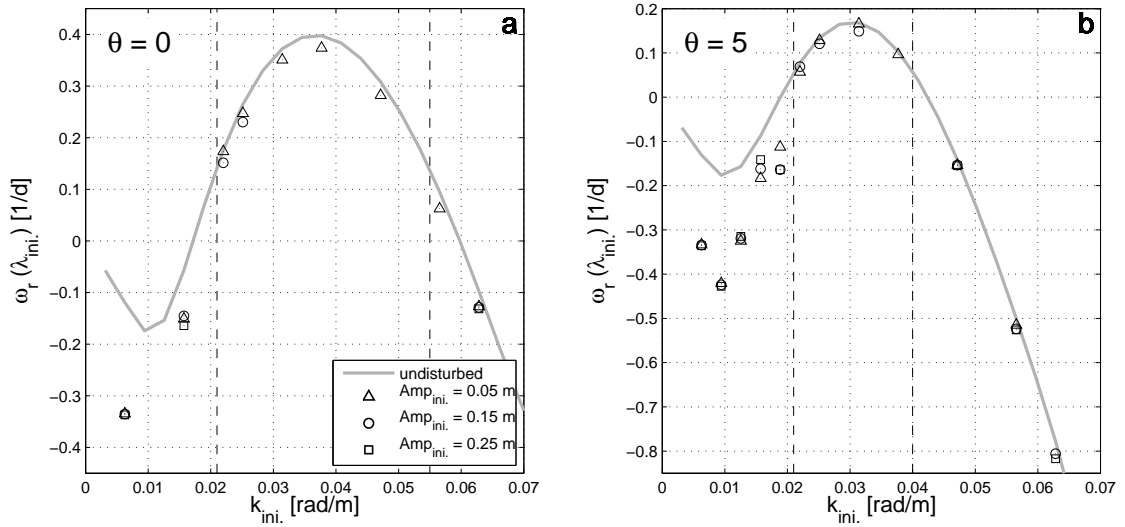


Figure 4.23: The linear growth and decay rates for various initial length scales and amplitudes ($Amp_{ini.} = 0.05$ m (' Δ '), 0.15 m (' \circ ') and 0.25 m (' \square ')) for both (a) normal, and (b) oblique wave incidence. These results are compared with the linear growth starting from an undisturbed bed, after five days of development (grey line). The dashed lines show the range of length scales that remain and do not break up or merge.

bigger value of $Amp_{min}(\lambda_{final})$ results in a more rapid development, and therefore a shorter linear growth period. The duration of the linear decay of $\lambda_{ini.}$ is also related to the value of $Amp_{ini.}$. An increase in initial amplitude of $\lambda_{ini.}$ results in an increase in decay period for $Amp_{ini.} \leq 0.2$ m. However, for values of $Amp_{ini.}$ that are larger still, a decrease in the decay period can be observed, and for $Amp_{ini.} = 0.35$ m linear decay cannot be determined. This is because the formation of the final length scale also happens faster, and soon dominates the linear decay. The growth rate during the linear growth periods as well as the linear decay rate are quasi-constant for various $Amp_{ini.}$ values (see Fig. 4.22(b, c)).

For various values of $\lambda_{ini.}$, a wide range of growth and decay rates can be observed (see Fig. 4.23). The figure only shows the behaviour of the initial pre-existing bed patterns. Length scales that do not break up or merge, but undergo further growth (in between the dashed lines) exhibit positive linear growth, while length scales that are outside this range decrease and therefore show negative growth rates. The pre-existing growth and decay rates show a close correspondence with the undisturbed growth rate curve. Differences mainly occur for disappearing bed-forms with big length scales ($k_{ini.} < 0.02 [rad/m]$), where the decay rate of the pre-existing bed-forms is much bigger than what is observed for the undisturbed development.

Not all $Amp_{ini.}$ show linear growth and decay rates. Only when $Amp_{ini.}$ is small do bed forms that remain show linear growth. The moment when the linear growth rate becomes significantly influenced by non-linear effects, and ceases to be constant, is generally when $Amp(total)$ of this transect reaches between 0.10 and 0.14 m. This threshold amplitude ($Amp_{thres.}$) can be related to $Amp_{end}(total)$: when $Amp(total)$ reaches between 0.4 and 0.6 of $Amp_{end}(total)$, non-linear effects will become significant and a linear model becomes unsuitable to describe the ongoing development. $Amp_{thres.}$ is variable for different initial and final length scales and initial amplitudes, however, $Amp_{thres.} \approx 0.5 Amp_{end}$ seems to form an indication of a boundary for linear development. This threshold amplitude is of interest for the determination of linear growth for pre-existing bed-forms that do not break up or merge. If the amplitude of the pre-existing bed-forms lies above the threshold amplitude, the development of this bed-form cannot accurately be

described using only linear growth. However, the cross shore location of $Amp_{thres.}$ is not at the maximum height of the initial pre-existing bed pattern ($Amp_{ini.}$), and so $Amp_{ini.}$ cannot be directly compared with $Amp_{thres.}$ it would be more correct to compare the amplitude of the pre-existing bed-form at day 1.8 (see Fig. 4.16(b)), when the shift in cross shore location of the pre-existing bed-form creates a peak in the amplitude of the pre-existing bed-forms, with the threshold amplitude for linear growth.

$Amp_{ini.}$ -values of 0.25 m result in a corresponding peak amplitude after 1.8 days of around 0.15 m. This amplitude is generally above the threshold for linear growth and the initial bed-forms show no constant linear growth. Length scales that do not break up or merge and $Amp_{ini.} = 0.15$ m can occasionally result in linear growth, whereas $Amp_{ini.} = 0.05$ m always shows linear growth (see Fig. 4.23). Whether linear growth is observed for initial amplitudes of 0.15 m seems to be dependent on the growth rate of the particular length scale. Linear growth is only assumed to exist when the the linear growth rate is close to constant over a day. The period of linear growth is reduced when the growth rate is big: the amplitude quickly reaches the threshold amplitude, and non-linear effects will take effect. If the period of linear growth is less than one day, this is determined to be too short to be regarded as linear growth. This occurs in particular for initial length scales that are close to the *FGM* for normal wave incidence, since these length scales show the highest linear growth rate.

Length scales that are on the boundary between decay and growth show different behaviour; for $\theta = 0^\circ$ these length scales are: $\lambda_{ini.} = 333$ and 111 m ($k_{ini.} =$

0.019 and 0.057 [rad/m], respectively), and for $\theta = 5^\circ$: $\lambda_{ini.} = 333$ m ($k_{ini.} = 0.019$ [rad/m]). As was described in section 4.4.2, these length scales show limited linear growth in the undisturbed case (see Fig. 4.14 and 4.15), but are at some point overwhelmed by faster developing length scales that occur in the centre of the growth rate curve. These initial length scales generally show only a very gradual increase or decrease in amplitude, and no linear growth. However, for one case linear growth is determined ($\theta = 0^\circ$, $k = 0.057$ [rad/m] and $Amp_{ini.} = 0.05$ m), which closely corresponds with the growth rate for the undisturbed case (*grey line*).

Figure 4.23(a, b) gives insight into the behaviour observed in Fig. 4.19(d), which shows that although $Amp_{min}(\lambda_{final})$ increases for increasing $k_{ini.}$, $Amp_{min}(total)$ decreases. Results presented in 4.19(a, c) suggest the opposite: for increasing $k_{ini.}$, the increasing $Amp_{min}(\lambda_{final})$ causes a more rapid development of λ_{final} , and therefore a higher level of $Amp_{min}(total)$. Results presented in Fig. 4.23(a, b) show a second contribution to the determination of the total minimum amplitude: the decay rate of the pre-existing bed-form also affects $Amp_{min}(total)$. The minimum total amplitude decreases, because the decay rate of $\lambda_{ini.}$ rapidly increases for increasing k -values, even while $Amp_{min}(\lambda_{final})$ increases.

The linear growth rate of the finally dominant length scales is shown in Fig. 4.24, for both normal (a, c, e) and oblique wave incidence (b, d, f). The undisturbed growth rate (originating from Fig. 4.8) of various length scales is taken as benchmark for the growth rate of bed patterns that develop under pre-existing conditions. Growth rates of the finally dominant length scales correspond well

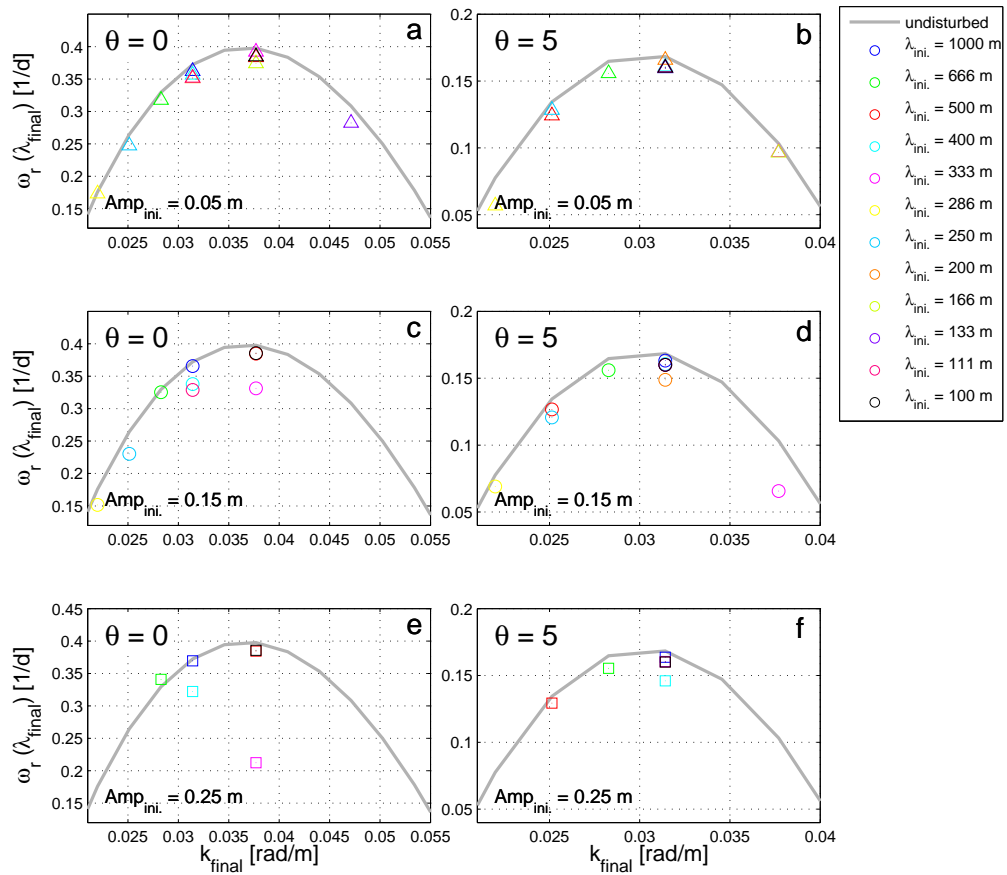


Figure 4.24: The linear growth rates of λ_{final} (in colour) for various initial amplitudes ($Amp_{ini} = 0.05$ m (\triangle), 0.15 m (\circ) and 0.25 m (\square)), compared with the linear growth for the undisturbed bed (after 5 days) (grey line), (a, c, e) for normal, and (b, d, f) oblique wave incidence.

with the growth rate in the undisturbed case, although the evolution of bed-forms from pre-existing bed patterns predict slightly smaller growth rates than what is observed in the undisturbed case. Smaller initial amplitudes are generally closer to the undisturbed growth rate than bigger initial amplitudes, and this effect is stronger for length scales that do not break up or merge. This is due to the non-linear effects that cause reduced or non-existent linear growth rates.

4.4.4 Migration rate

The migration rate of bed-forms has not been a major topic of investigation for the comparison of field observations with linear stability predictions presented in chapter 3. The field observations by van Enckevort et al. [2004] suggest migration rates of less than 40 m/d, but a day-to-day listing of the observed migration rates is not presented. However, migration rates are predicted by the linear stability analysis, and investigated is how these are affected by pre-existing bed-forms.

Previous research using a non-linear stability analysis has studied the development of one bed pattern length scale from both an alongshore constant, and a randomly disturbed beach. Migration rates have thus been relatively easy to obtain. Visual inspection of the results showed how rapidly a bed pattern migrated along a coast [Garnier, 2006]. However, the introduction of pre-existing bed-forms makes a visual determination of the migration rate insufficient. In this case the objective is to determine both the migration rate of the pre-existing bed-form as well as the finally dominant length scale. This behaviour is obscured by the decay

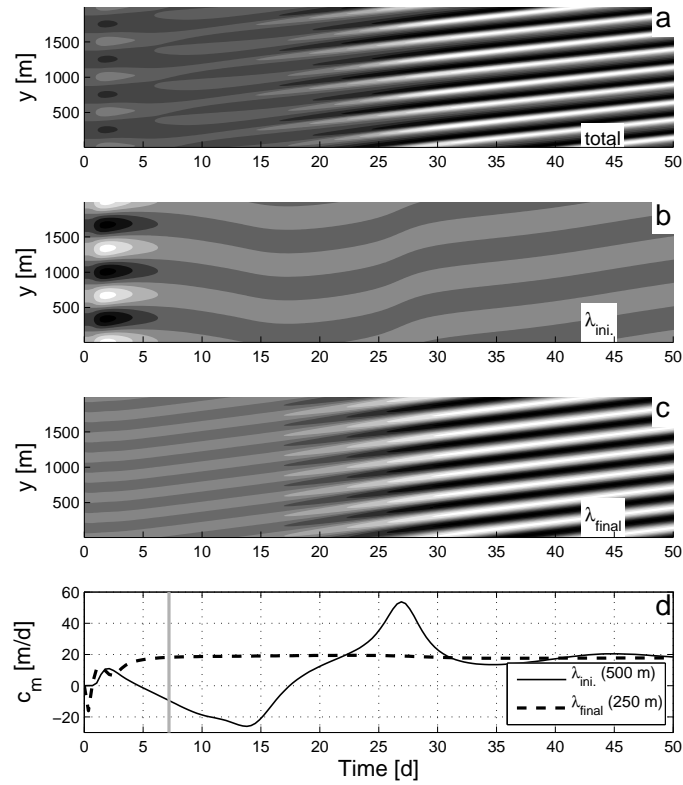


Figure 4.25: (a) The evolution of the nearshore bed in time when pre-existing bed patterns exist for oblique wave incidence ($\lambda_{ini.} = 500$ m, $Amp_{ini.} = 0.15$ m). (b, c) The reconstructed bed profile according to the Fourier analysis output for $\lambda_{ini.}$ and $\lambda_{final.}$. (d) The migration rate of the initial pre-existing bed-form and finally dominant length scale. The grey line at day 7 in (d) represents the moment when the dominant mode shifts from $\lambda_{ini.}$ to $\lambda_{final.}$.

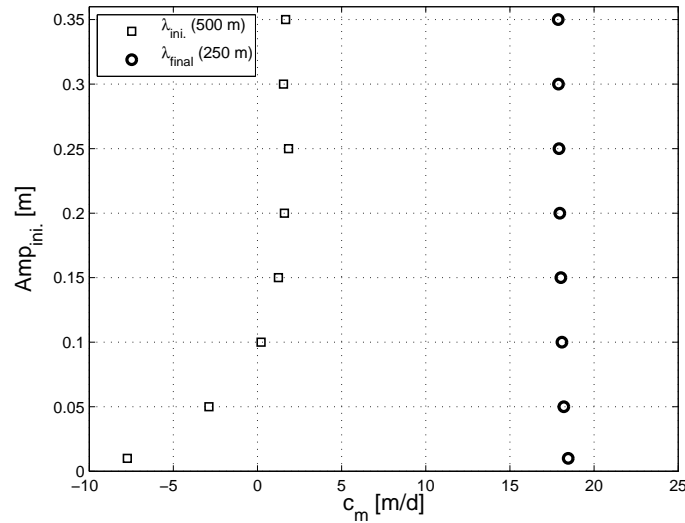


Figure 4.26: The migration rate of the pre-existing and the finally dominant bed-forms for various initial amplitudes ($\lambda_{ini.} = 500$ m, $\theta = 5^\circ$).

and growth of either bed-form, making visual determination unsuitable.

To calculate the migration rate of various length scales, a Fourier analysis is used to separate the various different processes corresponding to different length scales. The contribution of both $\lambda_{ini.}$ and λ_{final} are shown in Fig. 4.25(b, c). The shift in alongshore location of bar crests in both graphs gives the migration rate of both length scales (Fig. 4.25(d)). For λ_{final} this migration rate is rather constant, at around 18 m/d. The migration rate of $\lambda_{ini.}$ changes in time. Initially the migration rate fluctuates and averages around 0 m/d. When the final length scale becomes dominant, the migration rate of $\lambda_{ini.}$ converges to the migration rate of λ_{final} . The initial length scale diminishes in height, and the physical relevance of the migration rate after the dominant bed-form has become λ_{final} , is therefore reduced. For the quantification of the migration rate of both the initial and final

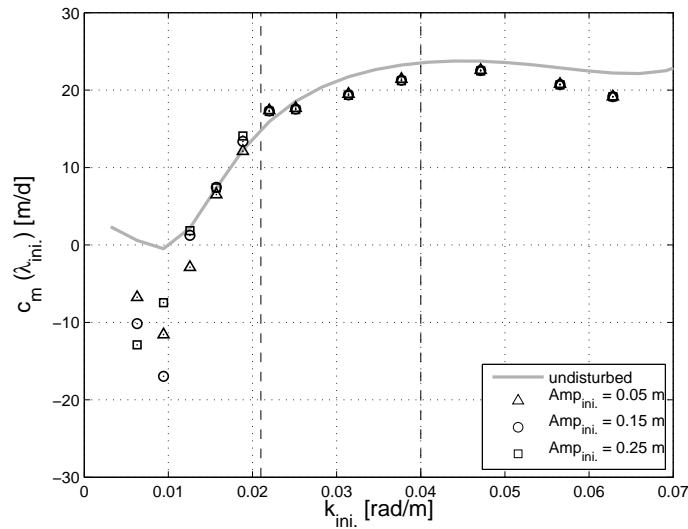


Figure 4.27: The migration rate of the initial pre-existing bed-forms with different length scales and amplitudes for oblique wave incidence. The average migration rate is plotted over the period for which λ_{ini} is dominant. The undisturbed migration rate (at day 5) of various length scales is plotted as a grey line. The dashed lines show the range within which the length scales remain, and do not break up or merge.

length scale, the average migration over the period of dominance of either length scale is chosen.

The influence of Amp_{ini} on the migration rate of both the pre-existing bed-forms and the finally dominant bed patterns is limited (see Fig. 4.26). The migration rate of the final length scale is not dependent on the initial amplitude. The migration rate of the initial length scale seems to be influenced by the initial amplitude, since the migration rate is negative for small initial bed patterns, but becoming positive for big pre-existing amplitudes. The reason for the changing

initial migration rate is the way this value is calculated and not due to changes in the migration rate in time. The migration rate is an average over the period where λ_{ini} is dominant. This decreases for increasing Amp_{ini} , reducing the number of negative migration rates that occur after day 5 that are included in calculation of the average migration rate (see Fig. 4.25(b)).

The migration rate of various initial bed-forms closely corresponds to the undisturbed migration rate curve (see Fig. 4.27). The migration rate curve for the undisturbed development was determined at day 5 of the modelling period. The migration rate curve fluctuates more in time than the growth rate curve, and the slight differences that occur between the pre-existing migration rate and the undisturbed migration rate can partially be attributed to this. The undisturbed migration rate curve at this time is depicted since it shows the most complete migration rate curve without non-physical fluctuations. Migration rates of the pre-existing bed-forms fluctuate (see Fig. 4.25(b)), but the average migration rate corresponds well with the undisturbed migration rate at day 5, especially for shorter length scales. It can also be concluded that the initial amplitude of the pre-existing bed-forms does not influence the migration rate significantly. Migration rates of length scales that are not breaking up or merging (in between the dashed lines) are an average of the migration rates over the entire modelling period. A possible explanation for why these length scales show a slightly lower migration rate than what is observed for the undisturbed development, is that during the initial stages of the run the migration rate is zero. This is probably due to the fact that wave conditions are still building up in the early stages of

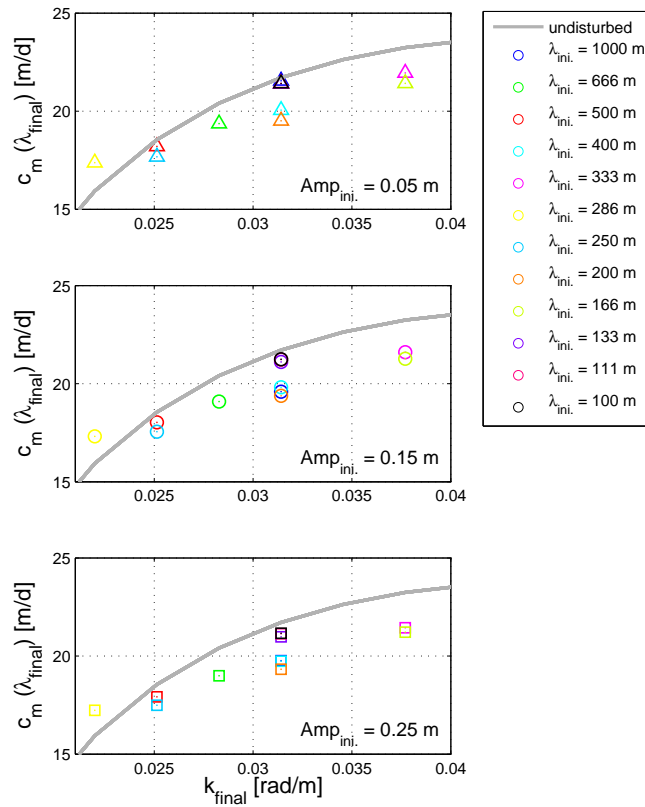


Figure 4.28: The migration rate of λ_{final} for different Amp_{ini} . ($Amp_{ini} = 0.05$ m (' \triangle '), 0.15 m (' \circ ') and 0.25 m (' \square ')), for oblique wave incidence. The average migration rates are plotted over the period for which each λ_{final} is dominant. The corresponding migration rate for the undisturbed evolution (after 5 days) is depicted as a grey line.

development, and because of the appearance of the pre-existing bed-forms; the implemented pre-existing bed-forms are designed to be shore normal. During the first days, the orientation of the bed pattern changes, while the constant migration rate establishes.

The migration rate of the finally dominant length scales (Fig. 4.28) is generally slightly underpredicted compared to the undisturbed migration rate. However, the difference between the undisturbed migration rate (*grey line*) and the migration rate of finally dominant length scales ('□', 'o' and '△') seems to be rather constant, suggesting that the undisturbed migration rate at this moment in time (after five days) might be a slight over-estimation of the average migration rate in time.

4.5 Discussion

To investigate the effects of pre-existing bed-forms on the development of crescentic bed patterns, a wide range of different pre-existing length scales, amplitudes and different wave conditions were examined. The results obtained show a clear relationship between the development of an undisturbed beach and the evolution of the nearshore zone in the case of pre-existing bed patterns.

A linear model has limitations that make difficult the direct application of model results to predict the development of crescentic bed-forms according to changing wave conditions. A non-linear model has more freedom to accurately describe field conditions. However, in order to observe specific behaviour that is related to the effects of pre-existing bed-forms, many conditions were set to create circumstances that resulted in the gradual evolution of bed-forms and the aim was not necessarily to create model predictions that are directly comparable with reality.

The time before a bed-form reaches its final height is significantly longer in the runs carried out in this research than is observed in reality. Observed bed-forms generally reach a final height within three weeks [van Enckevort et al., 2004]. The time before bed-forms reach a final height during these runs is dependent on various factors. The duration of the development of bed-forms is influenced by the value of the downslope term (γ) and the moderate wave conditions. The pre-existing bed characteristics resulted in development times ranging from 10 to over 100 days. Characteristics, such as the time at which a bed-form reaches its max-

imum height and the time when the dominant bed pattern length scale changes, are therefore not comparable with reality. However, other characteristics, such as the linear growth rate, the final amplitude and the migration rate, give a good insight into the processes involved in the evolution of crescentic bed-forms from an initial state where bed-forms already exist.

The initial amplitude of the finally dominant length scale ($Amp_{min}(\lambda_{final})$) depends on various factors: Not only will a bigger initial amplitude of the pre-existing bed-form result in an increased initial excitement of the finally dominant length scale, but also the initial pre-existing length scale will cause variations in the excitement of the range of length scales close to λ_{FGM} . Length scales that form a factor of the pre-existing length scale show a bigger initial amplitude (Amp_{min}), which subsequently results in a more rapid evolution, compared to other bed pattern length scales. The results presented in this chapter suggest, therefore, that when a pre-existing bed pattern breaks up, this will give rise to a new bed pattern whose length scale is closer to λ_{FGM} of the undisturbed development, and also forms a factor of λ_{ini} . In reality, a single dominant mode is generally not observed [van Enkevort et al., 2004]. This means that a much wider range of different length scales will be initially excited than what is assumed for these runs. A more realistic approach could be to implement random perturbations onto the pre-existing bed-forms, to cause large initial amplitudes for a wider range of bed pattern length scales. However, runs that included random perturbations show that although a wider range of length scales develop, the finally dominant length scale does not change. The application of random perturbation, however, also

results in a more disturbed development of bed-forms, making the analysis more complicated. It is noteworthy that pre-existing length scales that are significantly shorter than λ_{FGM} merge to become λ_{FGM} . The finally dominant length scale of these short pre-existing bed-forms is therefore not a whole number factor of the initial length scale, which results in smaller Amp_{min} values of the finally dominant bed-forms.

The periodic boundaries at either end of the alongshore modelling domain and the limitations of a Fourier analysis result in a reduction in the number of length scales that develop within the model runs. Only bed-forms that form a factor of the total width of this stretch of beach (2000 m) can be implemented as pre-existing bed-forms and can develop into a finally dominant length scale. This means that only a limited number of long pre-existing bed-forms can be examined. The application of moderate wave conditions, however, results in the development of finally dominant length scales that are reasonably short ($\lambda_{FGM} = 200$ m ($\theta = 0^\circ$) and $\lambda_{FGM} = 166$ m ($\theta = 5^\circ$)), and the range of possible length scales in that region is large enough to give quantified predictions of the finally dominant length scale.

In setting up the conditions for the non-linear model runs, the results from the linear stability analysis were used to create the pre-existing bed-forms. The Morfo60 output only gives physically accurate descriptions of bed pattern length scales that have a positive linear growth. A wide range of pre-existing length scales were generated by the application of extreme wave conditions ($H_{rms} = 1.5$ m, $T_p = 7.5$ s and $\theta = 0^\circ$). The cross shore location of the peak in the bed perturbation

is, however, further offshore than for the pre-existing runs of the non-linear model under moderate wave conditions, due to the increased wave height. The discrepancy between the offshore location of the peak in the bed pattern perturbation according to the extreme wave conditions in Morfo60 and the more moderate runs in Morfo55 is resolved at the start of each run: The bed patterns shift shorewards and reach the new optimum location after 1.8 days (see Fig. 4.16).

A second concern related to the application of linear stability results to create pre-existing bed-forms is the physical appearance of the bed-forms. In a linear stability analysis, bed patterns are assumed to be very small. The appearance of bed patterns according to the linear stability analysis might, therefore, not exactly correspond to the actual appearance of bed-forms of bigger initial amplitudes. Results from the non-linear model suggest that bed-forms not only grow in height but also expand in the cross shore direction, and this may not be represented by the linear model.

4.6 Conclusions

Results from a non-linear stability analysis of the effects of pre-existing bed-forms on the evolution and development of crescentic bed patterns, show that the existence of bed-forms at the start of the modelling period causes significant changes to the evolution of the nearshore seabed. The effects of these pre-existing bed-forms are, however, closely linked to the undisturbed evolution of bed-forms, i.e. when bed patterns develop from an alongshore constant beach profile. Pre-existing bed-forms, therefore, do not necessarily negate predictions made by a linear stability analysis. The existence of pre-existing bed-forms makes it necessary to interpret the predictions made by a linear stability analysis with care.

Non-linear stability analysis results of the evolution of the nearshore seabed with pre-existing crescentic bed-forms show that pre-existing bed patterns with a length scale that is close to the dominant length scale of the undisturbed case (λ_{FGM}) will undergo further growth and reach a final height within a short period of time. Initial length scales that are outside the linear growth rate curve of the undisturbed development will decrease in prominence and give rise to crescentic bed patterns with a length scale close to λ_{FGM} . When a pre-existing bed pattern breaks up, the finally dominant length scale generally forms a factor of the pre-existing length scale, this finally dominant length scale is closer to λ_{FGM} than the pre-existing length scale.

The rate of growth and decay of the pre-existing bed-forms as well as the finally dominant bed pattern both closely correspond to the undisturbed growth

rate curve. The development of pre-existing bed-forms with a length scale close to λ_{FGM} shows a similar linear growth to the undisturbed growth of that length scale, but only if the initial amplitude is small and the non-linear effects are negligible. If a new bed-form arises from a pre-existing bed pattern, a period of linear growth can also be observed. The growth rate of the newly arising bed-form is again very similar to the undisturbed growth rate of that length scale. Pre-existing bed-forms that are outside the undisturbed growth rate curve will decrease and give rise to the development of a length scale closer to λ_{FGM} . The rate of decay of the pre-existing bed-forms corresponds well with the negative part of the growth rate curve of the undisturbed development. However, the agreement is stronger for length scales that are shorter than λ_{FGM} , than for length scales that are significantly larger.

Different final length scales result in slight changes in the final amplitude and migration rate, which are similar to those observed in the undisturbed scenario. The migration rate of decreasing initial length scales, during their period of dominance, also corresponds with the undisturbed migration rate.

The results presented in this chapter show that the non-linear evolution from a periodically disturbed bed can be partially described using only a linear stability analysis. The finally dominant length scales are, independent of the pre-existing length scale, always near the peak of the undisturbed growth rate curve. There is also strong agreement between the growth rate and migration rate of both the growing and declining bed-forms and the final amplitude of the finally dominant length scale.

Chapter 5

Pre-existing bed patterns in a linear stability model

The results obtained using the non-linear model have shown that results from a linear stability model can be used to describe the development of bed-forms when bed patterns pre-exist. This chapter introduces a possible application of this knowledge to predict the development of crescentic bed patterns using a linear stability model, and describes the development of an algorithm to implement this new understanding.

5.1 Assumptions of the pre-existing algorithm

In the comparison of linear stability model predictions of the development of crescentic bed patterns with field observations (presented in chapter 3), each set of wave and tidal conditions resulted in a separate linear growth rate curve. The fastest growing mode (*FGM*) of each of these runs was assumed to dominate the development of the other length scales. However, the investigation into pre-

existing bed-forms has revealed that the entire linear growth rate curve is of importance, including the length scales that show linear decay rates. Pre-existing bed patterns, whose length scale shows significant linear growth under the present forcing circumstances, will remain and undergo further development. However, when the length scale of a pre-existing bed-form lies outside the range of currently growing modes, then this length scale will decay. The rate of initial decay of this pre-existing bed pattern corresponds to the linear decay rate of this length scale under the existing forcing conditions.

The implementation of the results obtained in chapter 4, has resulted in the following assumptions for a pre-existing bed-forms (*PEB*) algorithm, which can be applied to the linear stability results for the Duck conditions:

- After a storm, existing bed patterns are wiped out and all length scales start with the same initial amplitude (Amp_0).
- The amplitude of different length scales develops according to rate of growth or decay for that length scale, as presented in the linear growth rate curve. The growth rate curve changes over time, due to changing forcing conditions, and this will affect the development of the amplitude of different length scales.
- For any moment in time, it is assumed that any length scale cannot be smaller than a certain threshold. Decaying amplitudes can therefore not decay beyond Amp_0 .

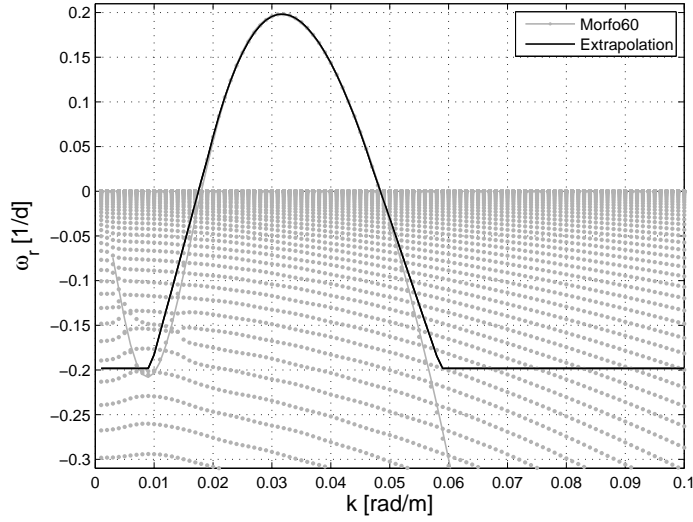


Figure 5.1: The positive part of the growth rate curve is extrapolated in order to obtain negative growth rates for length scales that are outside the positive part of the growth rate curve. The maximum decay rate is set at the negative value of the growth rate of the *FGM*. The results from Morfo60 are displayed in grey dots, with an approximation of the physically accurate modes depicted as a grey line. The extrapolated results are shown as a black line.

- The most likely length scale to be observed in reality is assumed to be the length scale with the biggest amplitude at each time step; the dominant length scale (λ_d).
- With the increase in amplitude of the bed patterns, the importance of non-linear effects in the governing equations also increases, reducing the accuracy of linear stability analysis predictions. A maximum amplitude (Amp_{max}) is therefore established to determine the moment when linear results are assumed to become inaccurate.

The Morfo60 model produces the same number of solutions to the system of equations, as there are computational nodes ($N_x = 300$), for each examined length scale ($N_\lambda = 109$) and set of wave conditions ($N_t = 500$). The data stored from the Morfo60 runs of Duck did, however, not contain all the decaying modes. As the focus so far has been on the prediction of the *FGM*, only the biggest growth rates of each length scale were stored for each set of wave conditions. The available data of the Duck model runs, therefore, only gives a very limited insight into the decay of bed patterns.

A large number of decaying solutions to the system of equations are numerical in nature, making the determination of the physically accurate decaying modes difficult. The ideal solution would be to do two sets of runs, one with, for example, double the number of computational nodes than the other one, for each length scale and each set of wave conditions. Numerical results change in growth rate, whereas physical results would remain approximately constant, making it possible to identify decay rates of the length scales that are outside the growth rate curve. However, this approach is cumbersome, and for a first analysis presented here, a different approach was chosen.

In order to be able to describe decaying bed patterns, the rate of decay of length scales that do not show linear growth is determined using a linear extrapolation based on the two smallest growing modes on either side of the growth rate curve. It is assumed that the rate of decay cannot exceed the maximum rate of growth under each set of forcing conditions: The rate of decay is limited to the negative value of the growth rate of the *FGM*: $\omega_{r_{min}} = -\omega_{r_{FGM}}$.

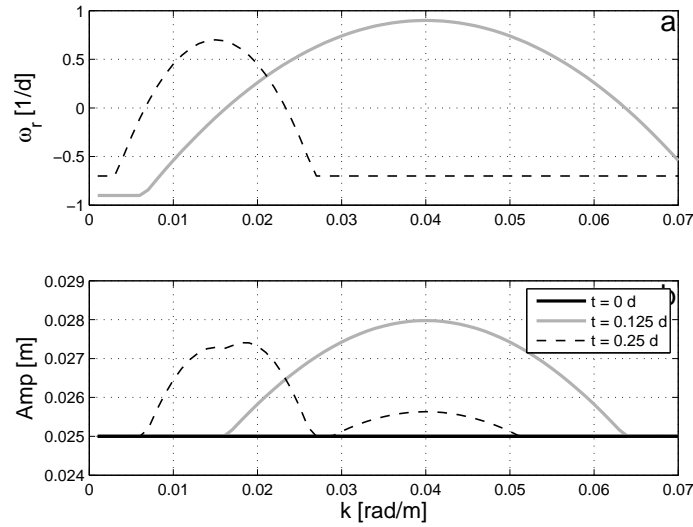


Figure 5.2: (a) Two different growth rate curves, at two time steps. (b) The development of the amplitude of various length scales according to the growth rates at the subsequent times. All length scales start with an amplitude of 0.025 m.

An example of the growth rate as well as the extrapolated rate of decay are presented in Fig. 5.1. In this figure, all solutions to the system are displayed (*grey dots*). In order to demonstrate the accuracy of the extrapolation, more than just the biggest growth rate for each length scale is shown. The extrapolated results (*black line*) show a slight underestimation of the negative part of the growth rate curve (*grey line*) when the decay rate does not exceed $-\omega_{rFGM}$. When the modelled decay rate exceeds $-\omega_{rFGM}$, extrapolated decay rates significantly underpredict the actual development. However, overall, a reasonably accurate description of the rate of decay can be achieved this way.

The development of the amplitude of different length scale can be described

by (see Fig. 5.2):

$$Amp(k_g, t_{j+1}) = Amp(k_g, t_j) e^{\omega(k_g, t_j) \Delta t}, \quad (5.1)$$

where $k_g = 0.001 - 0.11$ [rad/m], t_j represents the points in time when wave data were recorded, which have been modelled individually in Morfo60 ($j = 1 - 500$), and Δt represents the time step between two wave data records ($\Delta t = 3$ hours).

The runs presented in chapter 3 have shown that the development of bed patterns up to half their final height is the result of linear growth. The field measurements at Duck generally display an alongshore variation in the bar height of around 1 m, and therefore it is assumed that the maximum amplitude (Amp_{max}) is 25 cm.

The initial amplitude of all length scales after a storm (Amp_0) is set at 2.5 cm. The results presented in chapter 4 have shown that the initial amplitude of the finally dominant bed-form ($Amp_{min}(\lambda_{final})$) can be as high as 2.5 cm, when a single pre-existing bed pattern length scale is implemented (see Fig. 4.19). In reality, even after a storm, it is assumed that initial perturbations are at least as big as this value.

The determination of the value of both Amp_0 and Amp_{max} is rather arbitrary. The period for which the predictions of a linear stability analysis are assumed to be accurate, is therefore arbitrary as well. However, the period of time over which bed-forms grow by a factor of ten, as is used here, seems to correspond well with the previously presented time periods of linear growth after each storm (presented in section 3.5).

5.2 Comparison with field observations

The development of the dominant length scale according to the *PEB* algorithm is based on the entire growth rate curve for the various wave conditions and tidal levels recorded at Duck (see Fig. 5.3(a)). The implementation of the *PEB* algorithm can be seen in Fig. 5.3(b), where the evolution of the amplitudes of different length scales is depicted. The change from a filled plot, to only contour lines (at day 247 and 280) depicts the change from a linear regime to a supposedly non-linear regime, since the amplitude of the dominant length scale (Amp_d) surpasses Amp_{max} . However, the development beyond this moment in time is depicted since both Amp_0 and Amp_{max} are determined arbitrarily and the development may (under different initial and final conditions) still be defined to be within the range of a linear stability model. Fig. 5.3(c) depicts the normalised amplitude over time. At each time step, the value of the maximum amplitude is set at 1, and the amplitudes of all other length scales are scaled to this value.

A comparison of field observations with the *PEB* algorithm shows that immediately after the first and third storm (day 237 and 273), the predicted length scales correspond well with field observations. Both field observations and model predictions show the occurrence of a wide range of length scales. The *PEB* algorithm, however, overpredicts the length scale in between storms. This occurs especially after the first and second storms. After the first storm, a long period of relatively low wave activity results in stable bed-form length scales for both the algorithm and the observations. However, the *PEB* algorithm shows no development of shorter length scales during the initial post-storm stages, and when the

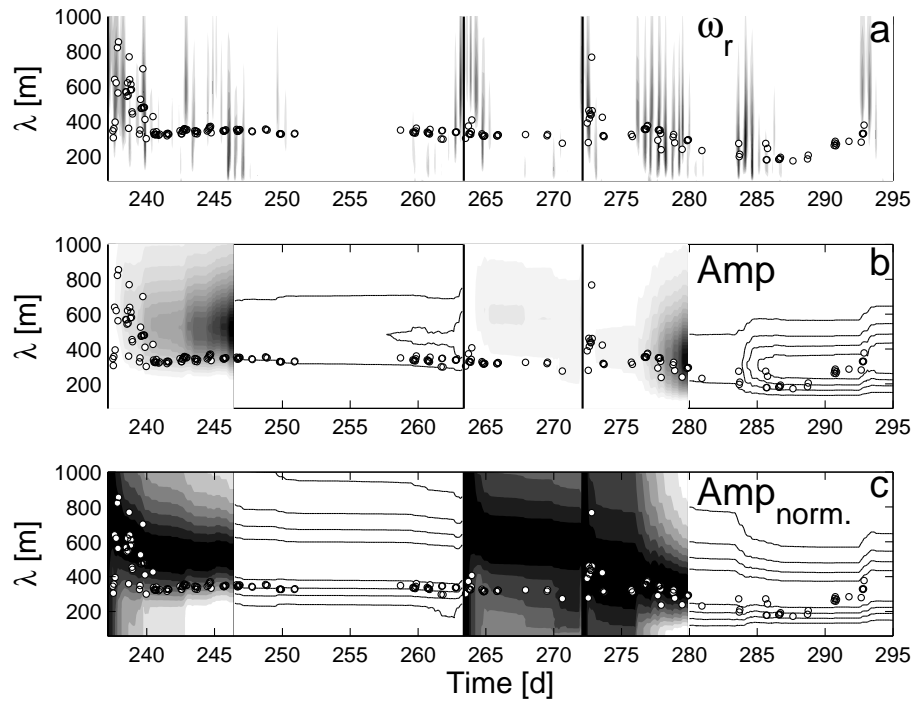


Figure 5.3: (a) The positive part of the growth rate curves predicted by Morfo60 for the different wave and tidal data over time recorded at Duck. The field measurements are shown in open black circles. (b) The development of the amplitudes of different length scales in time, according to the *PEB* algorithm. (c) the normalised amplitude of various bed pattern length scales at each time step. The vertical black lines represent storms (at day 237, 264 and 273). At these points in time, the amplitude of the various bed pattern length scales is set back to Amp_0 . The change from a filled plot to only contour lines (at days 247 and 280) depicts the points in time when Amp_d surpasses Amp_{max} .

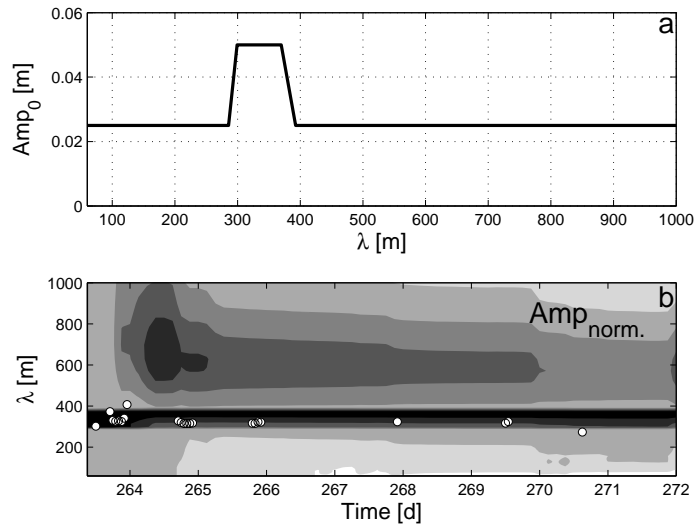


Figure 5.4: The results from the *PEB* algorithm after the second storm, when pre-existing bed patterns are preferentially initially excited. (a) The distribution of Amp_0 over the different length scales. Pre-existing length scales ($\lambda = 300 - 360$ m) are excited twice as much as the other length scales. (b) The normalised amplitude of various bed pattern length scales at each time step after the second storm.

wave conditions settle down, these shorter length scales do not become dominant. Contrastingly, the field observations show a significant decrease in length scale after the first days.

As was previously presented, the observed length scale after the second storm does not alter from the pre-storm conditions, suggesting that the pre-existing bed patterns are not fully wiped out. During this period, the *PEB* algorithm shows a significant overprediction of the dominant length scale compared to the field observations. However, the results presented in Fig. 5.3(b) show that the development of bed patterns is very small. If the observed pre-existing length scales

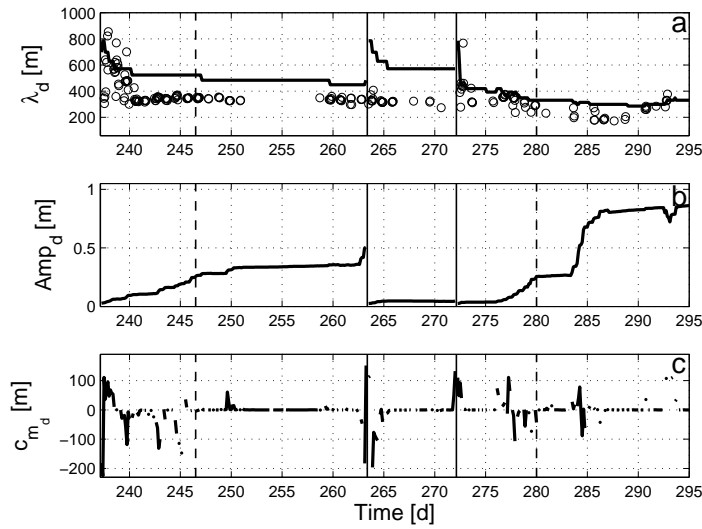


Figure 5.5: The development in time of the dominant length scale (a), the dominant amplitude (b) and the dominant migration rate (c). The solid vertical lines represent the storms, whereas the dashed vertical lines represent points in time when Amp_d surpasses Amp_{max} .

were to be excited more in Amp_0 than the other length scales, this would result in the continued dominance of these pre-existing length scales, after the second storm (see Fig. 5.4). However, this is not included in the ongoing comparison of model predictions with field observations, since knowledge concerning the occurrence of pre-existing bed patterns after this storm does not exist and an accurate description of the distribution of Amp_0 cannot be derived.

The predicted development after the third storm corresponds well with the field observations. Compared to the less accurate predictions after the first storm, it can be concluded that the occurrence of bigger growth rates for a longer period of time results in a longer period of development of the bed patterns after the third storm, resulting in a better correspondence.

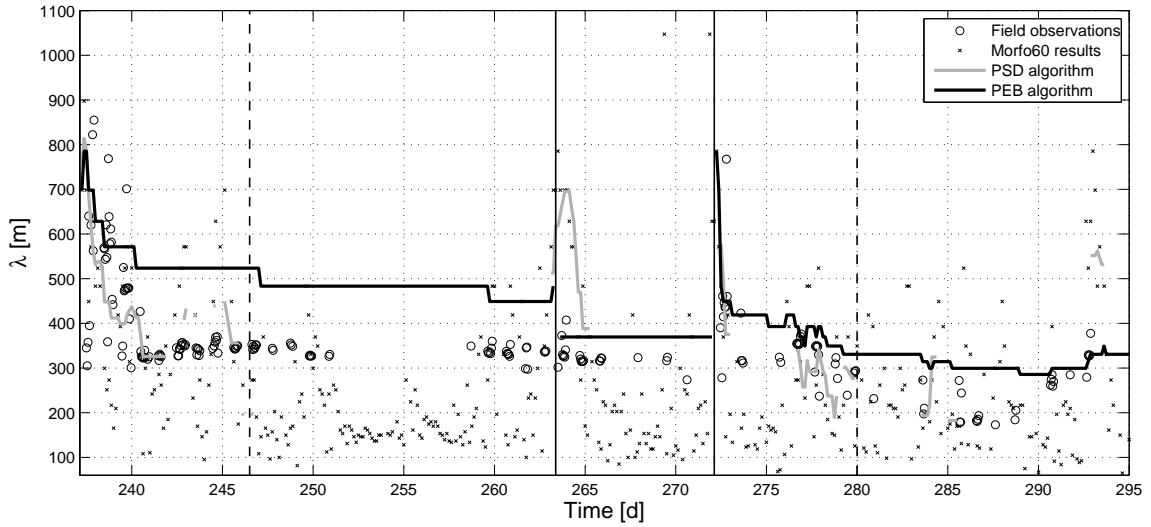


Figure 5.6: The observed length scale at Duck in time ('o') along with the original Morfo60 results ('x'), the output of the *PSD* algorithm (*grey line*) and the *PEB* algorithm (*black line*). The solid vertical lines represent the storms, whereas the dashed vertical represent the points in time when Amp_d surpasses Amp_{max} .

The dominant length scale (λ_d) as well as the amplitude (Amp_d) and the migration rate (c_{m_d}) of the dominant length scale at each time step are depicted in Fig. 5.5. The amplitude development shows a direct correspondence with the growth rate in Fig. 5.3(a). Periods with significant growth rates (after the first and third storm) result in significant amplitude gains. The determination of the migration rate is a direct result of conclusions drawn in chapter 4. The migration rate at a certain point in time is that of λ_d according to the migration rate curve at this moment, and not the migration rate of the *FGM* predicted at that moment. The migration rate distribution in time, however, shows a very similar behaviour to the original migration rate of the Morfo60 results (presented in section 3.3).

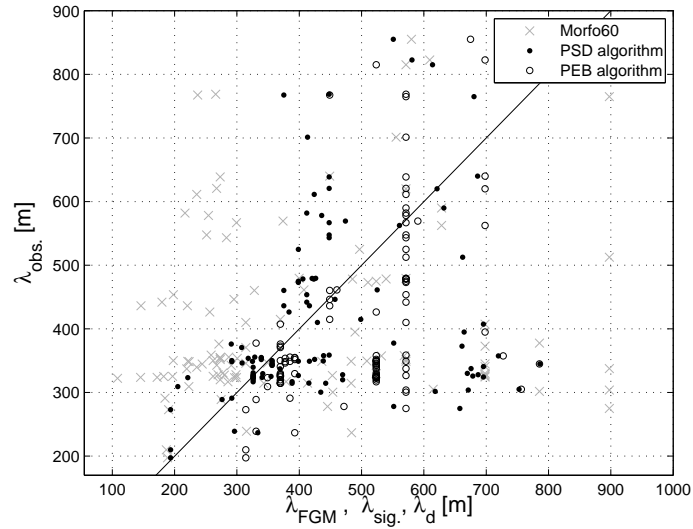


Figure 5.7: The predicted length scales according to the original Morfo60 results (λ_{FGM} : \times), according to the *PSD* algorithm (λ_{sig} : \bullet) and according to the *PEB* algorithm (λ_d : \circ), versus the observed length scales ($\lambda_{obs.}$) of the crescentic bed patterns at Duck. The solid line represents perfect correspondence between predicted length scales and those from field observations.

Generally, the migration rate is small, but can be as high as 200 m/d during extreme wave conditions.

A comparison between the observed and predicted length scale of crescentic bed patterns is presented Fig. 5.6 and 5.7. Both figures show the results from each of the previously presented attempts to use a linear stability model to describe real-world conditions. The actual Morfo60 output shows a very high rate of fluctuation (Fig. 5.6), due to the assumption of an alongshore uniform beach profile and the changing forcing conditions. The *PSD* algorithm identifies the more physically significant predictions at certain periods in time, and gives a much more

accurate description of the occurring bed-forms at these moments. Finally, the *PEB* algorithm shows a very gradual development of the dominant length scale. However, this algorithm also shows a continuous overprediction of the length scales occurring in between storms (see Fig. 5.7).

The implementation of the knowledge obtained from the study of pre-existing bed patterns only improves the predictive skills of the linear stability analysis locally, and the overall relative error of the *PEB* algorithm results is the same as the original raw Morfo60 results ($[\delta_{\lambda_{obs.}, \lambda_{FGM}}]_{entire\ period} = [\delta_{\lambda_{obs.}, \lambda_d}]_{entire\ period} = 0.44$). The development of crescentic bed patterns after the third storm shows a closer correspondence between field observations and *PEB* algorithm predictions. Wave conditions do not settle down as quickly as after the first storm, and a similar evolution of the bed pattern length scale is predicted with the *PEB* algorithm as that observed in the field, resulting in a small relative error. ($[\delta_{\lambda_{obs.}, \lambda_{FGM}}]_{Post\ storm\ 3} = 0.37$ and $[\delta_{\lambda_{obs.}, \lambda_d}]_{Post\ storm\ 3} = 0.18$).

A comparison between the predictions made by the *PEB* algorithm and the *PSD* algorithm shows that the *PSD* algorithm corresponds much more closely with the field observations much more closely than the *PEB* algorithm. However, where the *PSD* algorithm attempts only to identify periods in time where predictions and observations might converge, the *PEB* algorithm attempts to describe the continuous evolution of the bed patterns. The overall relative error between field observations and the *PEB* algorithm is therefore larger than the relative error of the periods predicted by the *PSD* algorithm. However, the relative error for

the *PEB* algorithm after storm 3 is the same as the error by the *PSD* algorithm. A possible improvement in the comparison between model predictions and field observations could be achieved through the combination of both algorithms. The *PEB* algorithm can be used for the accurate implementation of pre-existing bed patterns and an algorithm similar to the *PSD* algorithm can subsequently be used to identify the specific periods in time when predictions made by a linear stability model are assumed to be similar to field observations.

5.3 Discussion

The pre-existing bed-forms algorithm presented in this chapter is a first attempt at including the effects of pre-existing bed patterns into an analysis made by a linear stability model, in describing real-world conditions. This algorithm shows that the gradual evolution of the bed pattern length scale, as observed in the field, can be described by a linear stability analysis. However, discrepancies between model predictions and field observations remain significant. Improvements in the design of the algorithm might improve the comparison, although more field data is needed for the accurate quantification of such alterations.

The predictions made by the *PEB* algorithm generally show an overprediction of the dominant bed pattern length scale, compared to the field observations. Only directly after a storm do the results of the algorithm partially correspond with the observations made in the field. However, field observations suggest a continuous presence of short bed pattern length scales during the entire observation period. This is not predicted by the *PEB* algorithm, which predicts only bigger length scales to occur after a storm. A possible explanation might be that the model set-up favours longer length scales. The application of a description of the friction by Feddersen et al. [2000] resulted in a reduction of the predicted length scale of the *FGM* for oblique wave incidence (see section 2.2). However, it might be that the model settings still favour bigger length scales. An alternative explanation is that the model underpredicts the growth rate under mild wave conditions, resulting in the lack of development of shorter length scales during mild wave conditions in between storms. Alternatively, it might be that the error lies in the assumption

that all bed patterns are wiped out during each storm. It may be that periodic perturbations of shorter length scales still exist after a storm. Such a phenomenon was shown in our data to occur after the second storm, but it might be that this also occurs after the first and third storms.

The discrepancy between the field observations and the *PEB* algorithm can be partially accounted for by the assumption of a single dominant length scale at each time step. Both the field observations as well as the *PEB* algorithm show that a wide range of length scales exist immediately after a storm. In both cases, the actual occurrence of a wide range of length scales is reduced to one value. However, this single value is determined in a different way for the *PEB* algorithm than for the field observations: In the field observations, an average of the observed bed pattern length scales is shown, whereas the *PEB* algorithm only shows one single dominant length scale.

A first attempt at describing the decay rate of bed patterns is presented in this chapter. However, the extrapolation of the positive part of the growth rate curve in order to obtain decay rates is inaccurate. Not only does the extrapolation not exactly follow the physical predictions, but the lower limit of decay of $-\omega_{r_{FGM}}$ is inaccurate for shorter length scales. A more precise method would use all eigenvalues of the system, and identify the physically meaningful predictions by comparing the results of two different runs, one using twice the number of computational nodes as the other. Numerical results can then be identified as these will occur at different locations in the growth rate plot, whereas physical results

will remain at the same position along the growth rate curve.

The comparison with field observations has shown that the *PEB* algorithm only accurately predicts the development of crescentic bed patterns for brief periods of time. A careful determination of Amp_0 and Amp_{max} may result in an improved comparison with reality. Both the determination of Amp_0 and Amp_{max} are rather arbitrary in the presented study. A value of Amp_0 that is dependent on the pre-existence of different length scales will cause more accurate predictions over longer periods of time, for instance after the second storm. A more accurate determination of the value of Amp_{max} might result in time periods during which the development of crescentic bed patterns is more accurately described by the *PEB* algorithm. However, without further knowledge concerning the amplitude of the bed patterns at different stages of their development under real world conditions, the determination of a more accurate value of either Amp_0 or Amp_{max} is very complicated. The monthly bathymetric data collected at Duck are over a short domain, inhibiting the identification of specific bed patterns. Furthermore, the frequency at which these measurements are carried out is too low for the accurate determination of the final height of bed patterns.

Finally, the moment in time when Amp_0 is applied might be incorrect. It is assumed that at the peak of the storm, all bed patterns are erased, and immediately afterwards bed patterns start to re-develop. However, crescentic bed patterns might only develop under more moderate circumstances that occur later, when the storm has passed. This would mean that the applied reset after each storm

(Amp_0) would occur at a later stage, reducing the number of large length scales that is currently predicted during the first stages of post-storm development and possibly making the predictions by the *PEB* algorithm correspond more closely with field observations.

5.4 Conclusions

Research concerning the effects of pre-existing bed patterns (presented in chapter 4) have shown that pre-existing bed patterns initially show linear growth or decay, depending on the position of the length scale on the occurring linear growth rate curve. This understanding is implemented into the *PEB* algorithm, which is aimed at including the effects of pre-existing bed patterns into linear stability model predictions. The algorithm assumes that the amplitudes of all length scales develop according to the predicted linear growth and decay rates of these length scales.

A comparison between results from the *PEB* algorithm and field observations, as well as similar comparisons using the original linear stability model results and the physically significant (*PSD*) developments algorithm have shown that the *PEB* algorithm can describe the development of crescentic bed patterns, as was observed at Duck, at a higher accuracy for certain periods of time than the original linear stability results. Predictions made by the *PSD* algorithm generally correspond better with field observations than the *PEB* algorithm results. However, the *PSD* algorithm only shows predictions where field observations are most likely to converge with model predictions, whereas the *PEB* algorithm gives a continuous description of the dominant length scale.

The limitations imposed by a linear stability model and the field observations, mean that the discrepancies between predictions and field observations are generally significant. Including the effects of pre-existing bed patterns into the model

predictions of a linear stability analysis results in significantly improved predictions after the third storm ($[\delta_{\lambda_{obs.}, \lambda_{FGM}}]_{Post\ storm\ 3} = 0.37$ and $[\delta_{\lambda_{obs.}, \lambda_d}]_{Post\ storm\ 3} = 0.18$). After the first and second storms, however, the *PEB* algorithm significantly overpredicts the occurring length scale. In particular, the behaviour after the second storm is different compared to the field observations. This might be due to the possibly incomplete wipe-out of pre-existing bed patterns during this storm, whereas the *PEB* algorithm assumes a complete reset of the system at that point in time.

Chapter 6

Conclusions and recommendations

6.1 Answers to research questions

Question 1: How capable is a linear stability analysis in describing the observed development of crescentic bed patterns under variable wave forcing?

A linear stability model is used to describe the development of crescentic bed patterns at Duck. The modelled conditions closely correspond with recorded conditions over a two month period. Field observations of the crescentic bed pattern length scale over the same period at Duck by van Enkevort et al. [2004] are used for the comparison with model predictions. The results show that a linear stability analysis can predict the regeneration of crescentic bars at Duck after storms to a moderate degree of accuracy (relative error: $\delta_{\lambda_{obs.}, \lambda_{FGM}} = 0.44$). In line with the findings of van Enkevort et al. [2004], after storms, longer length scales are pre-

dicted than in between storms, when wave conditions are mild. Immediately after a storm, length scales between 500 and 800 m are predicted and can be observed. In between storm periods, observed and predicted length scales vary between 150 and 400 m.

However, fluctuations in the wave and tidal conditions cause the linear stability analysis predictions to show a much larger fluctuation than is actually observed. For each set of wave data, a linear stability analysis predicts the initial development of bed patterns, starting from an alongshore constant beach profile. Frequently changing wave conditions and tidal levels, therefore, cause fluctuating predictions of the bed pattern characteristics. In reality, a much more gradual development of bed-forms occurs after storms, and changes in the dominant length scale only occur gradually when wave conditions change more permanently.

Question 2: *Can current understanding of the development of crescentic bars be applied to improve the implementation of linear stability analysis predictions?*

To overcome the discrepancy between the fluctuating nature of linear stability analysis predictions and the gradual development of bed patterns in nature, a physically significant development (*PSD*) algorithm is developed. This algorithm can identify the more physically relevant model predictions with respect to growth rate and consistent length scale. Application of this algorithm to the results of the linear stability model produces a closer agreement between the predicted and observed bed patterns occurs ($\delta_{\lambda_{obs.}, \lambda_{sig.}} = 0.29$). The *PSD* algorithm partially addresses the limitations inherent in a linear stability analysis, however, it cannot

give continuous predictions over time.

Question 3: *How do pre-existing crescentic bed patterns interfere with the development of crescentic bed patterns?*

A non-linear stability analysis is used to investigate the effects of pre-existing bed patterns on the development of crescentic bed patterns, under constant wave forcing. A wide range of pre-existing bed pattern length scales and amplitudes was examined, along with two different offshore wave conditions. Results show that pre-existing bed patterns with a length scale that is close to the dominant length scale of the undisturbed case (λ_{FGM}) will undergo further growth and reach a final height within a short period of time. Initial length scales that are outside the linear growth rate curve of the undisturbed development will decrease in prominence and give rise to crescentic bed patterns with a length scale close to λ_{FGM} .

Not only can the finally dominant length scale be related to the linear growth rate curve for the undisturbed development, also the migration rate and linear growth and decay rate of pre-existing bed patterns and the finally dominant length scales correspond to the values from a linear model.

Question 4: *To what extent can a linear stability analysis be of use in describing the development of crescentic bed patterns, when these bed-forms already exist?*

An algorithm developed to implement the knowledge obtained from the investigation of the effects of pre-existing bed patterns is applied to the linear stability modelling results. This algorithm determines the dominant length scale over time,

based on the evolution of the amplitude of all length scales according to the complete growth rate curve, including decaying modes. The growth rate curve changes in time due to variations in the wave and tidal data, causing the amplitude of different length scales to dominate at different moments in time. A comparison of the outcomes of this algorithm with reality shows that although discrepancies remain in the overall comparison, significant improvements in the comparison between model predictions and field observations can be made during certain durations by implementing this algorithm.

6.2 Conclusion

In summary, we conclude that a linear stability analysis can describe the development of crescentic bed patterns for real-world cases with a reasonable degree of accuracy, but that an algorithm can be useful to overcome limitations of this modelling technique. The model predictions display fluctuations that are not observed in the field, due to the assumption of an alongshore constant bed profile under changing wave and tidal conditions. Over the course of this research, two algorithms have been developed that take into account the effects of both these fluctuations and the effects of pre-existing bed patterns. Firstly, the physically significant developments algorithm shows that, by identifying the periods where significant growth is predicted in combination with a relatively constant bed pattern length scale, better agreement can be achieved between predictions and observations, for the moments in time identified as significant periods. The second algorithm takes into account the interaction of pre-existing bed patterns on the development of crescentic bed patterns. This algorithm can give predictions for the entire period with a reasonable degree of accuracy. However, extensive knowledge of the occurring pre-existing bed patterns after storms, can improve the model predictions significantly. The results presented in this thesis have shown that a linear stability model, in combination with an algorithm for the identification of the more meaningful model results, can be used as a tool for coastal engineers to predict the development of crescentic bed patterns, and the likelihood of the occurrence of rip channels under changing forcing conditions.

6.3 Recommendations for further research

6.3.1 Comparison of linear model predictions with reality

The research presented in this thesis is based on the comparison of a single set of model runs by a linear stability model with one set of field observations. A more comprehensive investigation into the capabilities of a linear stability model in describing real-world conditions accurately would include other field sites. The available data, as well as the characteristics from this site, should fit the modelling attempt:

The field data available from the Field Research Facility of the United States Army Corps of Engineers at Duck is very extensive. A wide array of wave, tidal and bathymetric data is collected over the past decennia. This makes Duck an ideal source of data for coastal modelling. In this research only Argus images are used for the validation of the model predictions. Argus images only reveal the length scale of the observed bed patterns. Real bathymetric information concerning the development of the bed patterns could be used for a more extensive comparison of model predictions with field measurements. For instance, the development in height could be compared with the predicted growth rate curve. The bathymetric data at Duck consists of monthly measurements over a 1000 m long stretch of beach. Both the frequency as well as the length are insufficient for a successful quantification of crescentic bed pattern growth.

The characteristics of the field site should correspond with the assumed conditions in the model. The model assumes an alongshore constant, open coast and field data should therefore originate from a site whose conditions could be accu-

rately described by a linear stability model.

Various processes have been excluded from the modelling attempt. A more extensive investigation into the effects of these assumptions, could reveal which processes are critical for a more accurate description of field measurements.

Both the linear and non-linear stability analysis describe the nearshore zone in 2D. The depth varying processes, such as undertow, are not included. The effects of these processes are assumed to be limited, however, onshore and offshore migration of sediment could not be accurately described by this type of model. Currently, the alongshore average bed profile is fixed in both models, and only nearshore bed patterns can develop. The exclusion of 3D processes, mean that alongshore bars would disappear if the bed profile would not be fixed. As a result of this, bar migration cannot be described by either model. The position of the bar changes under different wave conditions. During storms, the bar migrates offshore, while during mild conditions the onshore bar migration occurs. The sparse bathymetric measurements at Duck only reveal that limited migration occurs between the start of the modelled period and the end of the modelled period. However, no further data is available and the bar could have migrated significantly in between. Different bar characteristics would result in significant changes to the predicted crescentic bed patterns [Calvete et al., 2007].

Differences between Morfo55 and Morfo60 results could also be investigated further. Although differences are limited, a better agreement could be useful for a more extensive incorporation of findings from the non-linear model in the analysis

by Morfo60.

A difference between Morfo60 and Morfo55 is that in Morfo60 the phase equation is excluded from the analysis of the perturbations. It was shown (in Fig. 2.8) that the influence on the growth rate curve is limited to smaller length scales. However, the accurate inclusion of this equation could give a more correct description of the occurring processes and therefore result in a better correspondence with reality.

The use of a more comprehensive model would enable us to incorporate more processes and variables into our modelling attempt. From the inclusion of the pier, to a variable grain size distribution, and a beach which shows pre-existing bed patterns.

Finally, refinements in the algorithms and their application could improve the predictive skills of the linear stability model. Combination of the *PEB* algorithm (for the inclusion of pre-existing bed patterns) and the *PSD* algorithm (for the identification of the moments in time when model results are most likely to correspond with field observations) might improve the comparison with reality. Also, a better understanding of the development of the bed patterns during a storm, might be of interest. It is assumed that all pre-existing bed patterns are wiped-out during a storm. However, especially after the second storm, strong indications exist that bed patterns remain, and dominate the subsequent period. This understanding could be easily included into the *PEB* algorithm. However, knowledge about the size of these pre-existing bed patterns is necessary for the accurate im-

plementation. Finally, the assumption that the development of new crescentic bed patterns starts immediately after the peak of the storm, might need refinement. Still persistent high wave conditions could inhibit the development of crescentic bars for a longer period of time, until more moderate wave conditions occur.

6.3.2 Comparison of a time-domain model with reality

Limitations that occur when using a linear stability model to investigate the development of crescentic bed patterns according to real-world conditions, could be overcome with the use of a more comprehensive model. Such a model could then be used to investigate which processes need including for a more accurate description of the development of bed patterns in the nearshore. This study might show similarities with the research presented in chapter 4, when the influence of pre-existing bed patterns was investigated. The use of a more comprehensive model to describe the actual development of crescentic bed patterns in time could reveal which processes excluded from a linear stability analysis, might be critical for the accurate description of the development of crescentic bed patterns. The depression at the pier, tidal variation, as well as pre-existing variability of the alongshore beach profile could be investigated, in order to determine their influence on the development of crescentic bed patterns.

6.3.3 Shoreface nourishments

Many coastlines across the world are under threat of erosion, and human interference is deemed necessary for the preservation of both the beach and the coastal zone. Shoreface nourishments are a new means of storm protection and erosion

mitigation in areas where hard defences (such as groins and seawalls) or beach nourishments are unsuitable. van Leeuwen et al. [2007] investigated the effects of shoreface nourishments using a linear stability analysis. However, results from this research suggest that an investigation using a non-linear model, could reveal both the sheltering effect of the beach behind the shoreface nourishment, and the influence of this type of human interference on the development of rhythmic features, such as crescentic bed patterns. The nourishment could even become part of the nearshore system, forming a second alongshore bar, which might also give rise to the development of crescentic bed patterns.

Bibliography

- Alexander, P. S. and Holman, R. A. (2004). Quantification of nearshore morphology based on video imaging. *Mar. Geol.*, 208:101–111.
- Battjes, J. A. (1975). Modeling of turbulence in the surfzone. In *Proc. Symp. Model. Tech.*, pages 1050–1061, San Francisco, U.S.A. A.S.C.E.
- Blondeaux, P. (2001). Mechanics of coastal forms. *Ann. Rev. Fluid Mech.*, 33:339–370.
- Bowen, A. J. (1969). Rip currents 1: Theoretical investigations. *J. Geophys. Res.*, 74(23):8467–8478.
- Bowen, A. J. and Holman, R. A. (1989). Shear instabilities of the mean longshore current. *J. Geophys. Res.*, 94(C12):18023–18030.
- Bowen, A. J. and Inman, D. L. (1969). Rip currents 2: Laboratory and field observations. *J. Geophys. Res.*, 74(23):8479–8490.
- Bowen, A. J. and Inman, D. L. (1971). Edge waves and crescentic bars. *J. Geophys. Res.*, 76:8662–8671.
- Caballeria, M., Coco, G., Falqués, A., and Huntley, D. A. (2002). Self-organization

- mechanisms for the formation of nearshore crescentic and transverse sand bars. *J. Fluid Mech.*, 465:379–410.
- Calvete, D., Coco, G., Falqués, A., and Dodd, N. (2007). (Un)predictability in rip channel systems. *Geophys. Res. Lett.*, 34(L05605).
- Calvete, D., Dodd, N., Falqués, A., and van Leeuwen, S. M. (2005). Morphological development of rip channel systems: Normal and near normal wave incidence. *J. Geophys. Res.*, 110(C10006).
- Canuto, C., Hussaini, M. Y., Quarteroni, A., and Zang, T. A. (1988). *Spectral Methods in Fluid Dynamics*. Springer–Verlag, New York, U.S.A.
- Castelle, B., Bonneton, P., Dupuis, H., and Sénéchal, N. (2007). Double bar beach dynamics on the high-energy meso-macrotidal french aquitanian coast: A review. *Mar. Geology*, 245(1-4):141–159.
- Chickadel, C. C., Holman, R. A., and Freilich, M. H. (2003). An optical technique for the measurement of longshore currents. *J. Geophys. Res.*, 108(C11).
- Church, J. C. and Thornton, E. B. (1993). Effects of breaking wave induced turbulence within a longshore current model. *Coastal Eng.*, 20:1–28.
- Coco, G. and Murray, A. B. (2007). Patterns in the sand: From forcing templates to self-organisation. *Geomorphology*, 91:271–290.
- Damgaard, J., Dodd, N., Hall, L., and Chesher, T. (2002). Morphodynamic modelling of rip channel growth. *Coastal Eng.*, 45:199–221.
- Dean, R. G. and Dalrymple, R. A. (1984). *Water wave mechanics for engineers and scientists*. World Scientific, Singapore.

- Deigaard, R., Drønen, N., Fredsoe, J., Jensen, J. H., and Jørgesen, M. P. (1999). A morphological stability analysis for a long straight barred coast. *Coastal Eng.*, 36(3):171–195.
- Dodd, N., Blondeaux, P., Calvete, D., de Swart, H. E., Falqués, A., Hulscher, S. J. M. H., Różyński, G., and Vittori, G. (2003). The use of stability methods in understanding the morphodynamical behavior of coastal systems. *J. Coastal Res.*, 19(4):849–865.
- Dodd, N. and Thornton, E. B. (1990). Growth and Energetics of Shear Waves in the Nearshore. *J. Geophys. Res.*, 95(C9):16075–16083.
- Dodson, I. (2009). Personal communication concerning the possible application of shoreface nourishments in the UK. Environment Agency.
- Dronen, N. and Deigaard, R. (2007). Quasi-three-dimensional modelling of the morphology of longshore bars. *Coast. Engineering*, 54. in press.
- Elgar, S., Guza, R. T., O'Reilly, W. C., Raubenheimer, B., and Herbers, T. H. C. (2001). Wave energy and direction observed near a pier. *J. Waterway, Port, Coastal and Ocean Eng.*, 127(1):2–6.
- Environment Agency (2008). Happisburgh to winterton sea defences stage 3b works. Technical Report <http://www.environment-agency.gov.uk/research/library/consultations/54395.aspx>, Environment Agency, Almondsbury, Bristol.
- Falqués, A. (2006). Wave driven alongshore sediment transport and stability of the Dutch coastline. *Coastal Eng.*, 53:243–254.

- Falqués, A., Coco, G., and Huntley, D. A. (2000). A mechanism for the generation of wave-driven rhythmic patterns in the surf zone. *J. Geophys. Res.*, 105(C10):24071–24088.
- Falqués, A., Dodd, N., Garnier, R., Ribas, F., MacHardy, L., Sancho, F., Larroudé, P., and Calvete, D. (2008). Rhythmic surf zone bars and morphodynamic self-organization. *Coastal Eng.*, 55(7-8):622–641.
- Falqués, A. and Iranzo, V. (1994). Numerical simulation of vorticity waves in the nearshore. *J. Geophys. Res.*, 99(C1):825–841.
- Feddersen, F., Guza, R., Elgar, S., and Herbers, T. (2000). Velocity moments in alongshore bottom stress parametrizations. *J. Geophys. Res.*, 105(C4):8673–8686.
- Fredsoe, J. and Deigaard, R. (1992). *Mechanics of Coastal Sediment Transport*. World Scientific, Singapore, first edition.
- Gallagher, E., Elgar, S., and Guza, R. T. (1998). Observations of sand bar evolution on a natural beach. *J. Geophys. Res.*, 103(C2):3203–3215.
- Garnier, R. (2006). *Nonlinear modelling of surf zone morphodynamical instabilities*. PhD thesis, Appl. Physics Dept., Univ. Politècnica de Catalunya, Barcelona, Spain.
- Garnier, R., Calvete, D., Dodd, N., and Falqués, A. (2007). Modelling the interaction between transverse and crescentic bar systems. In *Proceedings RCEM conference 2007*, volume 2, pages 931–937.

- Garnier, R., Calvete, D., Falqués, A., and Caballeria, M. (2006). Generation and nonlinear evolution of shore-oblique/transverse sand bars. *J. Fluid Mech.*, 567:327–360.
- Garnier, R., Calvete, D., Falqués, A., and Dodd, N. (2008). Modelling the formation and long-term behaviour of rip-channel systems from the deformation of a longshore bar. *J. Geophys. Res.*, 113(C07053).
- Grunnet, N. M. and Ruessink, B. G. (2005). Morphodynamic response of nearshore bars to a shoreface nourishment. *Coastal Eng.*, 52:119–137.
- Grunnet, N. M., Walstra, D. J. R., and Ruessink, B. G. (2004). Process-based modelling of a shoreface nourishment. *Coastal Eng.*, 51:581–607.
- Hamm, L., Capobianco, M., Dette, H. H., Lechuga, A., Spanhoff, R., and Stive, M. J. F. (2002). A summary of European experience with shore nourishment. *Coastal Eng.*, 47:237–264.
- Hanson, H., Brampton, A., Capobianco, M., Dette, H. H., Hamm, L., Lastrup, C., Lechuga, A., and Spanhoff, R. (2002). Beach nourishment projects, practices and objectives - a European overview. *Coastal Eng.*, 47:81–111.
- Hino, M. (1974). Theory on formation of rip-current and cuspidal coast. In *Coastal Eng. 1974*, pages 901–919, New York, U.S.A. Am. Soc. of Civ. Eng.
- Holman, R. A. and Stanley, J. (2007). The history and technical capabilities of Argus. *Coastal Eng.*, 54:477–491.
- Inman, D. L. and Guza, R. T. (1982). The origin of swash cusps on beaches. *Mar. Geol.*, 49:133–148.

- Iranzo, V. and Falqués, A. (1992). Some spectral methods for differential equations in unbounded domains. *Comp. Methods Applied Mech. Eng.*, 98:105–126.
- Kamphuis, J. W. (1995). Comparison of two-dimensional and three-dimensional beach profiles. *J. Waterway, Port, Coastal and Ocean Eng.*, 121(3):155–161.
- Klein, M. D. (2006). *Modelling rhythmic morphology in the surf zone*. PhD thesis, Tech. Univ. Delft, The Netherlands.
- Klein, M. D. and Schuttelaars, H. M. (2006). Morphodynamic evolution of double barred beaches. *J. Geophys. Res.*, 111(C06017).
- Klein, M. D., Schuttelaars, H. M., and Stive, M. J. F. (2003). Linear stability of a double-barred coast. In Smith, J. M., editor, *Coastal Eng. 2002*, vol. 3, pages 3396–3408, Singapore. World Scientific.
- Komar, P. D. (1998). *Beach Processes and Sedimentation*. Prentice Hall, second edition.
- Komar, P. D. and Holman, R. A. (1986). Coastal processes and the development of shoreline erosion. *Annual Review Earth and Planetary Sciences*, 14:237–265.
- Konicki, K. M. and Holman, R. A. (2000). The statistics and kinematics of transverse bars on an open coast. *Mar. Geol.*, 169:69–101.
- Lafon, V., Dupuis, H., Butel, R., Castelle, B., Michel, D., Howa, H., and Apoluceno, D. D. M. (2005). Morphodynamics of nearshore rhythmic sandbars in a mixed-energy environment (SW France): 2. physical forcing analysis. *Estuarine, Coastal and Shelf Science*, 65:449–462.

- Lippmann, T. C., Herbers, T. H. C., and Thornton, E. B. (1999). Gravity and shear wave contributions to nearshore infragravity motions. *J. Phys. Ocean.*, 29:231–239.
- Lippmann, T. C. and Holman, R. A. (1989). Quantification of sand bar morphology: a video technique based on wave dissipation. *J. Geophys. Res.*, 94(C1):995–1011.
- Longuet-Higgins, M. S. and Stewart, R. W. (1964). Radiation stresses in water waves: a physical discussion with applications. *Deep Sea Res.*, 11:529–562.
- MacMahan, J. H., Thornton, E. B., and Reniers, A. J. H. M. (2007). Rip current review. *Coastal Eng.*, 53:191–208.
- MacMahan, J. H., Thornton, E. B., Stanton, T. P., and Reniers, A. J. H. M. (2005). Ripex: Observations of a rip current system. *Mar. Geol.*, 218:113–134.
- Mei, C. C. (1989). *The Applied Dynamics of Ocean Surface Waves*, volume 1 of *Advanced Series on Ocean Engineering*. World Scientific, Singapore.
- Ojeda, E., Ruessink, B. G., and Guillen, J. (2008). Morphodynamic response of a two-barred beach to a shoreface nourishment. *Coastal Eng.*, 55:1185–1196.
- Phillips, O. M. (1966). *The Dynamics of the Upper Ocean*. Cambridge University Press, Cambridge, U.K.
- Plant, N. G., Holland, K. T., and Holman, R. A. (2006). A dynamical attractor governs beach response to storms. *Geophys. Res. Lett.*, 33:1–6.

- Plant, N. G., Holman, R. A., Freilich, M. H., and Birkemeier, W. A. (1999). A simple model for interannual sandbar behavior. *J. Geophys. Res.*, 104(C7):15755–15776.
- Pope, L., Ruessink, B. G., Wiering, A., and Turner, I. L. (2007). Recurrent neural network modeling of nearshore sandbar behavior. *Neural Networks*, 20:509–518.
- Press, W. H., Teukolsky, S. A., Vetterling, W. A., and Flannery, B. P. (1989). *Numerical Recipes: The Art of Scientific Computing*. Cambridge University.
- Reniers, A. J. H. M., Roelvink, J. A., and Thornton, E. B. (2004). Morphodynamic modeling of an embayed beach under wave group forcing. *J. Geophys. Res.*, 109(C01030).
- Ribas, F., Calvete, D., Falqués, A., de Swart, H. E., and Kroon, A. (2007). Comparing observed surfzone transverse finger bars with model results. In *Proceedings RCEM conference 2007*, volume 2, pages 713–720.
- Ribas, F., Falqués, A., and Montoto, A. (2003). Nearshore oblique sand bars. *J. Geophys. Res.*, 108(C43119).
- Ribas, F. and Kroon, A. (2007). Characteristics and dynamics of transverse finger bars. *J. Geophys. Res.*, 112(F03028). doi:10.1029/2006JF000685.
- Ruessink, B. G., Coco, G., Ranasinghe, R., and Turner, I. L. (2007). Coupled and noncoupled behavior of three-dimensional morphological patterns in a double sandbar system. *J. Geophys. Res.*, 112(C07002).
- Ruessink, B. G., Miles, J. R., Feddersen, F., Guza, R. T., and Elgar, S.

- (2001). Modeling the alongshore current on barred beaches. *J. Geophys. Res.*, 106(C10):22451–22463.
- Schielen, R. R., Doelman, A., and de Swart, H. E. (1993). On the dynamics of free bars in straight channels. *J. Fluid Mech.*, 252:325–356.
- Smit, M. W. J., Reniers, A. J. H. M., Ruessink, B. G., and Roelvink, J. A. (2008). The morphological response of a nearshore double sandbar system to constant wave forcing. *Coastal Eng.*, 55(10):761–770.
- Sorensen, R. M. (1993). *Basic Wave Mechanics*. John Wiley & Sons, New York, U.S.A.
- Soulsby, R. L. (1997). *Dynamics of Marine Sands*. Thomas Telford, London, U.K.
- Stauble, D. K. (1992). Long-term profile and sediment morphodynamics: field research facility case history. Technical report, US Army Corps of Engineers.
- Svendsen, I. A. (2006). *Introduction to nearshore hydrodynamics*. World Scientific, Singapore.
- The Open University (1989). *Waves, Tides and Shallow-water Processes*. Pergamon press.
- Thornton, B. and Guza, R. T. (1983). Transformation of wave height distribution. *J. Geophys. Res.*, 88(10):5925–5938.
- Thornton, E. B., MacMahan, J., and Sallenger Jr., A. H. (2007). Rip currents, mega-cups and eroding dunes. *Mar. Geology*, 240(1-4):151–167.

- Tiessen, M. C. H., van Leeuwen, S. M., Calvete, D., and Dodd, N. (2007). Analysis of the morphodynamical development of crescentic bed patterns at Duck over two months in 1998. In *Proceedings RCEM conference 2007*, volume 2, pages 729–736.
- Turner, I. L., Whyte, D., Ruessink, B. G., and Ratasinghe, R. (2007). Observations of rip spacing, persistence and mobility at a long, straight coast. *Mar. Geol.*, 236:209–221.
- van Enkevort, I. M. J. and Ruessink, B. G. (2001). Effects of hydrodynamics and bathymetry on video estimates of nearshore sandbar position. *J. Geophys. Res.*, 106(C8):16969–16979.
- van Enkevort, I. M. J. and Ruessink, B. G. (2003a). Video observations of nearshore bar behaviour. Part 1: alongshore uniform variability. *Cont. Shelf Res.*, 23:501–512.
- van Enkevort, I. M. J. and Ruessink, B. G. (2003b). Video observations of nearshore bar behaviour. Part 2: alongshore non-uniform variability. *Cont. Shelf Res.*, 23:513–532.
- van Enkevort, I. M. J., Ruessink, B. G., Coco, G., Suzuki, K., Turner, I. L., Plant, N. G., and Holman, R. A. (2004). Observations of nearshore crescentic sandbars. *J. Geophys. Res.*, 109(C06028).
- van Leeuwen, S., Dodd, N., Calvete, D., and Falqués, A. (2007). Linear evolution of a shoreface nourishment. *Coastal Eng.*, 54:417–431.
- van Leeuwen, S. M., Dodd, N., Calvete, D., and Falqués, A. (2006). Physics of

nearshore bed pattern formation under regular or random waves. *J. Geophys. Res.*, 111(F01023).

Wright, L. D., Chappell, J., Thom, B. G., Bradshaw, M. P., and Cowell, P. J. (1979). Morphodynamics of reflective and dissipative beach and inshore systems, Southeastern Australia. *Mar. Geol.*, 32:105–140.

Wright, L. D., Nielsen, P., Shi, N. C., and List, J. H. (1986). Morphodynamics of a bar-trough surf zone. *Mar. Geol.*, 70:251–285.

Wright, L. D. and Short, A. D. (1984). Morphodynamic variability of surf zones and beaches: A synthesis. *Mar. Geol.*, 56:93–118.

Yu, J. and Slinn, D. N. (2003). Effects of wave-current interaction on rip currents. *J. Geophys. Res.*, 108(C33088).

